

Use Authorization

In presenting this thesis partially fulfilling the requirements for an advanced degree at Idaho State University, I agree that the library shall make it freely available for inspection. I further state that permission for extensive copying of my thesis for scholarly purposes may be granted by the Dean of Graduate School, the Dean of my academic division, or the University Librarian. It is understood that any copying or publication of this thesis for financial gain shall not be allowed without my written permission.

Signature _____

Date _____

Numerical study of effect of wall thermal boundary conditions in non-premixed flame dynamics
in a confined channel

by
Nabin Raj Mahat

A thesis
Submitted in partial fulfillment
of the requirements for the degree of
Master of Science in the Department of Mechanical Engineering
Idaho State University
Fall 2022

Committee Approval

To the Graduate Faculty:

The committee members appointed to examine the thesis of Nabin Raj Mahat find it satisfactory and recommended that it be accepted.

Dr. Rajib Mahamud,

Major Advisor

Dr. Kenneth Bosworth,

Committee Member

Dr. James Mahar,

Graduate Faculty Representative

Acknowledgments

First and foremost, I would like to express my sincere gratitude to my advisor Dr. Rajib Mahamud for his continuous belief and support, and guidance beyond limitation whose door was always open whenever I had any problems regarding my research/writing and guiding me to the right direction. Thank you for being patient and always motivating me and pushing me beyond the boundaries and helping me recognize the ability I have which I was unaware of before. I would like to thank Dr. Kenneth Bosworth for always being available for any queries I had regarding the thesis and beyond. In addition, I would like to appreciate the academic and financial support provided by the mechanical engineering department and the graduate school at Idaho State university. I would not have been able to finish my thesis on time had the financial support from the department not given. I would also like to hugely thank my parents, grandparents, maternal uncle, maternal aunt, uncle, aunt for showering their continuous love, support, motivation and blessing throughout the ups and downs of my life and having a full faith in whatever I do. Finally, I would like to mention my brothers, sisters, relatives and my friends for always being there whenever I needed them.

Table of Contents

List of Figures.....	ix
List of Abbreviations/Symbols.....	xiii
Abstract.....	xv
CHAPTER 1. INTRODUCTION, BACKGROUND AND LITERATURE REVIEW	1
1.1 Introduction, Applications and Challenges:.....	1
1.2 Flame Modeling	4
1.2.1 Premixed Flame Modeling.....	6
1.2.2 Non-premixed Flame Modeling	7
1.3 Effects of Boundary conditions on flame propagation/characteristics.....	7
1.4 Motivations and Objectives.....	8
1.5 Thesis Outline	9
1.6 Background and literature review	9
CHAPTER 2. MATHEMATICAL AND NUMERICAL MODELING	15
2.1 Mathematical Modeling	15
2.1.1 LES Governing Equations	20
2.2 Numerical Modeling	26
2.2.1 Interpolation schemes	30
2.2.2 Surface normal gradient schemes (snGradSchemes).....	32
2.2.3 Gradient schemes.....	32
2.2.4 Laplacian schemes	33

2.2.5 Divergence schemes	34
2.2.6 Time schemes	35
Chapter 3. EXPERIMENTAL DESCRIPTION (SANDIA AND CAMBRIDGE SANDIA BURNERS) AND MODEL VALIDATION	37
3.1 Experimental Description.....	37
3.1.1 Flame Setup	37
3.2 Burner Geometry	37
3.3 Steps to simulate combustion of Sandia D flame using OpenFOAM.....	40
CHAPTER 4. RESULTS AND DISCUSSION.....	42
4.1 Results from validation	42
4.1.1 Results from validation without including the blocks	43
4.1.2 Results from validation by including just the inside block for the fuel.....	47
4.1.3 Results from validation by using all three blocks for fuel, pilot gases, and coflow.....	50
4.2 Results based on shape of burner	53
4.2.2 Parametric study of convergent burner at fuel velocity 20 m/s and $y/D = 30$ for (a) temperature, (b) velocity, and (c) mixture fraction	56
4.2.3 Parametric study of divergent nozzle at fuel velocity 20 m/s and $y/D = 30$ for (a) temperature, (b) velocity, and (c) mixture fraction	57
4.3 Results based on different inlet fuel velocities at different locations	60
4.3.1 Parametric study of inlet fuel velocity 15 m/s and $y/D = 15$ for temperature, velocity, and mixture fraction.....	60

4.3.2 Parametric study of inlet fuel velocity 20 m/s and $y/D = 15$ for temperature, velocity, and mixture fraction.....	62
4.3.3 Parametric study of inlet fuel velocity 15 m/s and $y/D = 30$ for temperature, velocity, and mixture fraction.....	63
4.3.4 Parametric study of inlet fuel velocity 20 m/s and $y/D = 30$ for temperature, velocity, and mixture fraction.....	65
4.3.5 Parametric study of inlet fuel velocity 15 m/s and $y/D = 45$ for temperature, velocity, and mixture fraction.....	67
4.3.6 Parametric study of inlet fuel velocity 20 m/s and $y/D = 45$ for temperature, velocity, and mixture fraction.....	68
4.4 Results based on heat flux wall boundary condition @ $U = 20$ m/s	71
4.4.1 Parametric study of heat flux at uniform gradient = 10 at $y/D = 15$ for temperature, velocity, and mixture fraction at inlet velocity 20 m/s	71
4.4.2 Parametric study of gradientEnergy at heat flux = 10 at $y/D = 30$ for temperature, velocity, and mixture fraction at inlet velocity 20 m/s	72
4.4.3 Parametric study of heat flux at uniform gradient = 50 at $y/D = 15$ for temperature, velocity, and mixture fraction at inlet velocity 20 m/s	74
4.4.4 Parametric study of heat flux at value = 50 at $y/D = 30$ for temperature, velocity, and mixture fraction at inlet velocity 20 m/s.....	75
4.4.5 Parametric study of heat flux at value = 500 at $y/D = 15$ for temperature, velocity, and mixture fraction at inlet velocity 20 m/s.....	77

4.4.6 Parametric study of heat flux at value = 500 at $y/D = 30$ for temperature, velocity, and mixture fraction at inlet velocity 20 m/s.....	78
4.4.7 Parametric study of heat flux at value = 1000 at $y/D = 15$ for temperature, velocity, and mixture fraction at inlet velocity 20 m/s	80
4.4.8 Parametric study of heat flux at value = 1000 at $y/D = 30$ for temperature, velocity, and mixture fraction at inlet velocity 20 m/s	81
4.5 Demonstration of temperature profile at 0.26 seconds during validation after all the blocks were added.....	84
4.6 Demonstration of velocity profile at 0.26 seconds during validation after all the blocks were added.....	85
4.7 Demonstration of mixture fraction profile at 0.26 seconds during validation after all the blocks were added	85
4.8 Demonstration of temperature profile at 0.26 seconds during validation after all the blocks were added for longer geometry (four times).....	86
4.9 Demonstration of velocity profile at 0.26 seconds during validation after all the blocks were added for longer geometry (four times).....	86
4.10 Demonstration of mixture fraction profile at 0.26 seconds during validation after all the blocks were added for longer geometry (four times)	87
Chapter 5. CONCLUSIONS AND RECOMMENDATIONS FOR FUTURE RESEARCH	90
5.1 Concluding remarks	90
5.2 Recommendations for future research.....	91

References	92
------------------	----

List of Figures

Figure 1: Change in flame type with gas velocity (Hottel and Hawthorne 1949)	2
Figure 2: Schematic diagram of Premixed combustion 3. non-premixed combustion flame.....	3
Figure 3: Schematic diagrams of non-premixed combustion	4
Figure 4: Flamelet approach schematic	23
Figure 5: Pre-flamelet computing and look up table for diffusion flame modeling	26
Figure 6: Flowchart of mixture fraction approach for diffusion flame numerical modeling.....	27
Figure 7: Burner schematic	38
Figure 8: Schematic of simulated burner	39
Figure 9: Geometry from blockMesh file	39
Figure 10: Commands to run the file	41
Figure 11: Cambridge-Sandia Stratified Burner	42
Figure 12: (a). x vs U_{mean} at 10 mm (b). x vs U_{mean} at 30 mm (c). x vs U_{mean} at 50 mm.....	43
Figure 13: (a). x vs U_{mean} at 70 mm (b). x vs T at 10 mm (c). x vs T at 70 mm	45
Figure 14: (a). x vs T at 10 mm (b). x vs T at 70 mm (c). x vs U_{mean} at 10 mm	47
Figure 15: (a). x vs U_{mean} at 30 mm (b). x vs U_{mean} at 50 mm (c). x vs U_{mean} at 70 mm.....	49
Figure 16: (a). x vs T at 10 mm (b). x vs T at 70 mm (c). x vs U_{mean} at 10 mm	50
Figure 17: (a). x vs U_{mean} at 30 mm (b). x vs U_{mean} at 50 mm (c). x vs U_{mean} at 70 mm.....	52
Figure 18: (a). Uniform burner (b) Convergent burner (c) Divergent burner.....	54
Figure 19: (a). Temperature profile (b). Velocity profile (c). Mixture fraction profile of uniform burner	55
Figure 20: (a). Temperature profile (b). Velocity profile (c). Mixture fraction profile of convergent burner	56

Figure 21: (a). Temperature profile (b). Velocity profile (c). Mixture fraction profile of divergent burner	58
Figure 22: (a) Temperature vs $y/D = 15$ at inlet velocity = 15 m/s, (b) Velocity vs $y/D = 15$ at inlet velocity = 15 m/s, (c) Mixture fraction vs $y/D = 15$ at inlet velocity = 15 m/s	61
Figure 23: (a). Temperature vs $y/D = 15$ at inlet velocity = 20 m/s, (b) Velocity vs $y/D = 15$ at inlet velocity = 20 m/s, (c) Mixture fraction vs $y/D = 15$ at inlet velocity = 20 m/s	62
Figure 24: (a). Temperature vs $y/D = 30$ at inlet velocity = 15 m/s, (b) Velocity vs $y/D = 30$ at inlet velocity = 15 m/s, (c) Mixture fraction vs $y/D = 30$ at inlet velocity = 15 m/s	64
Figure 25: (a). Temperature vs $y/D = 30$ at inlet velocity = 20 m/s, (b) Velocity vs $y/D = 30$ at inlet velocity = 20 m/s, (c) Mixture fraction vs $y/D = 30$ at inlet velocity = 20 m/s	65
Figure 26: (a). Temperature vs $y/D = 45$ at inlet velocity = 15 m/s, (b). Velocity vs $y/D = 45$ at inlet velocity = 15 m/s, (c). Mixture fraction vs $y/D = 45$ at inlet velocity = 15 m/s	67
Figure 27: (a). Temperature vs $y/D = 45$ at inlet velocity = 20 m/s, (b). Velocity vs $y/D = 45$ at inlet velocity = 20 m/s, (c). Mixture fraction vs $y/D = 45$ at inlet velocity = 20 m/s	68
Figure 28: (a). Temperature vs $y/D = 15$ at inlet velocity = 20 m/s for heat flux = 10, (b). Velocity vs $y/D = 15$ at inlet velocity = 20 m/s for heat flux = 10, (c). Mixture fraction vs $y/D = 15$ at inlet velocity = 20 m/s for heat flux = 10.....	71
Figure 29: (a). Temperature vs $y/D = 30$ at inlet velocity = 20 m/s for heat flux = 10, (b). Velocity vs $y/D = 30$ at inlet velocity = 20 m/s for heat flux = 10, (c) Mixture fraction vs $y/D = 30$ at inlet velocity = 20 m/s for heat flux = 10.....	73
Figure 30: (a). Temperature vs $y/D = 15$ at inlet velocity = 20 m/s for heat flux = 50, (b). Velocity vs $y/D = 15$ at inlet velocity = 20 m/s for heat flux = 50, (c). Mixture fraction vs $y/D = 15$ at inlet velocity = 20 m/s for heat flux = 50.....	74

Figure 31: (a). Temperature vs $y/D = 30$ at inlet velocity = 20 m/s for heat flux = 50, Velocity vs $y/D = 30$ at inlet velocity = 20 m/s for heat flux = 50, (c). Mixture fraction vs $y/D = 30$ at inlet velocity = 20 m/s for heat flux = 50.....	76
Figure 32: (a). Temperature vs $y/D = 15$ at inlet velocity = 20 m/s for heat flux = 500, (b). Velocity vs $y/D = 15$ at inlet velocity = 20 m/s for heat flux = 500, (c). Mixture fraction vs $y/D = 15$ at inlet velocity = 20 m/s for heat flux = 500.....	77
Figure 33: (a). Temperature vs $y/D = 30$ at inlet velocity = 20 m/s for heat flux = 500, (b). Velocity vs $y/D = 30$ at inlet velocity = 20 m/s for heat flux = 500, (c). Mixture fraction vs $y/D = 30$ at inlet velocity = 20 m/s for heat flux = 500.....	79
Figure 34: (a). Temperature vs $y/D = 15$ at inlet velocity = 20 m/s for heat flux = 1000, (b). Velocity vs $y/D = 15$ at inlet velocity = 20 m/s for heat flux = 1000, (c). Mixture fraction vs $y/D = 15$ at inlet velocity = 20 m/s for heat flux = 1000	80
Figure 35: (a). Temperature vs $y/D = 30$ at inlet velocity = 20 m/s for heat flux = 1000, (b). Velocity vs $y/D = 30$ at inlet velocity = 20 m/s for heat flux = 1000, (c). Mixture fraction vs $y/D = 30$ at inlet velocity = 20 m/s for heat flux = 1000	82
Figure 36: Temperature profile after validation for 0.26 seconds	84
Figure 37: Velocity profile after validation for 0.26 seconds	85
Figure 38: Mixture fraction profile after validation for 0.26 seconds	85
Figure 39: Temperature profile after validation for 0.26 seconds for longer geometry (four times)	86
Figure 40: Velocity profile after validation for 0.26 seconds for longer geometry (four times) ..	86
Figure 41: Mixture fraction profile after validation for 0.26 seconds for longer geometry (four times).....	87

Figure 42: Temperature contour	87
Figure 43: Velocity contour	88
Figure 44: Mixture fraction contour	88

List of Abbreviations/Symbols

CO_2	Carbon dioxide.
CH_4	Methane.
CO	Carbon monoxide.
NO_x	Nitric oxide and nitrogen dioxide.
Da	Damkohler number.
C_V	Heat capacity at constant volume.
C_P	Heat capacity at constant pressure.
c	Speed of the sound.
Z	mixture fraction.
Z''	mixture fraction variance.
L_f	Flame thickness.
χ	Scalar dissipation rate.
L_c	Cell length.
m	Constant molar mass.
Ma	Mach number.
P	Pressure.
Pr	Prandtl number.
Q	Specific energy released in a chemical reaction.
r	Radial position.
R	Flame tip position along the conduit.
Re	Reynolds number.
R_p	Universal gas constant.

S_c	Schmidt number.
T	Temperature.
T_w	Wall temperature.
t	Time.
u	Velocity component.
Y	Mass fraction of the fuel.
z	Axial position.
α	Thermal diffusivity
γ	Adiabatic exponent.
ε	Total energy per unit volume.
ζ	Stress tensor.
η	Dynamic viscosity.
Θ	Thermal expansion coefficient.
ρ	Density.
σ	Acceleration rate.
τ	Scaled time.
τ_f	Scaled time with respect to the flame.
ν	Kinematic viscosity.
m/s	meter per second (velocity unit).
mm	millimeter.
mJ	millijoule.

Numerical study of effect of wall thermal boundary conditions in non-premixed flame dynamics in a confined channel

Thesis Abstract-Idaho State University (2022)

Most of the combustion and propulsion applications are designed such that fuel and oxidizer are injected independently, mostly with multi-hole nozzles, into the chamber where it is mixed by turbulent diffusion and could achieve higher flame stability and fire protection. In non-premixed flames in a confined chamber, detailed modeling of flame wall interactions is crucial in predicting local heat release rates, flame quenching, and flame propagation and extinction. Wall thermal boundary conditions are pivotal in influencing combustion and flame propagation. In recent years, there have been many studies studying the effects of boundary conditions on flame propagation using a fully-compressible Navier-Stokes solver with different thermal conditions such as adiabatic and isothermal walls with various Lewis numbers and the Reynolds number correlated with the flame propagation. It is apparent that there is a necessity to determine the prediction of flame structure of a flame using Large Eddy Simulation (LES) and flame interaction with fluid motion and boundary conditions considering the importance of combustion. Flamelet/progress variable approach was applied to the large eddy simulation of a diffusion flame in a confined channel to flame propagation, calculate mixture variable and scalar dissipation rate in the CFD solver and update species concentration from the tabulated data. The OpenFOAM C++ platform that solves the transport equation of mass, energy, momentum, and species is used to explore and investigate the effects of wall thermal boundary conditions of a turbulent piloted methane/air diffusion flame in a confined channel configuration. It evaluates velocity and temperature profile during the flame progression along with the mixture fraction

and intermediate chemical formations in an effective manner. As the flow passes through the concentric nozzle, the flow develops from a transition region to a flame propagation region and the flame wall interaction takes place. The model was applied to validate the experimental results of the Cambridge-Sandia burner. The approach at the lower fuel velocities have shown the accurate predictions and well reproduced results. Also, the attention is equally shifted to identify the smallest Damkohler number which basically represents the weakest burning intensity of the flame by the use of diffusion flame in order to see the effects of controlling parameters on flame propagation. Additionally, parametric studies were performed with different fuel flow rates in order to evaluate the minimum Damkohler number for the optimum steady burning in a constant geometry and study how the flame propagation varies with the fluctuation of the Damkohler number.

Keywords: OpenFOAM; Combustion; Non-premixed; Diffusion flame; Flamelet; Sandia Burner; Flame Propagation; Validation; Parametric Study; Velocity; Temperature; Mixture Fraction

CHAPTER 1. INTRODUCTION, BACKGROUND AND LITERATURE REVIEW

1.1 Introduction, Applications and Challenges:

Numerous pieces of machinery used in various sectors include combustion. For the design and optimization, it is crucial to be able to model combustion. The visible gaseous part of a fire which is caused by a highly exothermic chemical reaction between fuel and oxidizer is called flame. The chemical reaction between the fuel and the oxidant is called combustion, which is accompanied by the emission of light in the visible region of the spectrum and by the release of heat [1]. The flame temperatures can be about 2200K or even down to 1300K depending on the fuel-air ratio [1]. The color and temperature of the flame depend on the type of fuel involved during combustion. There are different methods of distributing the required components of combustion to a flame. On the basis of mixing arrangement, flames can be:

- **Non-premixed/Diffusion Flame:** In a diffusion flame, the flame occurs when oxygen and fuel diffuse into each other, where they meet. Examples of non-premixed combustion include the common flame of a candle.
- **Premixed Flame:** The oxygen and fuel are premixed beforehand in a premixed flame. In premixed combustion, fuel and oxidizer are mixed at the molecular level prior to ignition. Combustion occurs as a flame front propagating into the unburnt reactants. Examples of premixed combustion include aspirated internal combustion engines, lean premixed gas turbine combustors, and gas-leak explosions. Premixed combustion is much more difficult to model than non-premixed combustion because premixed combustion usually occurs as a thin, propagating flame that is stretched and contorted by turbulence.

On the basis of gas velocity, flames can be:

- **Laminar:** If the gas flow rate is relatively low, it is considered as laminar flow
- **Turbulent:** If the gas flow rate is relatively high, it is considered as turbulent flow. The careful analyses of solutions to the Navier-Stokes equations show that turbulence develops as an instability of a laminar flow. It results from the interaction of chemistry and turbulence.

The rate of combustion is determined by the extent of fuel-oxygen pre-mixing. That means, there will be different reaction and temperature paths, resulting in different color hues. As the temperature increases, the color of the flame changes from red to orange to yellow to white. Similarly, the flame may be laminar or turbulent depending on the low or high gas flow rates. Hence, flames can be laminar diffusion, laminar premixed, turbulent diffusion, or turbulent premixed flames, where the transition from laminar to turbulent occurs as the flow velocity increases. Figure 1 shows flame and figure 2 shows change in flame type with increase in gas velocity.

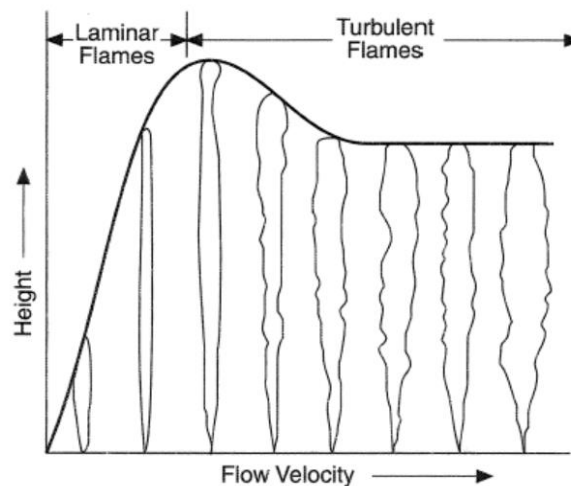


Figure 1: Change in flame type with gas velocity (Hottel and Hawthorne 1949)

The most commonly used flames are those of hydrocarbons with air, some other combinations can be:

- Propellants: e.g., Liquid hydrogen, liquid oxygen, ammonium perchlorate, rubber polymer binder
- Self-decomposition flames: e.g., Acetylene which burn without the addition of oxidizer.
- High temperature flames: They are produced by oxygen-fuel combinations such as ethyne with oxygen for welding
- Unusual flames: They are produced by the combustion of air or oxygen with a variety of unusual fuels like carbon disulphide.

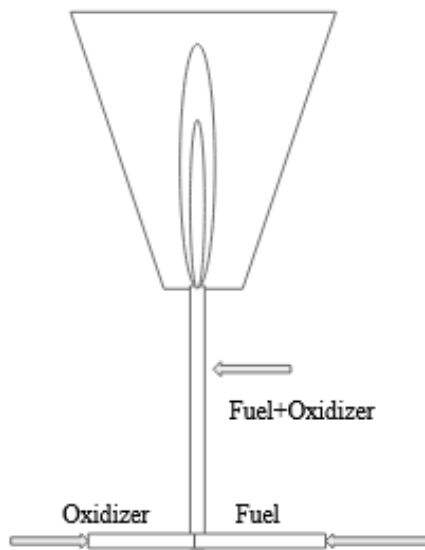


Figure 2: Schematic diagram of Premixed combustion

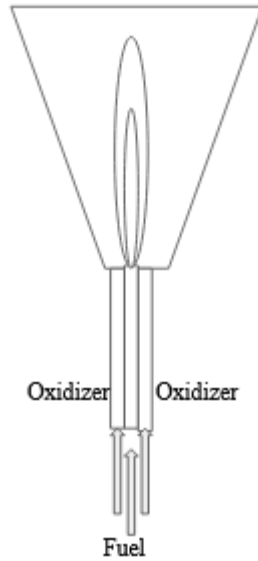


Figure 3: Schematic diagrams of non-premixed combustion

1.2 Flame Modeling

In instances of premixed as well as non-premixed combustion, the interaction of turbulence and chemistry is crucial. As a result, in many circumstances, the effectiveness of turbulence modeling is dependent on the performance of combustion modeling. Up until recently, industrial applications have used RANS-based flow models with varying types of combustion models to suit the application area with some success. However, the performance of the RANS-based models has been hampered in more complex conditions such as powerful swirling flows and very dynamically propagating flames. For the study of turbulent reactive flows, Large Eddy Simulation (LES) has developed into a very effective technique. Unsteady (time accurate) models of realistic geometries are required due to the significance of vortical structures and instability processes inside combustors.

The Reynolds Averaged Navier-Stokes (RANS) methodology is now the most popular method for creating combustion chamber designs. RANS, on the other hand, employs a steady state method that filters the Navier-Stokes equations over time. This method calls for ad hoc closure techniques that differ for each unique geometry and does not capture the flow's transitory properties. The Direct Numerical Simulation (DNS) method, on the other hand, resolves the full turbulent spectrum and yields an unsteady solution. Though considering the actual speed of supercomputers, the computational cost of DNS makes the modeling of an entire combustor impractical.

LES is a filtered, unstable solution to the Navier-Stokes equations. The large-scale turbulence structures are resolved by LES, but modeling is still needed for the small-scale structures. Since the small scales are locally isotropic, LES closure may be universal, meaning that sub-grid size models can be used in most situations as long as the turbulent Kolmogorov spectrum is sufficiently resolved. In part because of environmental laws aimed at lowering NO_x, the majority of land-based gas turbines are run in a premixed mode. Accurate premixed flame forecasts are desired for the proper design of premixed combustion systems.

Numerical simulations of reacting flows based on large eddy simulations (LES) have been pursued because they are well-suited to provide accurate and cost-effective predictions. This is because the capability of the classical approach is limited, using Reynolds averaged Navier-Stokes (RANS) equations in conjunction with phenomenological combustion models.

To sum up, whereas the RANS approach predominated in numerical simulations of turbulent combustion in the 1980s and 1990s, large-eddy simulation (LES) is quickly overtaking it as the dominant numerical tool for combustion modeling in the twenty-first century.

The foundation of LES is the resolution of large-scale turbulent eddies and the simulation of how small-scale eddies affect premixed flames. The strategy is particularly appealing for real-world use, especially when simulating phenomena involving the unstable dynamics of massive vortices. The basic understanding of the physics of premixed turbulent combustion has not yet been greatly advanced by LES, as the combustion models employed in it are frequently based on models created earlier for RANS applications.

1.2.1 Premixed Flame Modeling

Any homogeneous combination in which the fuel and the oxidant have already been mixed prior to the reaction results in premixed flames. That means reactants are thoroughly blended in premixed flames before entering the flame zone. Examples include the flame from a Bunsen burner and that from the majority of spark-ignited motors. Diffusion flames, on the other hand, develop at the point where air and fuel vapor collide. The fuel vapor and the oxidant are separate before burning, in contrast to premixed flames. There are four zones in a premixed flame: preheat zone (where the reactants are heated up), inner-layer (where there is radical formation), oxidation-layer (where there is the finishing of the remaining reactions), and post-flame zone (where there is formation of hot products and NO_x [57]. The ability of a premixed flame to spread normally toward itself while burning rapidly is its key characteristic [58]. A premixed flame develops when the Damkohler number is very low because mixing is quick compared to reaction [59].

1.2.2 Non-premixed Flame Modeling

The stoichiometric, counter diffusion of fuel and oxidizer sustains a non-premixed flame. The Damkohler number "Da" is used to compare the timescale of mixing to the timescale of chemical reaction in the case of non-premixed flames [59]. The reaction happens in a very thin zone between the fuel and oxidizer when the Damkohler number is very high, and the flame speed is constrained by the diffusion rate [59]. Zhang et al [63] came to the conclusion that from the perspective of fundamental modeling, large-eddy simulation (LES) methods with various sub-grid models had proven to be superior to Reynolds-averaged Navier-Stokes (RANS) methods, particularly in terms of foretelling the turbulent mixing process. They concluded that scalar dissipation and scalar variance are crucial modeling parameters for non-premixed turbulent combustion simulations, for example in mixture fraction-based models like flamelet models and the conditional moment closure. For the prediction of local extinction and re-ignition effects in turbulent diffusion flames, Pierce & Moin's flamelet/progress variable technique has been expanded [64]. There are two models that both incorporate the time scale ratio. The Sandia flames D and E were simulated using a large-eddy approach using the extended FPV model [64]. The outcomes for both examples are in good accord with the experimental findings. This exemplifies the extended FPV model's capacity to forecast local extinction and re-ignition effects in turbulent diffusion flames [64].

1.3 Effects of Boundary conditions on flame propagation/characteristics

It is found that a flame accelerates due to the boundary conditions. Boundary conditions like temperature, temperature gradient, heat flux, wall friction, wall heat transfer is one of the key factors influencing flame propagation shape and propagation velocity. In recent years, there have

been many studies scrutinizing the role of boundary conditions in flame acceleration scenarios by means of analytical formulations, numerical studies or experimental measurements. However, the majority of these works was limited to equidiffusive flames, where the thermal-to-mass diffusivity ratio (the Lewis number; Le) is unity [13]. Different thermal conditions such as isothermal and adiabatic walls can be applied to see the effect on flame propagation. Some studies have found that the increase in the Lewis number results in moderation of flame tip acceleration. It is also found that there is a change in the burning rate and surface area of the flame front at the lower Lewis numbers, where flames appear unstable against the diffusional-thermal flame instability [13]. Some studies demonstrate that higher wall temperatures promote slower propagation as they reduce the thermal expansion rate, as a result of the post-cooling of the burn matter [14]. As for the wall temperature effect, it has been found that isothermal walls provide weaker flame acceleration as compared to adiabatic ones [14]. The burning intensity and the flame-generated flow can be significantly modified by the momentum and energy transferred at the walls.

1.4 Motivations and Objectives

The effects of nozzle geometry and confinement and wall thermal boundary conditions on the dynamics of non-premixed flames have been extensively investigated numerically. However, there have not been even attempts on using the diffusion flame in the effects they have on flame structure and stability. Therefore, further research is needed in order to help develop the numerical study of the effect of wall thermal boundary conditions in a confined channel in a non-premixed flame dynamic.

This study uses 75% CH_4 and 25% CO_2 as the fuel supply, similar to the Sandia Flame D. This study aims to experimentally examine the effect of different burner configurations (regular,

nozzle, diffuser), effect of Damkohler number, effect of heat flux, effect of high velocities on the flow field and stability of non-premixed flame. The Cantera Solver and OpenFOAM platform were used for numerical modeling and obtaining simulation results, respectively, for collecting experimental data.

1.5 Thesis Outline

The thesis is organized as follows:

- **Chapter 1** presents the introduction, background, applications and challenges, along with motivations and objectives towards the end of the chapter.
- **Chapter 2** provides the emphasis on literature review and the works that have been done on the effects of boundary conditions on flame stability in a confined channel so far.
- **Chapter 3** describes the experimental setup, the design platform used, the solver method used, and the simulation platform used to generate the simulation plots. Furthermore, it puts emphasis on the plots that have been generated under different boundary conditions and configurations.
- **Chapter 4** presents the results based on the OpenFOAM simulations and their subsequent discussion.
- **Chapter 5** summarizes the results and outlines the main conclusions. Moreover, it provides recommendations for future works.

1.6 Background and literature review

In order to determine the possible air swirl and maintain a stable combustion of flame, combustion tests including the flame stability test have been performed (23). Masudi et al. [23] carried out the combustion tests at 834,330 Btu/hr., 669,488 Btu/hr. and 508, 215 Btu/hr. where

the combustion was relatively complete at 834,330 Btu/hr., 669,488 Btu/hr., but they showed no significant effect of swirl settings on NO_x, SO₂ and CO₂ respectively (23). In an attempt to provide a visually stable flame, burner settings may be adjusted (23). They showed that the parameters like coal particle size, volatile matter, ash content and excess air affect the flame stability (23). On the other hand, they also conducted the test that showed the gaseous concentrations at different locations of the burner are a function of residence time for each of the firing rates (23). Koirtyohann et al. [24] showed that the effect of flame shape should be the same for flame emission intensity as for atomic absorption response which is backed up by the experimental evidence (24). They have lowered the required electrical gain and used the narrower spectrometer slits to reduce noise levels eventually depending on the background structure in the vicinity of the line backed up by three cases (24). Lee CW et al experimentally investigated various kinds of pilot burners to study the effects of geometry (25). They also studied fuel equivalence ratios to analyze the feasibility of the novel pilot burner for the conventional burner application by which they concluded that the novel pilot burner with multi air holes had a thin, straight, long and stable pilot flame, while the conventional pilot burner had a thick, lifted, short and unstable flame (25). Also, it is shown that the pilot burner with an upper air flow hole led to less thermal damage to the burner combustor since it had a straight pilot flame (25). On the other hand, they concluded that the combustor durability is affected by the vertical location of the pilot burner from the main burner combustor. In order to investigate the effect of the coflow on the flame stability and flame structure, Lee CW et al performed experimental research for partially premixed turbulent flames (25). A swirler has been a broadly utilized agent device to progress combustion solidness and combustion effectiveness simultaneously since it can stabilize fire with the assistance of distribution zone and advance

homogeneous air/fuel blending (25). Numerous analysts have examined the impact of burner geometry on fire shape and its stabilization condition Aggarwal [26] conducted numerical and test inquire about for extinction and blowout of laminar in part premixed blazes that was spurred by contemplations of fire security and concealment. Syred [27] examined the swirl combustion system which permits coupling between the acoustics, combustion and swirling stream flow to occur. Lee et al. [28] explored combustion instabilities, which were watched for various combustion geometries and working conditions and which on a very basic level comprise interactions between acoustic wave waves and flame discharge. Masri et al. [29] studied experimental works on laboratory-scale swirl fire burners where critical reporting comes about or information bases exist. This paper centered on chosen gaseous fuel burners that span premixed, mostly premixed and non-premixed combustion over unconfined and confined conditions. Cookroom et al. [30] explored a laboratory-scale swirling burner, showing numerous similarities. Lee et al. [31] examined the characteristics of in part premixed turbulent flames. They were explored utilizing a burner plan that permits for a variety within the level of premixing between fuel and air. Some have detailed that as well solid a swirl concentrated with a swirl number of more than 3 has appeared unsteady fire and carbon monoxide (CO) arrangement, which comes about from a flame extinguishing impact caused somewhat by solid force of combustion discuss and mostly by incomplete combustion due to a critical sum of inactive gas of burnt gas. Yang et al. [32] studied the impact of fuel arrangement, combustor geometry, and working conditions on combustion characteristics in a swirl-stabilized combustor. Meanwhile, another vital figure that impacts fire steadiness is spout geometry. Akbarzadeh and Birouk [34] performed an exploratory investigation to study the impact of fuel spout geometry on the solidness of non-premixed turbulent methane fire. They concluded that the lift-off speed did not

change significantly with shifting co-airflow rates. In any case, it was higher for the rectangular and triangular spouts, taken after by the square and circular spouts. Wang et al. [35] examined the potential part that the breadth of a burner plays in fire structure and fire instability and the impact of burner distance across on the turbulent premixed fire structure. As of late, Yu et al. [36] considered the impact of pilot fire on a guided fly fire. They detailed that the response zone of the guided fly fire was within the mixing layer of the most jet and the hot coflow from the pilot fire. The proportionality proportion within the reaction zone could be altogether higher than that within the fuel/air blend of the most fire, particularly for the fundamental fire that had a much higher proportionality proportion than that of the pilot flame. They too detailed that the burning speed of the most fire was uncaring to the hot gas composition from the pilot fire, demonstrating that the warm exchange from the pilot flame to the most fire had a more noteworthy effect on the most fire than the exchange of radicals and combustion intermediates (such as CO and H₂) from the pilot fire to the main fire. Flame shape and measure are pivotal parameters, which ought to be carefully considered when designing and working a combustion gadget since they decide numerous combustion highlights, e.g., the temperature field, poison emanation, combustion efficiency, and fabric security (37). Recently, the burner geometry and fuel proportionality proportion of the pilot burner were changed to explore their impact on the pilot fire methodically. In expansion, the separation between the pilot burner and the main burner was moreover changed to tentatively explore its impact on fundamental fire. Pilot burner geometry and fuel proportionality proportion influences pilot fire structure, in this way making fire length longer and fire temperature higher for the most exceedingly bad case. The study carried out by Abdullah [38] uncovered that the cone shaped burner advanced higher fire uniqueness than the cylindrical one, and subsequently gets to be in coordinate contact with the

burner internal divider. The experimental results moreover appeared that recessing the center body, when employing a round and hollow burner geometry, enhances fire steadiness. The opposite scenario happens when employing a cone shaped burner geometry. The impact of burner arrangement (round and hollow or funnel shaped) on premixed biogas flames stability is found more noteworthy at tall swirl numbers. Lewis et al. [39] studied that the condition of correspondence of gas and burning speeds, required for stabilization of a fire over a burner, is established near the rim of the orifice. The conversion of biogas to biomethane (97–99% CH₄) enables it to be compressed or liquefied for use in gas turbines, boilers, and CHP as well as in cars and consumer uses [40]. Biogas has a low volumetric energy level, which causes unstable combustion and flame blowouts [41-42]. According to the review of Chomiak [43], limits on flammability are strongly influenced by temperature, which is dependent on the fuel's composition and concentration. In practical applications, diffusion flames are recognized for their safety and manipulation over the fee of energy launch as well as their balance throughout a wide variety of operating parameters [44]. Lean premixed flame stability is significantly impacted by a number of downsides, including autoignition, flashback, an increase in CO emissions, and combustion instabilities [45] and the reason for the drawback is the limited heat release intensity and low flame temperature of lean combustion [46]. Hence, implementing a swirl [47-48], changing the burner geometry [49-50], or/and applying a confinement [51-53] are three non-blending technique approaches that can be used to address stability difficulties. Another study [41] reported that the flame topology, blowout, and stability of premixed flames are greatly affected by increasing the confinement and swirl number. This is because the mixing layer thickness has increased and the velocity has decreased, making the flow velocity more equal to the flame propagation speed [42]. Low calorific value gaseous fuels' structure and

stabilization in conical burners were also researched, and it was found that the cone's internal vorticity structure increased flame stability [43]. But an excessive cone (quarl) angle allowed for additional ambient air entrainment, which caused the stabilization core to lengthen and narrow [54]. Another strategy for improving biogas flame stability involves mixing with fuels with higher calorific values [55]. In comparison to pure biogas flames, this method can result in better heating value, laminar flame speed, and heat release, which widens stability limits [55]. There are, however, a number of problems with blending procedures, including higher NO_x emissions, a greater potential for flashback, and higher capital and operating expenses [43]. The burner with a slot that is typically used for atomic absorption using premixed flames also produces fantastic outcomes when used to work on emissions. This prompted more thorough research into the impact of flame form. The triple flame's propagation speed must be accurately modeled in a simulation in order to accurately forecast the flame stabilization physics [56]. Additionally, the triple flame must be placed in such a way that its propagation speed is equal to the incident flow velocity [56]. The swirl (to create an internal recirculation zone that creates low velocity regions where the flame can anchor) leads to shorter, more compact flames, enhanced flame stabilization, improved mixing, and decreased nitric oxides [56]. Even if the flame would seem to be stable, it could still experience high-speed periodic flame motions because of periodic flame liftoff and flashback as well as a precessing vortex core [56] which could result in a combustion instability that needs to be detected with high-speed diagnostics.

CHAPTER 2. MATHEMATICAL AND NUMERICAL MODELING

2.1 Mathematical Modeling

Turbulence models are ways to incorporate the impact of turbulence in the simulation of fluid flows in computational fluid dynamics (CFD). Since turbulent flows are common in both natural and industrial flows, as well as in the majority of engineering applications, turbulence models are necessary for the majority of simulations. When fluid flows are regular and move in an organized fashion, they might be laminar [60]. Convective forces in the flow outweigh the fluid's viscous forces when the flow's speed or characteristic length is raised, causing the laminar flow to change into a turbulent one [60]. The Reynolds number is the ratio of convective to viscous forces. The greater the number, the more turbulent the flow, and it can be used to categorize different types of flows [60].

DNS (Direct Numerical Simulation)

This method is generally restricted to simple geometries and low Reynolds numbers due to the large computational resources required in terms of CPU time and memory. Using DNS, turbulence may be better understood and simplified turbulence models that are less expensive to calculate while still being helpful for predicting the primary impact of turbulence on the flow can be created [60]. RANS can be used to solve complex industrial challenges, while DNS and LES are often used for simple geometries and academic settings.

RANS (Reynolds-Averaged Navier-Stokes Simulations)

The Navier-Stokes equations can be averaged to produce the Reynolds Averaged Navier-Stokes (RANS) equations, which are the mean equations for fluid flows [60]. The most popular and

widely used method in industrial applications is RANS modeling. It is based on time averaging of the dependent variables and the governing equations. In the paper “Assessment of modeling approaches for the simulation of non-premixed and partially premixed turbulent combustion processes”, Jan E. Anker, Kilian Claramunt and Charles Hirsch mentioned two variants of the flamelet generated manifolds (FGM) technique to construct a manifold based on a set of flamelets and the Reaction Diffusion-Manifolds (REDIM) method for the simulation of non-premixed and partially premixed turbulent combustion processes. In their modeling approaches, they used the RANS-equations which are solved together with a transport equation for the mixture fraction f and its variance g . A transport equation for the progress variable Y is solved to parameterize the evolution of the overall reaction. It is assumed that the variance of the progress variable plays a negligible role in the turbulence-chemistry interaction compared to the variance of the mixture fraction. The governing equations were:

$$\partial_t \rho + \vec{\nabla} \cdot (\rho \vec{u}) = 0 \dots \dots \dots (1)$$

$$\partial_t (\rho \tilde{u}) + \vec{\nabla} \cdot (\rho \tilde{u} \otimes \tilde{u} - \underline{\underline{\sigma}}) = 0 \dots (2)$$

$$\partial_t (\rho \tilde{f}) + \vec{\nabla} \cdot (\rho \tilde{u} \tilde{f} - \rho D_e \vec{\nabla} \tilde{f}) = 0 \dots (3)$$

$$\partial_t (\rho \tilde{g}) + \vec{\nabla} \cdot (\rho \tilde{u} \tilde{g} - \rho D_e \vec{\nabla} \tilde{g}) = 2 D_e (\vec{\nabla} \tilde{f})^2 - C_\chi \rho \tilde{g} \tilde{\epsilon} / \tilde{k} \dots (4)$$

$$\partial_t (\rho \tilde{Y}) + \vec{\nabla} \cdot (\rho \tilde{u} \tilde{Y}) = \vec{\nabla} \cdot (\rho D_e \vec{\nabla} \tilde{Y}) + \tilde{\omega}_Y \dots (5)$$

with the velocity vector \vec{u} , the density ρ , the effective stress tensor $\underline{\underline{\sigma}}$, the source term of the progress variable $\tilde{\omega}_Y$ &, the turbulent kinetic energy k , the outer product \otimes and its dissipation rate ϵ . Here, the RANS equations were solved in conjunction with the standard k - ϵ model and a turbulent Schmidt number of $\sigma_D = 0.7$ was used. They concluded that the non-premixed FGMs

account for finite rate effects and are able to accurately resolve the formation of intermediate species as well as the lifting of partially premixed flames. But they found out that the use of REDIM approach and the use of premixed FGM tables did not prove to have significant advantages over the use of flamelets for which the work is on-going for investigation.

LES (Large Eddy Simulation)

For some applications, it can be necessary to employ more intricate methods that, rather than simulating all turbulence scales, focus on resolving the flow patterns that hold the most energy. This method is referred to as large eddy simulations (LES) [60]. This turbulence modeling is based on volume filtering. It is a relatively young technique that requires large computational resources but less than DNS. LES spatially filters out the tiniest turbulence scales while directly resolving the largest, most energetic scales.

W. Malalasekera, S.S. Ibrahim, A.R. Masri, S. K. Sadasivuni, and S. R. Gubba [61] summarized their experience in using the Large Eddy Simulation (LES) technique for the modeling of premixed and non-premixed combustion. The application of LES based combustion modeling technique to two well defined experimental configurations where high-quality data is available for validation where they used Smagorinsky eddy viscosity model with a localized dynamic procedure as the sub-grid scale turbulence model was described [61]. For non-premixed combustion modeling, a conserved scalar mixture fraction based steady laminar flamelet model was used [61]. A radiation model incorporating the discrete transfer method was included in the non-premixed swirl flame calculations. Whereas, for premixed combustion, a model based on dynamic flame surface density (DSFD) was used [61]. They concluded that in both cases LES based combustion models perform remarkably well and results agree well with the experimental

data [61]. For the combustion chemistry of non-premixed, the Steady Laminar Flamelet Model (SLFM) was used to form the combustion modeling aspect where a presumed probability density function (PDF) of the mixture fraction was chosen as a means of modeling the sub-grid scale mixing [61].

Valerio Parisi [62] compared three Large Eddy Simulation (LES) combustion models (Eddy Break-Up [EBU], Steady Flamelet [SF] and Linear Eddy Model [LEM]) for non-premixed combustion where LES simulations were carried out for a non-reactive case in order to analyze the turbulent mixing inside the combustor. It was concluded that the LEM-LES simulation achieved the best agreement with the observed flame structure and was the only model that captured the stabilization processes observed in the experiments whereas EBU-LES and SF-LES did not predict the correct flow pattern because of the inaccurate modeling of sub-grid scale mixing and turbulence-combustion interaction [63].

Modeling of Turbulent Combustion:

1. Direct Numerical Simulation (DNS):
 - It solves the entire set of governing equations
 - Used for 2D
 - Used for low Reynold's number flames
2. Statistical Approach (RANS)
 - Modeling of turbulent non-premixed flames
 - i. Presumed PDF Burke-Schumann flame sheet model
 1. It says all the species mass fractions, temperature, density is uniquely related to mixture fraction (Z)
 - ii. Flamelet models

- iii. Eddy dissipation concept (Magnussen) model
 - iv. Conditional moment closure (CMC) models
 - v. Probability density function (PDF) models
 - vi. Infinitely Fast Chemistry
 - vii. Laminar flame
 - viii. Flame surface density
 - ix. etc....
- Modeling of turbulent premixed flames (says a unified model does not exist)
 - i. K- ε model
 - ii. Global chemistry + EDC/EBU
 - iii. Detailed chemistry + G-equation + presumed pdf + flamelet library
 - iv. Bray-Moss-Libby (BML)
 - v. Flame surface density models
 - vi. Zimont's model
 - vii. Renormalization group theory
 - viii. Eddy Break Up
 - ix. etc....

RANS (Reynolds-averaged Navier-Stokes) equations were proposed by Osborne Reynolds which are time-averaged equations of motion for fluid flow primarily used to describe turbulent flows. It refers to an application of time averaging to the Navier-Stokes equations, which is often used to reduce complex systems of differential equations into simpler forms by partially or fully eliminating the time variable.

3. LES (Large Eddy Simulation)

Some of the characteristics of LES are as follows.

- It filters away the small scales
- It retains the large eddies
- Its models are similar to RANS models
- It is computationally cheaper than DNS but expensive than RANS
- Large scale unsteady motion is resolved
- Eddies smaller than filter size need to be modeled
- Models are needed to account for unresolved cases

2.1.1 LES Governing Equations

2.1.1.1 Navier-Stokes Equations

For a compressible, reacting, multi-species fluid, the Navier-Stokes continuity, momentum, energy and species equations are:

$$\partial \rho / \partial t + \partial \rho u_i / \partial x_i = 0 \dots (5)$$

$$\partial \rho u_i / \partial t + \partial / \partial x_j [\rho u_i u_j + p \delta_{ij} - \tau_{ij}] = 0 \dots (6)$$

$$\partial \rho E / \partial t + \partial / \partial x_i [(\rho E + p) u_i + q_i - u_j \tau_{ji}] = 0 \dots (7)$$

$$\partial \rho Y_m / \partial t + \partial / \partial x_i [\rho Y_m u_i - \rho Y_m V_{i,m}] = \dot{\omega}_m \dots (8)$$

where ρ is the density, p is the pressure, τ is the viscous stress tensor, u_i ($i=1,2,3$) are the velocity components, δ_{ij} is the Kronecker delta, Y_m is the mass fraction of species m , $V_{i,m}$ is the diffusion velocity, $\dot{\omega}_m$ is the mass reaction rate per unit volume, q_i is the heat flux vector and E is the total energy per unit mass.

τ_{ij} is given as:

$$\tau_{ij} = \mu [\partial u_i / \partial x_j + \partial u_j / \partial x_i] - \frac{2}{3} [\mu \partial u_k / \partial x_k] \delta_{ij} \dots (9)$$

where μ is the molecular viscosity approximated using Sutherland's Law:

$$\mu = \mu_0 (T/T_0)^{3/2} (T_0 + S)/(T + S) \dots (10)$$

where S is the Sutherland constant, equal to an effective temperature characteristic of the gas, T is the temperature, T_0 and μ_0 are reference temperature and molecular viscosity respectively.

$$p = (\rho T / W_m) \sum_{m=1}^N Y_m R_u \dots (11)$$

$$E = e + \frac{1}{2} (u_k \cdot u_k) \dots (12)$$

$$e = \text{internal energy per unit mass} = \sum_{m=1}^N Y_m h_m - p/\rho \dots (13)$$

$$V_{i,m} = -D_m / Y_m \partial Y_m / \partial x_i \dots (14)$$

$$q_i = -k \partial T / \partial x_i + \rho \sum_{m=1}^N Y_m h_m V_{i,m} \dots (15)$$

$$k = C_p \nu / Pr \dots (16)$$

$$h_m = \Delta h_{f,m}^0 + \int_{T_0}^T C_{p,m}(T') dT' \dots (17)$$

Where h_m = static enthalpy per unit volume, k = mixture averaged thermal conductivity,

C_p = mixture averaged specific heat at constant pressure and Pr = Prandtl number

2.1.1.2 Navier-Stokes LES Filtered Equations

The LES approach to the numerical simulation of turbulent reacting flows applies a filter in space to the Navier-Stokes equations. The filtering operation decomposes the flow field quantities into a filtered (resolved) component and a sub grid scale (modeled) component.

One of the methods to decompose the variables is Favre filtering defined as:

$$\tilde{f} = \bar{\rho} f / \bar{\rho} \dots (18)$$

Where the over bar denotes spatial filtering.

2.1.1.3. LES Subgrid Closure Models

Chemical kinetic mechanisms take place at the tiny scales of turbulence that an LES technique cannot address. In order to account for reactions and the interplay between combustion and the resolved flow field, sub-grid closure models for the species equations are required. The following describes a few non-premixed sub-grid closure models.

2.1.1.3.1 Eddy Break-Up Model

This approach was first developed by Spalding in 1971 [9] and then by Magnussen and Hjertager in 1976 [9]. This model makes an effort to account for both the turbulence-related mixing time and the combustion reaction's chemical kinetic time. EBU is based on the energy cascade theory and presupposes that chemical kinetic and turbulent time scales both have an impact on the local reaction rate. The energy cascade theory states that large-scale eddies disintegrate into progressively smaller ones.

2.1.1.3.2 Steady State Flamelet Model

The sub grid closure is approached differently by the SF model. The main goal is to detach combustion from the flow solution and reduce the number of transported scalars in the system of LES equations. Tracking a number of scalars that are conveyed in the flow field and include information about the reactions can be used to characterize non-premixed combustion. Only the mixture percent is tracked in the SF approach. In a flamelet technique, the temperature is still computed by solving the filtered energy conservation equation, and the species concentration scalars are functions of three factors that are utilized to determine the species concentrations.

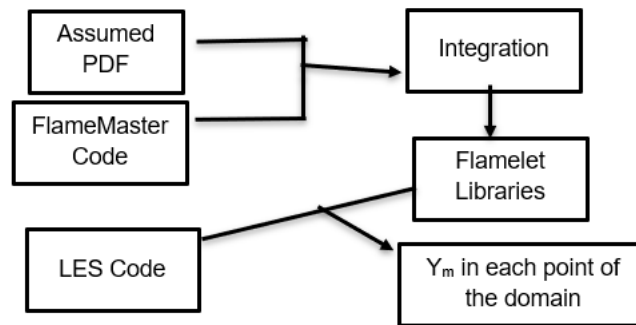


Figure 4: Flamelet approach schematic

2.1.1.3.3 Linear Eddy Model

The Linear Eddy Model (LEM) was originally formulated by Kerstein for non-reacting flows and was later extended by the same Kerstein to reactive flows. LEM attempts to solve turbulent mixing, molecular diffusion and chemical reactions by means of a one-dimensional domain embedded in the LES domain. This method has been successfully validated on both premixed and non-premixed combustion.

Classification of Combustion Models

The Damköhler number (Da) is dimensionless numbers used in reactive flow to relate the chemical reaction timescale (reaction rate) to the transport phenomena rate (flow time scale) occurring in a system. That is: $Da = \text{Turbulent flow time} / \text{Chemistry time}$

If $Da \sim 1 \Rightarrow$ slow chemistry

If $Da \gg 1 \Rightarrow$ fast chemistry

Overview of Models for Combustion

Zimont Flame Speed Model

- The turbulent flame speed can be written in terms of flow and chemistry time scales

$$S_t = A * (\text{Turbulent time scale} / \text{chemical time scale})^{.25} \text{ where } A = 0.52$$

Extended Coherent Flame Model (ECFM)

- The turbulent flame area (A_t) is of critical importance. The ECFM tracks an additional parameter, the flame area density (Σ) along with the progress variable C .

The above models are for premixed turbulent flames.

Modeling of Non-Premixed Combustion Model

The most frequently used models for the prediction of non-premixed turbulent combustion are

- Flamelet models
 - flamelet/progress variable (FPV) model
- Transported probability density function (TPDF) method
- Conditional moment closure (CMC) method

This model solves transport equations for mixture fraction (Z or f) and mixture fraction variance (instead of the individual species equations).

Applicability of Non-premixed Combustion Models

- Flow Regime: Turbulent flow (high Re)
- Chemistry: Equilibrium or moderately non-equilibrium (flamelet)
- Configuration: Non-Premixed

Applications of Diffusion Flame Models:

- Gas reaction (furnaces, burners). This is usually the model of choice if assumptions are valid for gas phase combustion problems.

- Accurate tracking of intermediate species concentration and dissociation effects without requiring knowledge of detailed reaction rates (equilibrium).

Limitations of Models

- Unreliable when mixing and kinetic time scales are comparable
- Cannot realistically model phenomena which depend on detailed kinetics (such as ignition, extinction).

Flamelets

A turbulent flame brush as an ensemble of discrete, steady laminar flames, called flamelets. The individual flamelets are assumed to have the same structure as laminar flames in simple configurations, and are obtained by experiments or calculations.

Diffusion Flame Models

- In this approach, the pre-calculated table of mixture fraction based on probability density function using thermodynamic data is used to calculate the flame brush for diffusion flame.
- Use of mixture fraction to decouple the chemical kinetics from the flow dynamics and reduce the burden of solving a large number of species transport equations.
- Under certain assumptions for non-premixed combustion, the thermochemistry can be reduced to a single parameter: the mixture fraction (f or Z)
- The mixture fraction is the mass fraction that originated from the fuel stream
- It is a conserved scalar quantity. Hence, its transport equation does not have a source term
- Combustion is simplified to a mixing problem, and the difficulties due to the closing non-linear mean reaction rates are avoided.
- Once fuel and oxidizer are mixed, the chemistry can be modeled as being in chemical equilibrium with the Equilibrium (chemistry) mode,

- Being near chemical equilibrium with the Steady Laminar Flamelet model, or significantly departing from chemical equilibrium with the Unsteady Laminar Flamelet model can be used

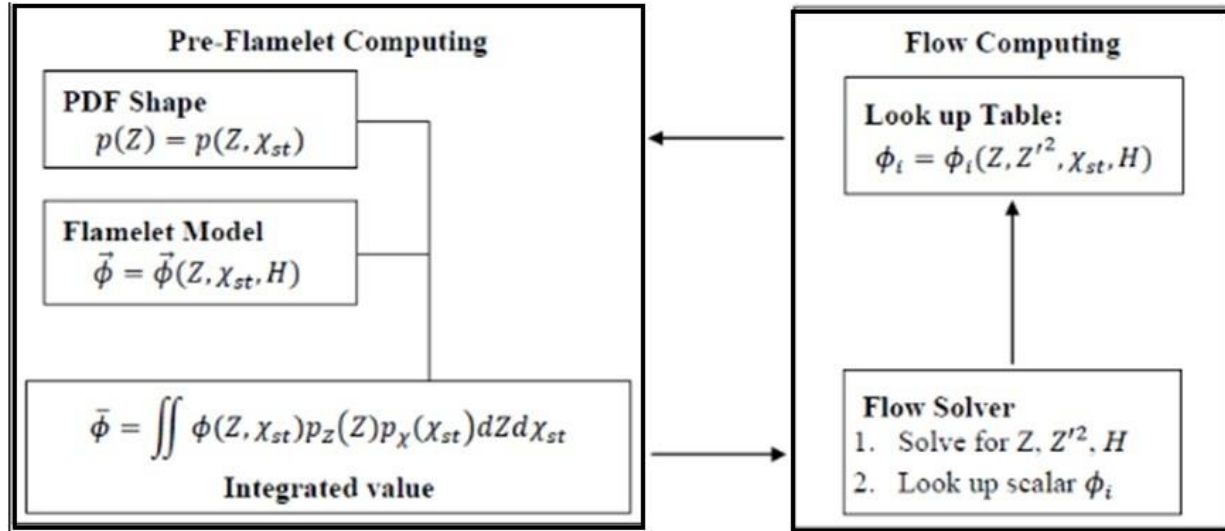


Figure 5: Pre-flamelet computing and look up table for diffusion flame modeling

2.2 Numerical Modeling

The OpenFOAM(Open Source Field Operation and Manipulation) computational toolbox is a free, open source software package written in C++. It is capable of simulating a wide variety of fluid flow processes. It has been developed primarily by OpenCFD Ltd since 2004[12]. The features it has can solve anything from complex fluid flows involving chemical reactions, turbulence and heat transfer, to acoustics, solid mechanics and electromagnetics. OpenFOAM contains a number of solvers having different computational properties. Those solver modules are available for both compressible and incompressible flows, chemical reactions and fluid–structure interactions. Also, for grid generation, pre-processing, and post-processible, many utilities are available. Some of the solcers from the OpenFOAM software package are:

- **rhoCentralFoam:** It is a combination of central difference and upwind schemes. It is useful to achieve good solvability for discontinuous solutions like shock waves and viscous phenomena.
- **sonicFoam:** It is based on the PISO algorithm (Pressure Implicit with Splitting of Operator) where two different equations are used to calculate the pressure for the correction of the pressure field obtained from discrete analogs of the equations of moments and continuity. Here, a second corrector is introduced which allows us to calculate the velocities and pressures satisfying the linearized equations of momentum and continuity.
- **rhoPimpleFoam:** It is a combination of the PISO and SIMPLE (Semi-Implicit Method for PressureLinked Equations) algorithms. It is because of the PISO algorithm that allows counting with the Courant number greater than 1 and makes the method iterative.
- **pisoCentralFoam:** It is a combination of a KurganovTadmor scheme and the PISO algorithm.

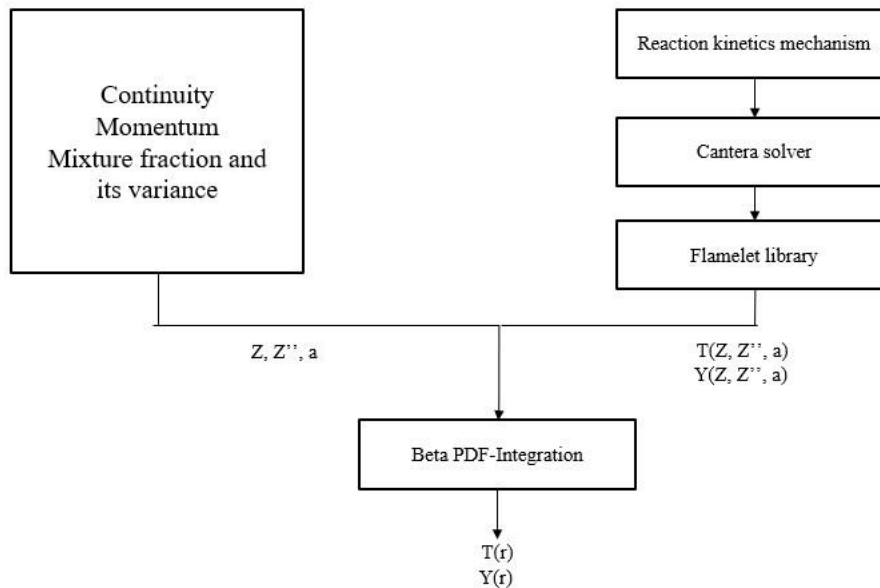


Figure 6: Flowchart of mixture fraction approach for diffusion flame numerical modeling

OpenFOAM uses the finite volume method for numerical representation of the equations governing fluid motion and the message passing interface (MPI) method for parallel computing. Reynolds averaged Navier–Stokes (RANS), hybrid RANS/LES (HRL), and LES are some of the turbulent models available. OpenFOAM provides three different pressure– velocity coupling methods for solving the governing equations for incompressible fluid flow, which are called Navier-Stokes equations.

Finite Volume Method (FVM)

The solution domain can be divided into a finite number of arbitrary control volumes of any shape where the solution is sought. It is required that the elements are convex and the faces that made up the control volume are planar. The Gauss or Divergence theorem which states that the outward flux of a vector field through a closed surface is equal to the volume integral of the divergence over the region inside the surface, is fundamental in the FVM. It is used to convert the volume integrals appearing in the governing equations into surface integrals.

OpenFOAM

OpenFOAM discretizes in space and time the governing equations in arbitrary polyhedral control volumes over the whole domain. It solves this system of discrete algebraic equations (DAE) to find the solution of the transported quantities after assembling a large set of linear DAE. Hence, the information like discretization of the solution domain or the mesh contained in the directory *constant/polyMesh*, boundary conditions and initial conditions contained in the directory *0*, physical properties such as density, gravity, diffusion coefficient, viscosity, etc. contained in the directory *constant*, physics involve, such as turbulence modeling, mass transfer, source terms,

etc. contained in the directories *constant* and/or *system*, how to discretize in space each term of the governing equations (diffusive, convective, gradient and source terms) contained in the directory *system/fvSchemes*, how to discretize in time the obtained semi-discrete governing equations contained in the directory *system/fvSolution*, set runtime parameters and general instructions on how to run the case (such as time step and maximum CFL number) contained in the directory *system/controlDict*, set sampling and functionObjects for post-processing contained in the directory *system/* has to be given.

Similarly, all the discretization schemes in OpenFOAM can be set as follows:

- The fvSchemes dictionary contains the information related to the discretization schemes for the different terms appearing in the governing equations.
- The discretization schemes can be chosen on a term-by-term basis.
- The keyword ddtSchemes refers to the time discretization.
- The keyword gradSchemes refers to the gradient term discretization.
- The keyword divSchemes refers to the convective terms' discretization.
- The keyword laplacianSchemes refers to the Laplacian terms discretization.
- The keyword interpolationSchemes refers to the method used to interpolate values from cell centers to face centers.
- The keyword snGradSchemes refers to the discretization of the surface normal gradients evaluated at the faces.

Similarly, OpenFOAM has many times discretization schemes where the source code can be found under *finiteVolume/ddtSchemes* directory. The time discretization schemes like steadyState are used for steady state simulations(implicit/explicit), Euler is used for time dependent first

order(implicit/explicit), bounded, backward and CrankNicolson are used for time dependent second order (implicit), bounded/unbounded. Both steady and unsteady simulations can be solved in OpenFOAM where steady simulations are much faster and require less computational power than unsteady simulations.

We can find the fvSchemes dictionary in the system directory in the OpenFOAM case setup. The fvSchemes dictionary in the system directory sets the numerical schemes for terms that appear in applications being run. They define different numerical schemes to discretize different terms in governing equations. If a default scheme is specified, it is assigned to all of the terms to which the sub-dictionary refers. However, if the *none* entry is selected, the user has to specify all terms in that sub-dictionary individually. The brief description of all the fvschemes available in OpenFOAM are described below:

2.2.1 Interpolation schemes

This sub dictionary contains values which are interpolated from cell centers to face centers. The interpolation schemes are divided into 4 categories: 3 categories of schemes used in conjunction with Gaussian discretisation of convection terms in fluid flow, which are general convection, normalized variable (NV), and, total variation diminishing (TVD), and one category of general schemes, specified by quoting the keyword and entry.

- Centered schemes
 - Linear
 - CubicCorrection
 - midPoint
- Upwind convection schemes
 - Upwind

- LinearUpwind
- skewLinear
- filteredLinear2
- TVD schemes
 - limitedLinear
 - vanLeer
 - MUSCL
 - LimitedCubic
- NVD schemes
 - Self-filtered central differencing (SFCD)
 - Gamma differencing

2.2.1.1 Schemes for strictly bounded scalar fields

These are for scalar fields that are bounded between 0 and 1. For example, the user would specify *default vanLeer01*; to bound the vanLeer scheme strictly between 0 and 1.

2.2.1.2 Schemes for vector fields

We get schemes for vector fields when *V* is added to the name of the general scheme, e.g., *limitedLinearV* for *limitedLinear*.

2.2.2 Surface normal gradient schemes (snGradSchemes)

This sub dictionary has surface normal gradient terms which are evaluated at a cell face. It is also required to evaluate a Laplacian term using Gaussian integration. The available schemes are described below.

- Limited
 - Limited non-orthogonal correction
- Corrected
 - Explicit non-orthogonal correction
- Uncorrected
 - No non-orthogonal correction
- Bounded
 - Bounded correction for positive scalars
- Fourth
 - Fourth order

All of the schemes are quoted with the keyword and entry, e.g., *default corrected*; But the limited schemes require an additional coefficient, e.g., *default limited 0.3*; The coefficient of 0 corresponds to uncorrected, 0.5 corresponds to non-orthogonal correction \leq orthogonal part, and 1 corresponds to corrected.

2.2.3 Gradient schemes

This sub-dictionary contains gradient terms. The following are the discretization schemes for each term. The Gradient is calculated using integrals over faces as

$$\int_{V_P} \nabla \phi dV = \oint_{\partial V_P} ds \phi = \sum_f s_f \phi_f \quad \dots (19)$$

The face value of ϕ from cell center values is evaluated as

$$\phi_f = f_x \phi_P + (1 - f_x) \phi_N \quad \dots (20)$$

where $f_x = \overline{fN}/\overline{PN}$

- Gauss <interpolationScheme>
 - Second order, Gaussian integration which specifies the standard finite volume discretisation of Gaussian integration which requires the interpolation of values from cell centers to face centers, e.g., *grad(p) Gauss linear*;
- leastSquares
 - Second order, least squares
- Fourth
 - Fourth order, least squares
- cellLimited <gradScheme>
 - Cell limited version of one of the above schemes
- faceLimited <gradScheme>
 - Face limited version of one of the above schemes

2.2.4 Laplacian schemes

This scheme contains Laplacian terms which requires Gauss scheme for discretization, a surface normal gradient scheme, and an interpolation scheme for the diffusion coefficient, e.g.

laplacian(nu,U) Gauss linear corrected; Here, the schemes are selected accordingly. The behavior of surface normal schemes used in `laplacianSchemes` are as follows.

- Corrected scheme: Unbounded, second order, conservative
- Uncorrected scheme: Bounded, first order, non-conservative
- Limited scheme: Blend of corrected and uncorrected
- Bounded scheme: First order for bounded scalars
- Fourth scheme: Unbounded, fourth order, conservative

2.2.5 Divergence schemes

This scheme contains divergence terms. The syntax of the entry is given as *div(phi,U)* where *phi* denotes flux. It uses the Gauss scheme for discretization and requires an interpolation scheme for the dependent field that can be selected from both general and convection-specific schemes, e.g.

div(phi,U) Gauss upwind;

The interpolation schemes used in `divSchemes` are described below.

- Linear scheme: Second order, unbounded
- SkewLinear scheme: Second order, (more) unbounded, skewness correction
- CubicCorrected scheme: Fourth order, unbounded
- Upwind scheme: First order, bounded
- LinearUpwind scheme: First/second order, bounded
- Quick scheme: First/second order, bounded
- TVD schemes: First/second order, bounded
- SFCD: Second order, bounded
- NVD schemes: First/second order, bounded

2.2.6 Time schemes

In this scheme, the first-time derivative terms are specified. It is also called ddt schemes where the discretization scheme for each term is selected as follows.

- Euler scheme: First order, bounded, implicit
- LocalEuler scheme: Local-time step, first order, bounded, implicit
- CrankNicholson scheme: Second order, bounded, implicit
- Backward scheme: Second order, implicit
- SteadyState scheme: Does not solve for time derivatives

Boundary Conditions in OpenFOAM

The main types of boundary conditions are:

- Basic: calculated, fixed value, fixed gradient, zero gradient
- Constraint: symmetry, wedge, cyclic, jump, cyclic AMI
- Derived: slip, no-slip, fan pressure, inlet-outlet, outlet inlet, total pressure

System specifications:

- Ubuntu Linux OS version 14.1
- OpenFOAM version 2.3.0
- ParaView version 5.6.0
- Gedit Text editor

Commands to be used:

- ls: This command in the terminal shows the folders available inside the directory.
- cd: This command stands for changing the directory.
- cd. : This commands helps to go one step back from the directory.

- `Gedit .bashrc` : This command displays the `gedit` file in order to change the alias `paraFoam` or alias `paraView` depending on the version of `openfoam` we are using. Suppose we are using the `paraFoam 2.3.0`, we save the alias file accordingly. Also, while in the terminal, we always go into the respective directory to run the case and always start with `of230` command. To summarise, the following are the commands used to run a sample case:
 - `Of230`: because this is the version of `openFoam` we are using.
 - `blockMesh`: generates the `blockMesh`
 - `canteraToFoam`: creates the tables by using the `cantera` solver
 - `diffusionflame`: First, we compile the `diffusion flame` and then use this command because this is what the research is based on.

CHAPTER 3. EXPERIMENTAL DESCRIPTION (SANDIA AND CAMBRIDGE SANDIA BURNERS) AND MODEL VALIDATION

3.1 Experimental Description

3.1.1 Flame Setup

The experimental setup consists of a burner. The flame that was simulated is a Sandia D flame from the Sandia laboratories and it was selected for validation rather than E or F because of the high Reynolds number and the small probability of local extinction [20]. The burner consists of a central block of walls. The fuel is a mixture of one part methane and three parts air by volume, and the boundary conditions in the zero folder are set accordingly. The mixture allows improved accuracy in the scalar measurements, reduces the flame length, and produces a more robust flame than pure methane [20,21]. As a result, flames are operated with little to no local extinction, with a modest pilot [20,21]. Because of the high mixing rates, the flames burn as diffusion flames [20]. The flames are confined. The pilot is a mixture of C_2H_2 , H_2 , air, CO_2 , and N_2 with the same nominal enthalpy and equilibrium composition as methane/air at this equivalence ratio [20].

3.2 Burner Geometry

The flame is made up of two concentric cylinders; the pilot jet emerges from the annulus and the main jet flow emerges from the center cylinder. Figure 6 displays a straightforward schematic of the flame and its surrounds. The burner has an inner fuel diameter of 5 mm, pilot diameter of 10 mm, and the coflow diameter of 50 mm and the total length of the burner was kept at 150 mm. The coflow velocity was set at 0.9 m/s, pilot velocity was set at 3.5 m/s, and the fuel velocity was set at 20 m/s. Similarly, the boundary field for temperature was set at 294 K for fuel, pilot,

and coflow. The axial profiles of scalar measurement in the flame includes locations $x/D = 15$, $x/D = 30$, and $x/D = 45$.

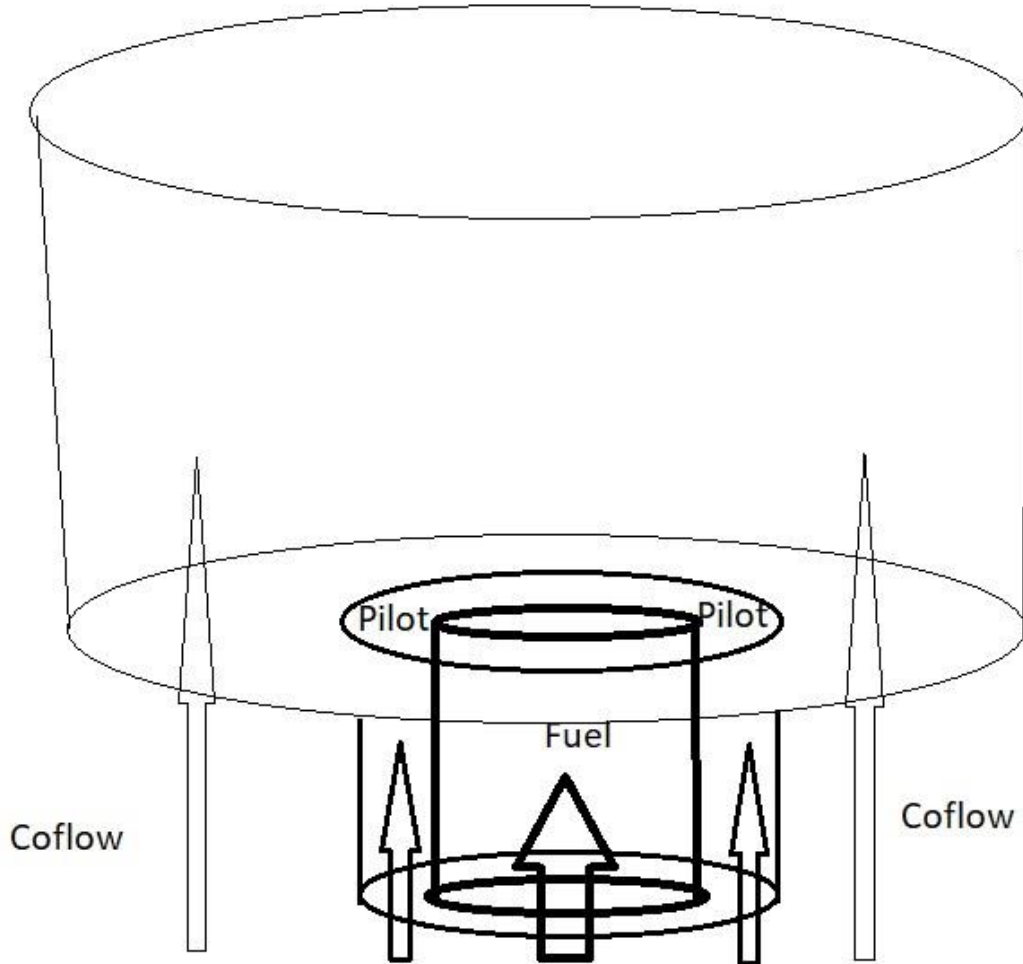


Figure 7: Burner schematic

In the actual simulation, the geometry was halved symmetrically so that we can get the same results but in a much shorter period of time. The schematic of the simulated geometry is shown in figure 7.



Figure 8: Schematic of simulated burner

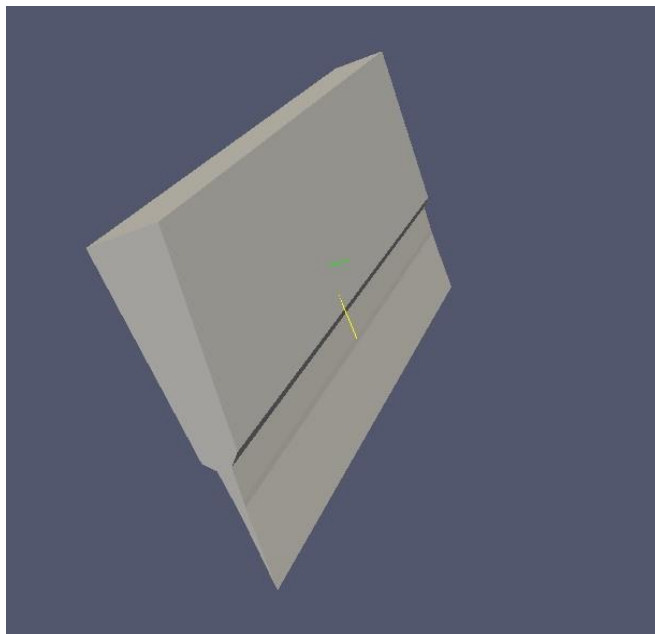


Figure 9: Geometry from blockMesh file

3.3 Steps to simulate combustion of Sandia D flame using OpenFOAM

Ubuntu 14.1 was used as a Linux platform and Open FOAM 2.3.0 was used to simulate the burner model. The simulated results were viewed using paraview. Simulation setup files for Open FOAM 2.3.0 and paraview were obtained from the OpenFOAM website and were extracted after downloading those files. Cantera solver is a transient solver that is used for simulating laminar/turbulent systems that uses stoichiometry expressions and kinetic data of reactions to obtain consumption and production rate of species [22]. OpenFOAM needs to know molecular weight, density, enthalpy/internal energy, transport properties and all kinds of species which are selected accordingly. In system.blockMeshDict, the geometry was defined. The chemkin subfolder contains the reaction mechanism and kinetics, thermophysical, and transport data. Constant/thermophysicalProperties file contains the thermodynamic settings of simulation. The Constant/turbulenceProperties file contains the turbulence properties of the system that uses the k- ϵ turbulence model. The 0 folder contains the initial and boundary conditions of the field variables. Properties such as velocity, temperature, pressure, etc. are located in the 0 folder. We set the start and end time inside the controlDict file which is inside the system folder. We can also save the data according to the timesteps we set inside the controlDict file with the command writeInterval.

We run the following commands to run the simulation.

- `cd Open Foam` (the case is inside this directory)
- `cd New_run 09222022` (the case we are running that was inside Open FOAM directory)
- `0f230` (to activate the open Foam version 2.3.0)
- `blockMesh` (to create the geometry from the blockMesh file)
- `canteraToFoam` (using the cantera solver to generate the species)

- diffusionflame (compiles the diffusion flame)
- paraFoam (views the geometry after simulation)

- blockMesh
- canteraToFoam
- diffusionflame

Figure 10: Commands to run the file

CHAPTER 4. RESULTS AND DISCUSSION

4.1 Results from validation

The mean velocities of inner tube, outer tube, and the outer annulus tube are 8.31 m/s, 18.7 m/s, and 0.4 m/s respectively. The temperature was set at 294 K and the results were taken at the runtime of 0.26 seconds. Figure 11 was used for validation.

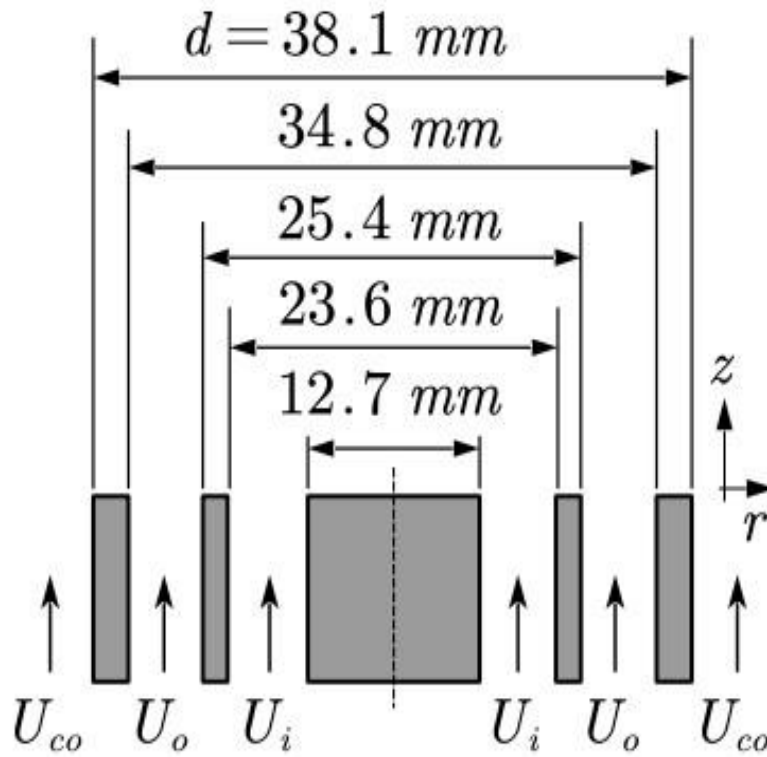


Figure 11: Cambridge-Sandia Stratified Burner

4.1.1 Results from validation without including the blocks

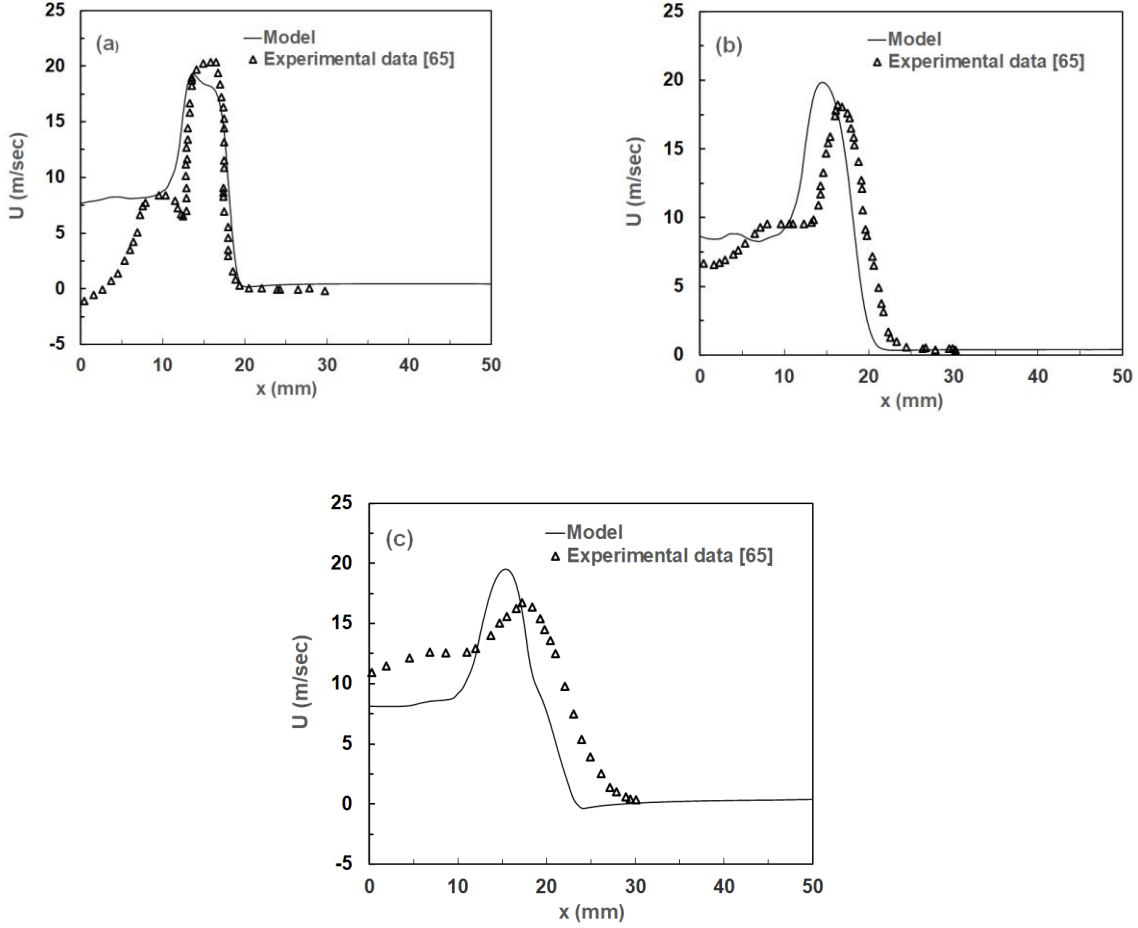


Figure 12: (a). x vs U_{mean} at 10 mm (b). x vs U_{mean} at 30 mm (c). x vs U_{mean} at 50 mm

Fig. 12(a) compares the axial mean velocity profiles from the experimental data with the data from the model without the inclusion of any blocks at axial distance of 10 mm. Prediction can be improved with the inclusion of the three blocks inside for the well reproduced velocity plot. The velocity first increases with the rate up to a maximum of 20 m/s, then decreases instantaneously before attaining a plateau. Hence, a very good agreement is obtained between LES results and experiments for the axial profiles of the mean axial velocity at the different axial location even though some discrepancies appear in the first measurement plane, where the mean values are

underestimated in the entrance region of the central main jet. This may be a consequence of the flow injection with slipping velocity at walls. After that discrepancy observed in the evolution of the velocity along the centerline, the axial velocity levels are rapidly recovered at the measurement planes located downstream. Fig. 12(b) compares the axial mean velocity profiles from the experimental data with the data from the model without the inclusion of any blocks at axial distance of 30 mm. Prediction can be improved by including three blocks inside for the well reproduced velocity plot. The velocity first increases with the rate up to a maximum of 20 m/s, then decreases instantaneously before attaining a plateau. Hence, a very good agreement is obtained between LES results and experiments for the axial profiles of the mean axial velocity at the different axial location even though some discrepancies appear in the first measurement plane, where the mean values are overestimated in the entrance region of the central main jet. This may be a consequence of the flow injection with slipping velocity at walls. After that discrepancy observed in the evolution of the velocity along the centerline, the axial velocity levels are rapidly recovered at the measurement planes located downstream. Fig. 12(c) compares the axial mean velocity profiles from the experimental data with the data from the model without the inclusion of any blocks at axial distance of 50 mm. Prediction can be improved with the inclusion of the three blocks inside for the well reproduced velocity plot. The velocity first increases with the rate up to a maximum of 20 m/s, then decreases instantaneously before attaining a plateau. Although a very good agreement is not obtained between LES results and experiments for the axial profiles of the mean axial velocity at the different axial location and some discrepancies appear in the first measurement plane, the newly generated plot from the model still follow the same trajectory format with a little shift on the left. This may be a consequence of the flow injection with slipping velocity at walls. That means the axial mean

velocity shown in Fig. 15 is slightly under-predicted upstream then over-predicted after finally following the almost same trajectory with a shift to the left.

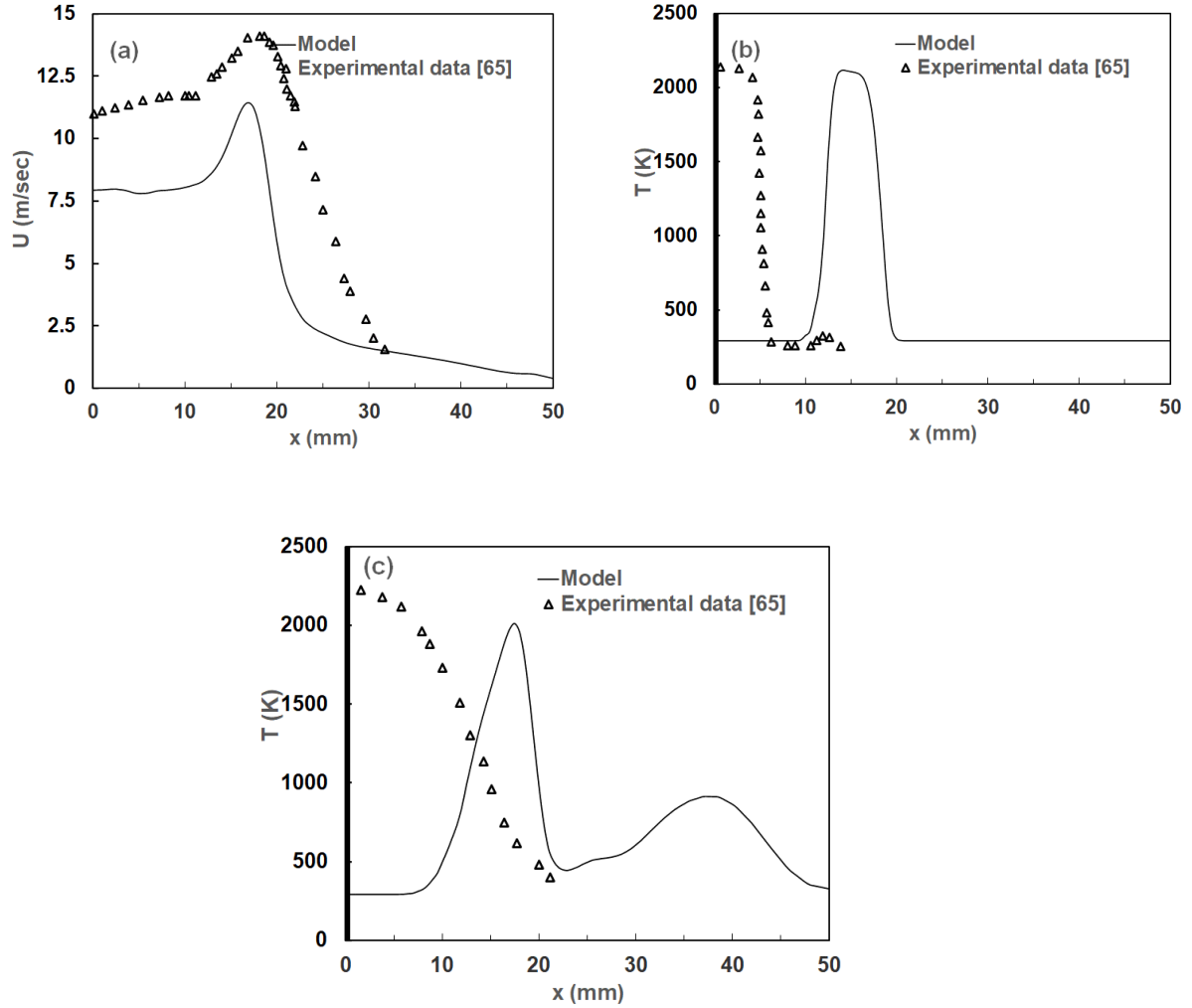


Figure 13: (a). x vs U_{mean} at 70 mm (b). x vs T at 10 mm (c). x vs T at 70 mm

Fig. 13(a) compares the axial mean velocity profiles from the experimental data with the data from the model without the inclusion of any blocks at axial distance of 70 mm. The velocity first increases with the rate up to a maximum of 14 m/s, then decreases instantaneously. Although a very good agreement is not obtained between LES results and experiments for the axial profiles of the mean axial velocity at the different axial location and some discrepancies appear in the

first measurement plane, the newly generated plot from the model is underestimated but still follow the same trajectory format with a little shift on the left. That means the axial mean velocity shown in Fig. 16 is slightly under-predicted upstream of the axial position $z = 70$ mm. Fig. 13(b) compares the axial temperature profiles from the experimental data with the data from the model without the inclusion of any blocks at axial distance of 10 mm. The temperature first increases with the rate up to a maximum of about 2200 K, then decreases instantaneously before becoming a plateau. Here, a very good agreement is obtained between LES results and experiments for the axial profiles of the temperatures at the different axial location except the fact that the newly generated plot from the model is shifted to the right while still following the same trajectory. Fig. 13(c) compares the axial temperature profiles from the experimental data with the data from the model without the inclusion of any blocks at axial distance of 70 mm. The temperature first increases with the rate up to a maximum of about 2000 K, then decreases instantaneously upto 500 K. Again, it increases upto 900 K before becoming a plateau. Here, a very good agreement is not obtained between LES results and experiments for the axial profiles of the temperatures at the different axial locations.

4.1.2 Results from validation by including just the inside block for the fuel

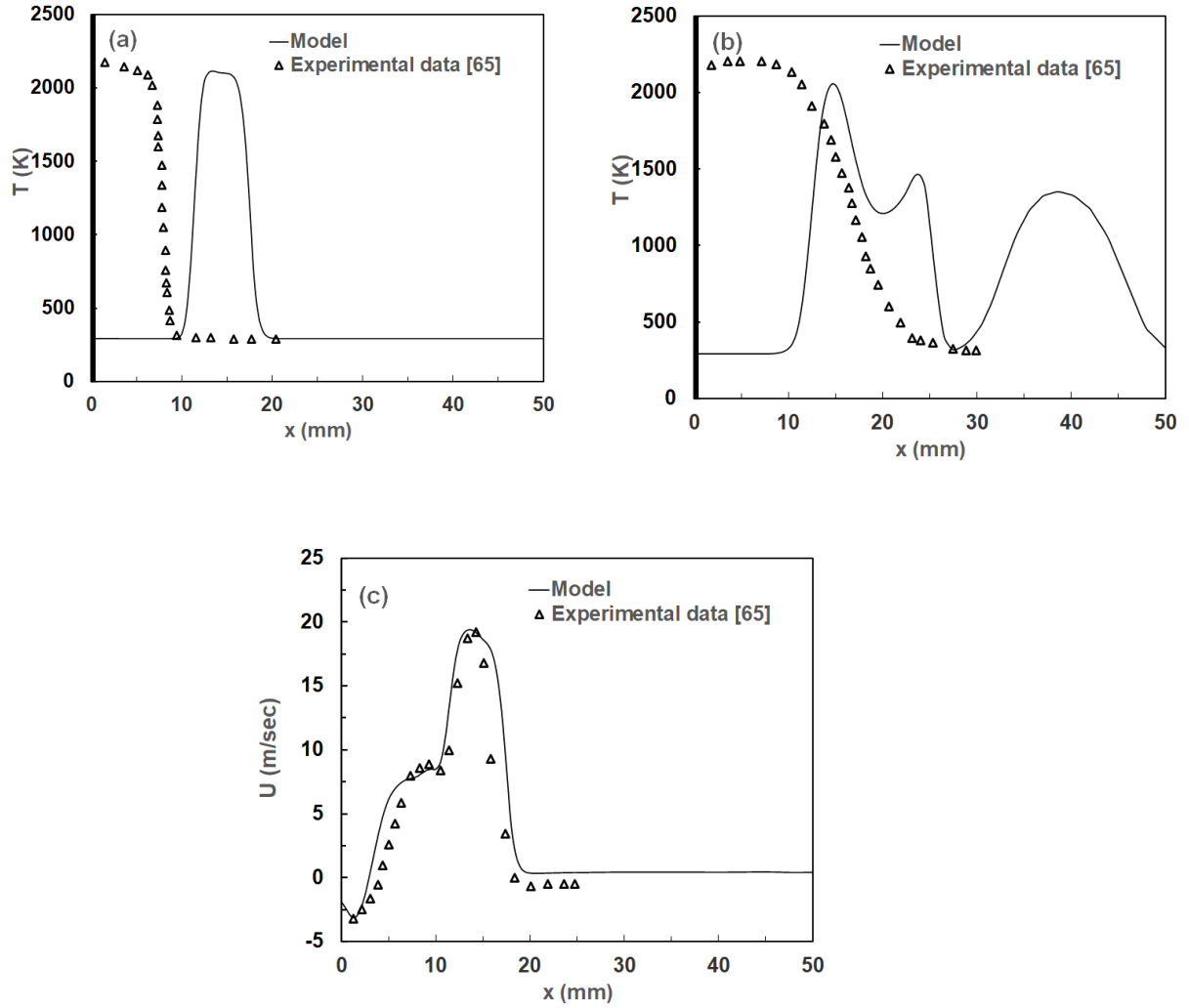
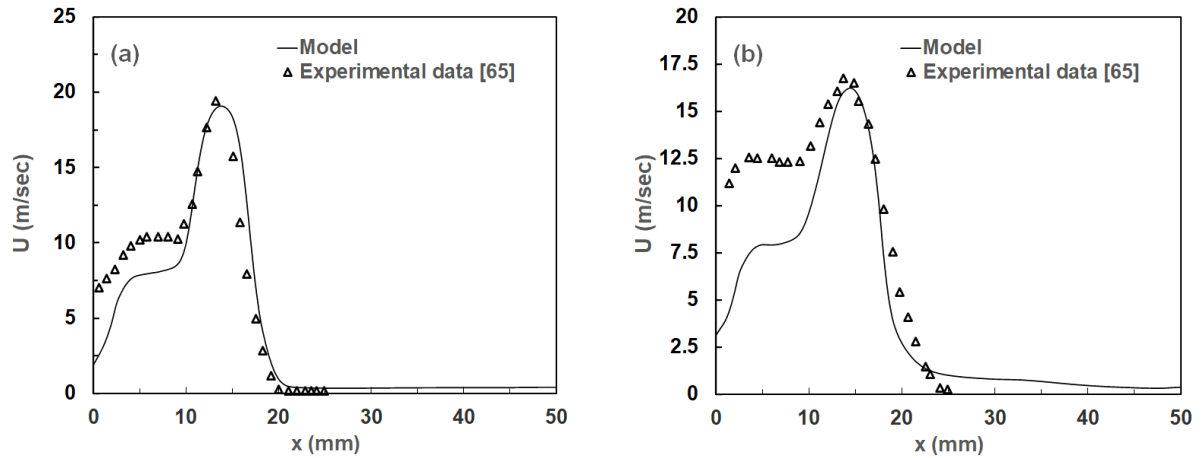


Figure 14: (a). x vs T at 10 mm (b). x vs T at 70 mm (c). x vs U_{mean} at 10 mm

Fig. 14(a) compares the axial temperature profiles from the experimental data with the data from the model at an axial distance of 10 mm with the inclusion of one inside block. The temperature first increases with the rate up to a maximum of about 2100 K, then decreases instantaneously before becoming a plateau. Here, a very good agreement is obtained between LES results and experiments for the axial profiles of the temperatures at the different axial location except the fact that the newly generated plot from the model is shifted to the right while still following the

same trajectory. Fig. 14(b) compares the axial temperature profiles from the experimental data with the data from the model at an axial distance of 70 mm with the inclusion of one inside block. The temperature first increases with the rate up to a maximum of about 2000 K, then decreases instantaneously up to 1400 K. Again, it increases up to 1500 K, then decreases to about 400 K. Again, it reaches to about 1300K before eventually becoming a plateau. Here, a very good agreement is not obtained between LES results and experiments for the axial profiles of the temperatures at the different axial locations. Fig. 14(c) compares the axial mean velocity profiles from the experimental data with the data from the model at an axial distance of 10 mm with the inclusion of one inside block. The velocity can be well predicted for validation. The velocity first increases with the rate up to a maximum of 20 m/s, then decreases instantaneously before attaining a plateau. Hence, a very good agreement is obtained between LES results and experiments for the axial profiles of the mean axial velocity at the different axial locations.



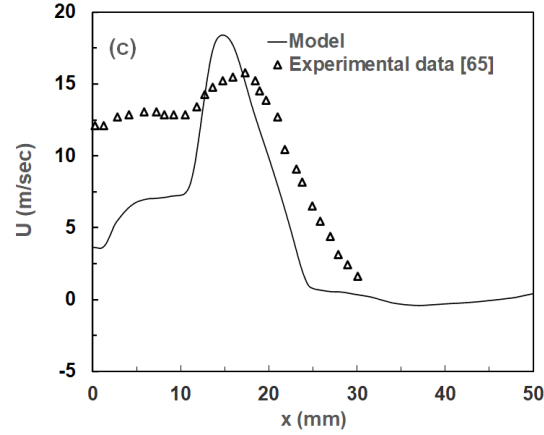


Figure 15: (a). x vs U_{mean} at 30 mm (b). x vs U_{mean} at 50 mm (c). x vs U_{mean} at 70 mm

Fig. 15(a) compares the axial mean velocity profiles from the experimental data with the data from the model at an axial distance of 30 mm with the inclusion of one inside block. The velocity can be well predicted for validation except the fact it is underpredicted in the first upstream before eventually picking up with the experimental data. The velocity first increases with the rate up to a maximum of 20 m/s, then decreases instantaneously before attaining a plateau. Hence, a very good agreement is obtained between LES results and experiments for the axial profiles of the mean axial velocity at the different axial locations. Fig. 15(b) compares the axial mean velocity profiles from the experimental data with the data from the model at an axial distance of 50 mm with the inclusion of one inside block. The velocity can be well predicted for validation except the fact it is underpredicted in the first upstream which starts at about 4 m/s before eventually picking up with the experimental data. The velocity first increases with the rate up to a maximum of 16 m/s, then decreases instantaneously before attaining a plateau. Hence, a very good agreement is obtained between LES results and experiments for the axial profiles of the mean axial velocity at the different axial locations. Fig. 15(c) compares the axial mean velocity profiles from the experimental data with the data from the model at an axial distance of

70 mm with the inclusion of one inside block. The velocity can be well predicted for validation except the fact it is underpredicted in the first upstream which starts at about 4 m/s and over-predicted after that up to about 18 m/s before eventually picking up with the experimental data. Hence, a very good agreement is obtained between LES results and experiments for the axial profiles of the mean axial velocity at the different axial locations.

4.1.3 Results from validation by using all three blocks for fuel, pilot gases, and coflow.

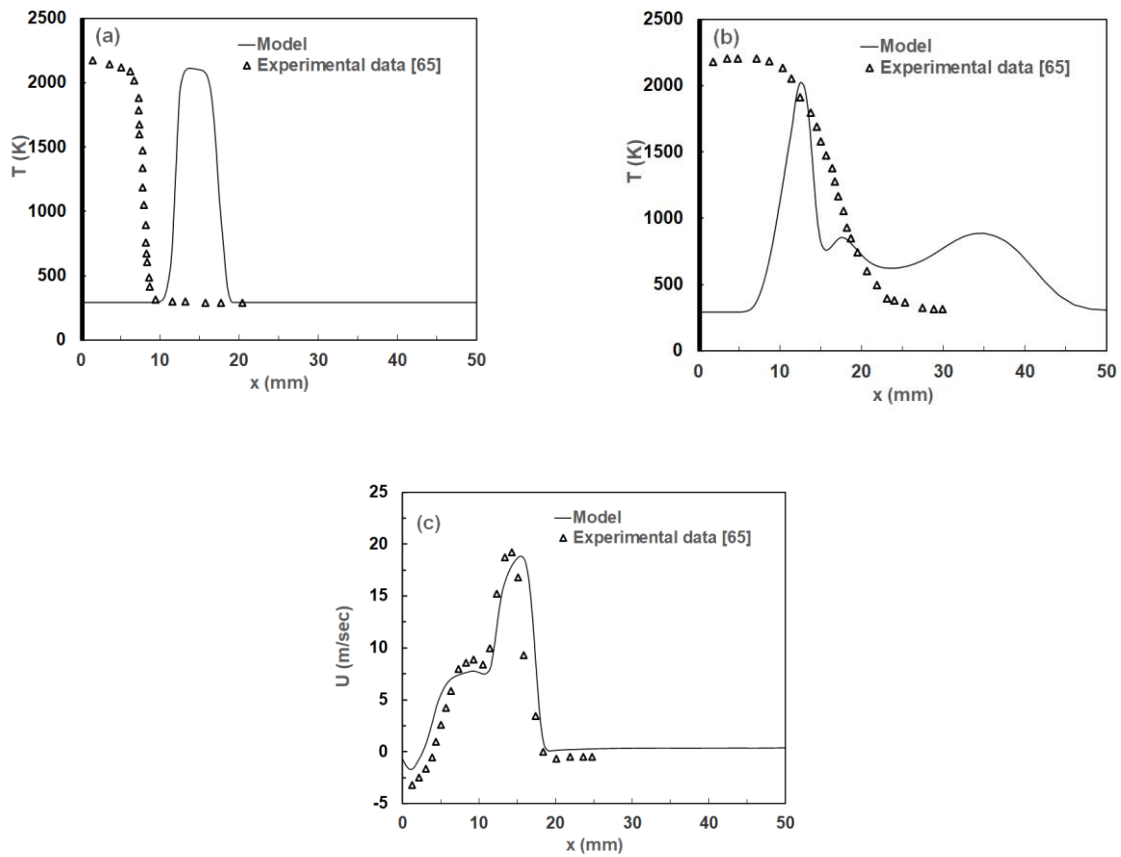


Figure 16: (a). x vs T at 10 mm (b). x vs T at 70 mm (c). x vs U_{mean} at 10 mm

Fig. 16(a) compares the axial temperature profiles from the experimental data with the data from the model at an axial distance of 10 mm with the inclusion of all three blocks. The temperature first increases with the rate up to a maximum of about 2100 K, then decreases instantaneously before becoming a plateau. Here, a very good agreement is obtained between LES results and experiments for the axial profiles of the temperatures at the different axial location except the fact that the newly generated plot from the model is shifted to the right while still following the same trajectory. Fig. 16(b) compares the axial temperature profiles from the experimental data with the data from the model at an axial distance of 70 mm with the inclusion of all three blocks. The temperature starts at about 300 K which is under-predicted and then increases with the rate up to a maximum of about 2000 K, then decreases instantaneously up to 800 K. Again, it increases up to 8500 K, then decreases to about 650 K. Again, it reaches to about 900 K before eventually becoming a plateau. Here, a very good agreement is not obtained between LES results and experiments for the axial profiles of the temperatures at the different axial locations. Fig. 16(c) compares the axial mean velocity profiles from the experimental data with the data from the model at an axial distance of 10 mm with the inclusion of all three blocks. The velocity can be well predicted for validation. The velocity first increases with the rate up to a maximum of 19 m/s, then decreases instantaneously before attaining a plateau. Hence, a very good agreement is obtained between LES results and experiments for the axial profiles of the mean axial velocity at the different axial locations.

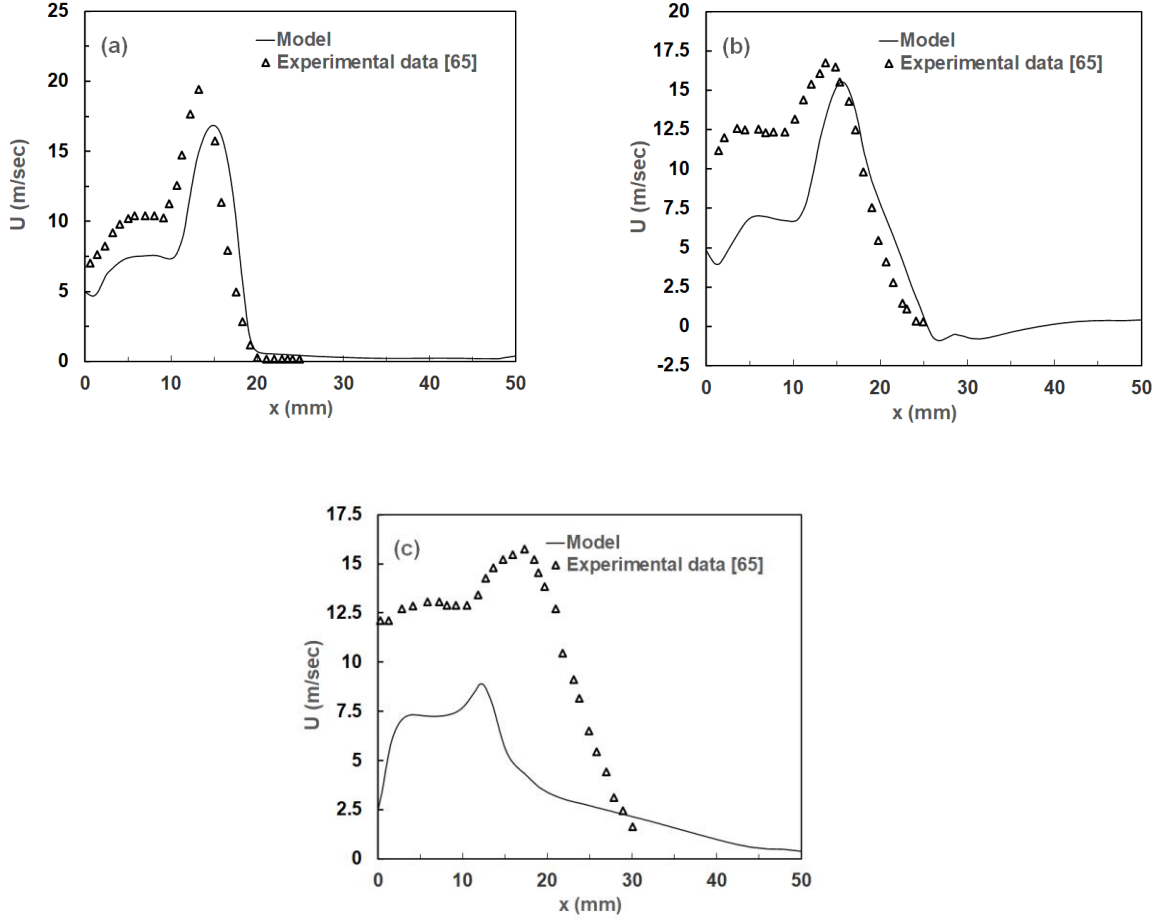


Figure 17: (a). x vs U_{mean} at 30 mm (b). x vs U_{mean} at 50 mm (c). x vs U_{mean} at 70 mm

Fig. 17(a) compares the axial mean velocity profiles from the experimental data with the data from the model at an axial distance of 30 mm with the inclusion of all three blocks. The velocity can be well predicted for validation except the fact it is underpredicted in the first upstream that begins at about 5 m/s and still under-predicted when it increases at about 17 m/s before eventually picking up with the experimental data and attaining a plateau afterwards. Hence, a very good agreement is obtained between LES results and experiments for the axial profiles of the mean axial velocity at the different axial locations. Fig. 17(b) compares the axial mean velocity profiles from the experimental data with the data from the model at an axial distance of

50 mm with the inclusion of all three blocks. The velocity can be well predicted for validation except the fact it is underpredicted in the first upstream which starts at about 5 m/s before eventually picking up with the experimental data. The velocity first increases with the rate up to a maximum of 16 m/s, then decreases instantaneously before attaining a plateau. Hence, a very good agreement is obtained between LES results and experiments for the axial profiles of the mean axial velocity at the different axial locations. Fig. 17(c) compares the axial mean velocity profiles from the experimental data with the data from the model at an axial distance of 70 mm with the inclusion of all three blocks. The velocity can be predicted for validation except the fact it is underpredicted in the first upstream which starts at about 3 m/s and again under-predicted after that up to about 9 m/s before flattening out. However, it never picks up with the experimental data. Hence, a very good agreement is not obtained between LES results and experiments for the axial profiles of the mean axial velocity at the different axial locations.

4.2 Results based on shape of burner

The parametric studies were conducted based on the shape of the burner. The shapes were uniform, convergent, and divergent. Figure. 30(a), (b), (c) depict the shape of burners.

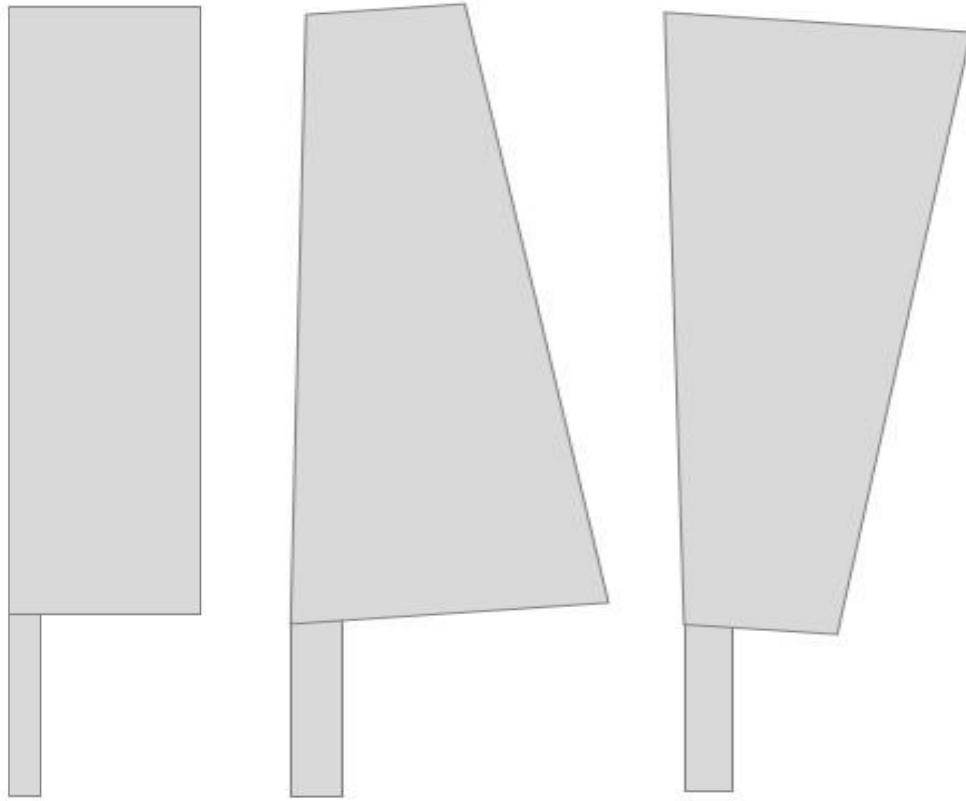
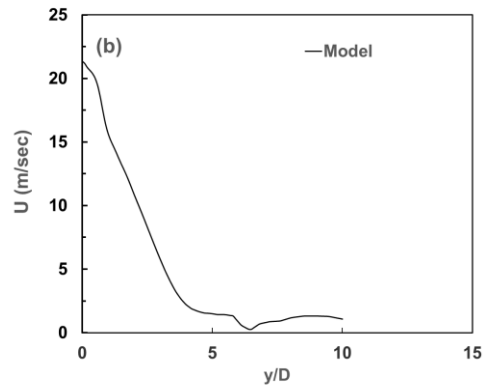
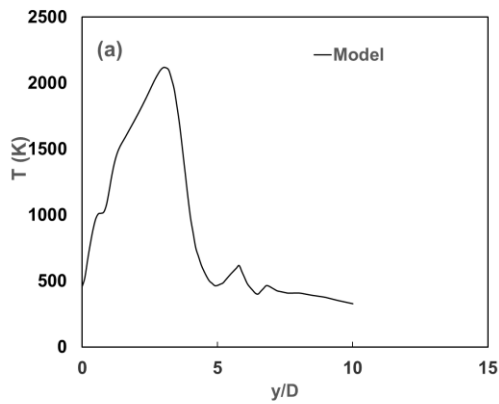


Figure 18: (a). Uniform burner (b) Convergent burner (c) Divergent burner

4.2.1 Parametric study of uniform burner at fuel velocity 20 m/s and $y/D = 30$ for temperature, velocity, and mixture fraction



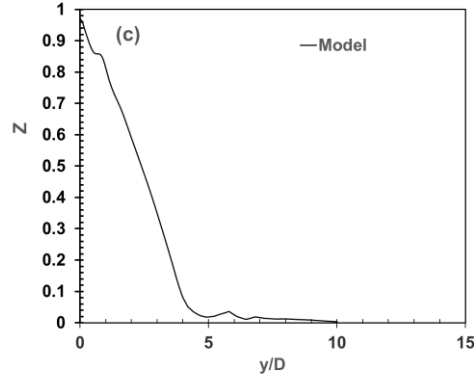


Figure 19: (a). Temperature profile (b). Velocity profile (c). Mixture fraction profile of uniform burner

Fig. 19(a) depicts the plot for the parametric study of uniform nozzles at fuel velocity 20 m/s and $y/D = 30$ for temperature. Temperature plot is sensitive to the geometry of the burner. Hence, the geometry of the burner has a limited impact. The temperature profile starts at around 500 K and rises to a value of around 2200 K before decreasing to a value of about 500 K and finally coming to about 300 K after some moderate fluctuations. Fig. 19(b) depicts the plot for the parametric study of uniform nozzles at fuel velocity 20 m/s and $x/D = 30$ for velocity. Velocity plot is sensitive to the geometry of the burner. Hence, the geometry of the burner has a limited impact. The velocity profile starts at around 21 m/s and finally reaches a value of about 1 m/s after some moderate fluctuations. Fig. 19(c) depicts the plot for the parametric study of uniform nozzles at fuel velocity 20 m/s and $y/D = 30$ for mixture fraction. Mixture fraction plot is sensitive to the geometry of the burner. Hence, the geometry of the burner has a limited impact. The mixture fraction profile starts at around 0.9 and finally dies to zero after some moderate fluctuations.

4.2.2 Parametric study of convergent burner at fuel velocity 20 m/s and $y/D = 30$ for (a) temperature, (b) velocity, and (c) mixture fraction

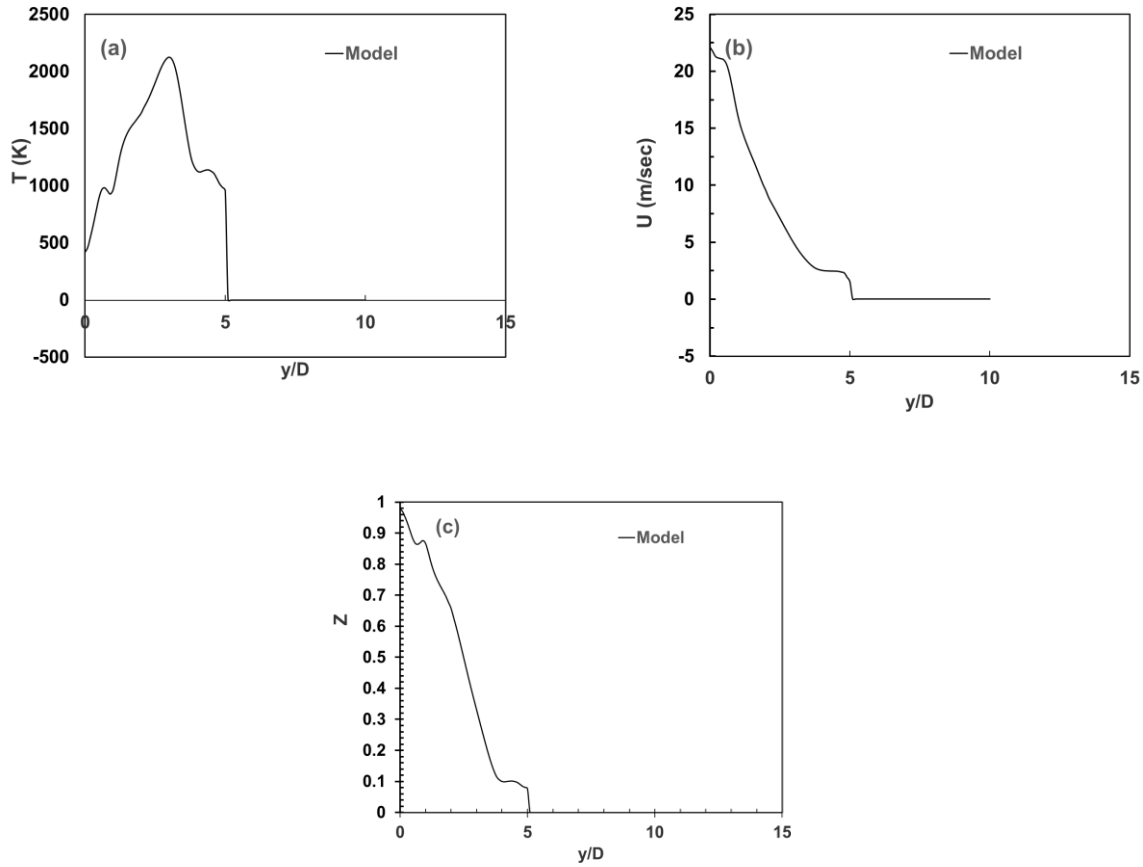
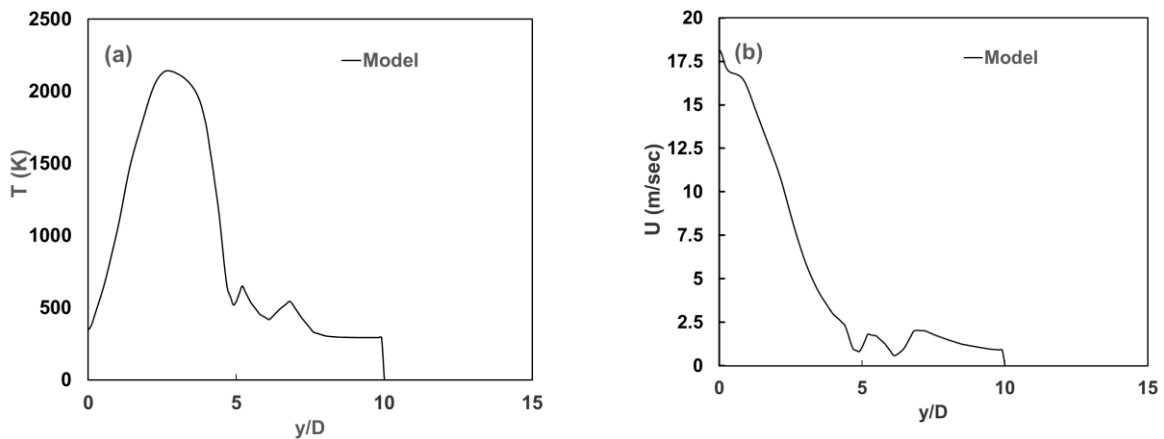


Figure 20: (a). Temperature profile (b). Velocity profile (c). Mixture fraction profile of convergent burner

Fig. 20(a) depicts the plot for the parametric study of convergent nozzles at fuel velocity 20 m/s and $y/D = 30$ for temperature. The temperature plot is sensitive to the geometry of the burner. The temperature profile starts at around 500 k and rises to a value of around 2200 K after having a dip during the rise at 1000 K. Then it decreases to a value of about 1200 K and finally dipping to zero afterwards immediately. But in the case of a uniform nozzle, the value was still fluctuating in the downstream section. Hence, the geometry of the burner has a limited impact.

Fig. 20(b) depicts the plot for the parametric study of convergent nozzles at fuel velocity 20 m/s and $y/D = 30$ for velocity. Velocity plot is sensitive to the geometry of the burner. Hence, the geometry of the burner has a limited impact. The velocity profile starts at around 21 m/s and finally reaches a value of about 0 m/s after some moderate fluctuations. But in the case of a uniform nozzle, the value was still fluctuating in the downstream section instead of directly dipping down to zero. Hence, the geometry of the burner has a limited impact. Fig. 20(c) depicts the plot for the parametric study of convergent nozzles at fuel velocity 20 m/s and $y/D = 30$ for mixture fraction. Mixture fraction plot is sensitive to the geometry of the burner. Hence, the geometry of the burner has a limited impact. The mixture fraction profile starts at around 0.9 and finally dies to zero after some moderate fluctuations with not much of a difference compared to the uniform nozzle except the fact that there is a small plateau before eventually hitting the zero.

4.2.3 Parametric study of divergent nozzle at fuel velocity 20 m/s and $y/D = 30$ for (a) temperature, (b) velocity, and (c) mixture fraction



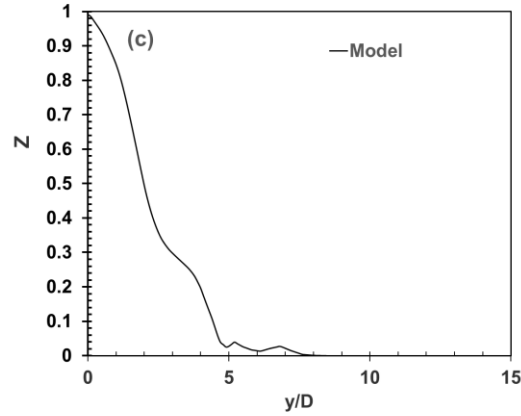


Figure 21: (a). Temperature profile (b). Velocity profile (c). Mixture fraction profile of divergent burner

Fig. 21(a) depicts the plot for the parametric study of divergent nozzles at fuel velocity 20 m/s and $y/D = 30$ for temperature. The temperature plot is sensitive to the geometry of the burner. The temperature profile starts at around 500 k and rises to a value of around 2200 K without any rises in the middle stream. Then it decreases with some fluctuations. But in the case of convergent nozzles, the profile decreases to a value of about 600 K and finally dips to zero afterwards immediately. And in the case of a uniform nozzle, the value was still fluctuating in the downstream section. Hence, the geometry of the burner has a limited impact in the downstream with just a minimal impact in the upstream. Fig. 21(b) depicts the plot for the parametric study of divergent nozzles at fuel velocity 20 m/s and $y/D = 30$ for velocity. Velocity plot is sensitive to the geometry of the burner. Hence, the geometry of the burner has a limited impact. The velocity profile starts at around 18 m/s and finally reaches a value of about 0 m/s after some moderate fluctuations. But in the case of a uniform nozzle, the value was still fluctuating in the downstream section instead of directly dipping down to zero. And in the case of a convergent nozzle, the velocity profile started at about 21 m/s. Hence, the geometry of the

burner has a limited impact. Fig. 21(c) depicts the plot for the parametric study of divergent nozzles at fuel velocity 20 m/s and $y/D = 30$ for mixture fraction. Mixture fraction plot is sensitive to the geometry of the burner. Hence, the geometry of the burner has a limited impact. The mixture fraction profile starts at around 1. and finally dies to zero after some moderate fluctuations. Whereas in the case of convergent nozzles, it starts at 0.9 and finally dies to zero after some moderate fluctuations with not much of a difference compared to the uniform nozzle except the fact that there is a small plateau before eventually hitting the zero.

To summarize, we can see the plots together as shown below:

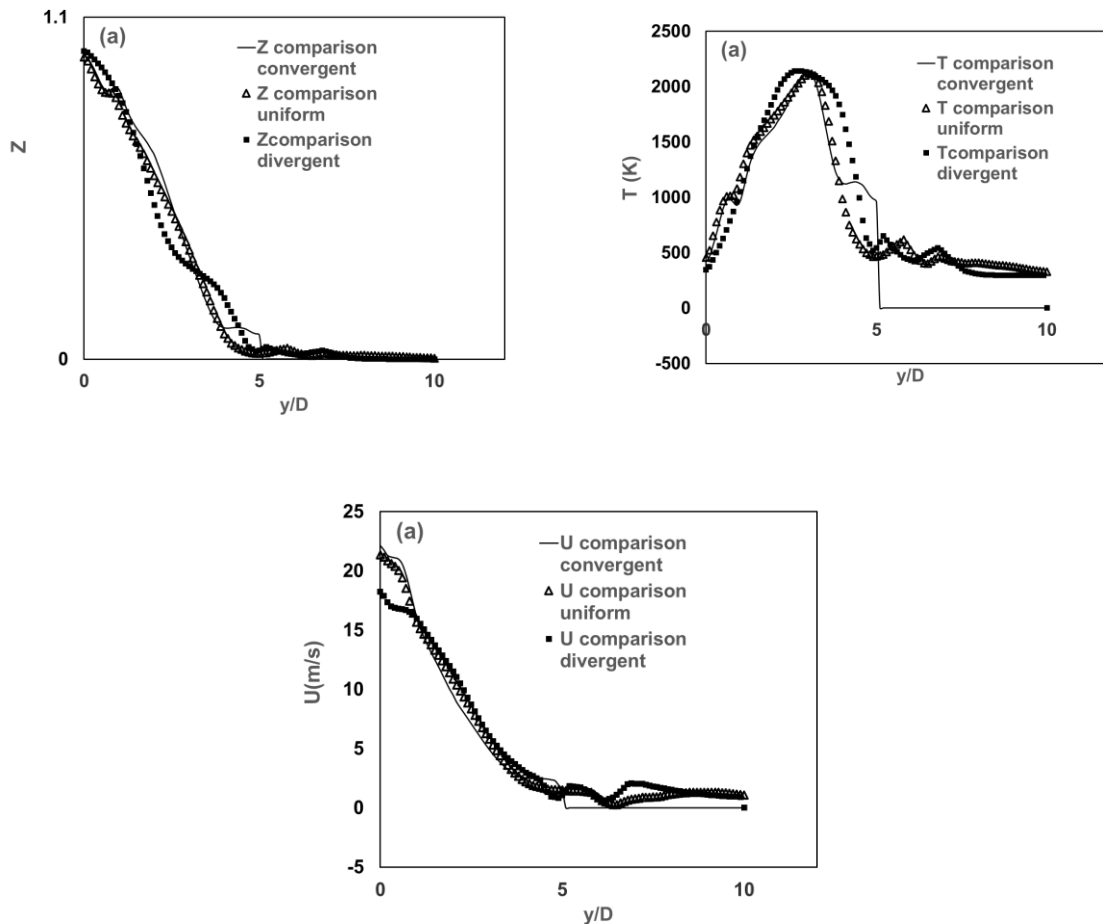
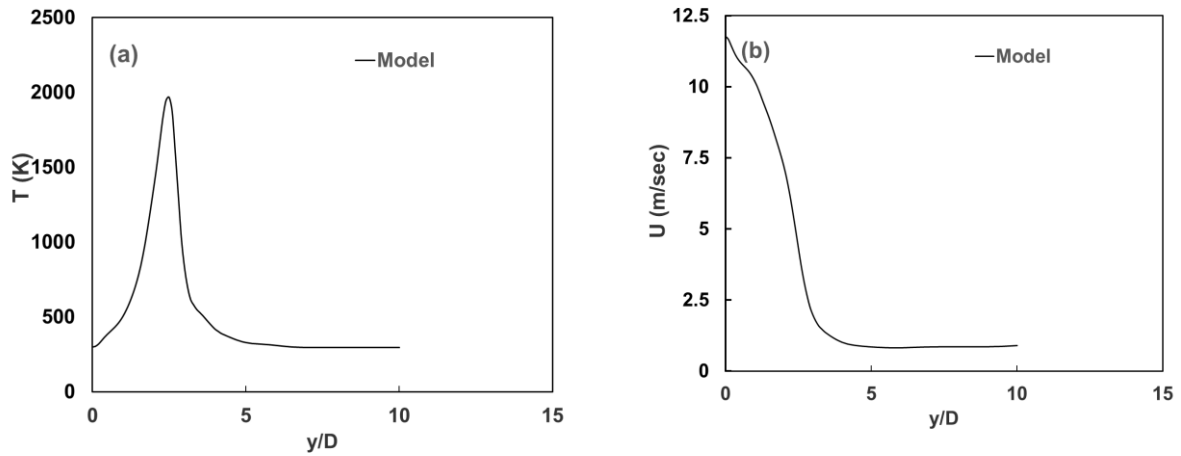


Fig 21 (d): Summary of comparison of results based on burner shape

4.3 Results based on different inlet fuel velocities at different locations

The study was conducted for inlet velocity 15 m/s and $y/D = 15$, inlet velocity 20 m/s and $y/D = 15$, inlet velocity 15 m/s and $y/D = 30$, inlet velocity 20 m/s and $y/D = 30$, inlet velocity 15 m/s and $y/D = 45$, inlet velocity 20 m/s and $y/D = 45$.

4.3.1 Parametric study of inlet fuel velocity 15 m/s and $y/D = 15$ for temperature, velocity, and mixture fraction



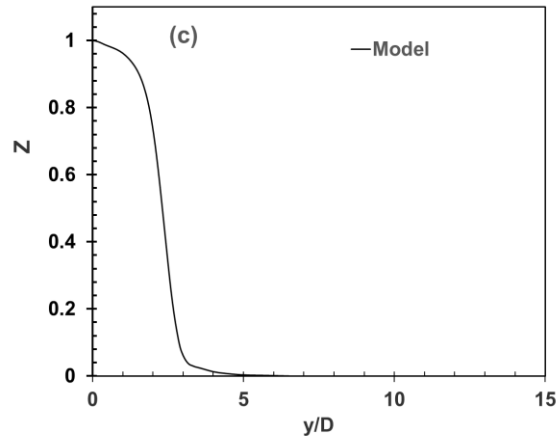


Figure 22: (a) Temperature vs $y/D = 15$ at inlet velocity = 15 m/s, (b) Velocity vs $y/D = 15$ at inlet velocity = 15 m/s, (c) Mixture fraction vs $y/D = 15$ at inlet velocity = 15 m/s

Fig. 22(a) depicts the temperature plot for the parametric study at inlet fuel velocity 15 m/s and $y/D = 15$. The temperature profile starts at around 300 K and rises to a value of around 2000 K without any fluctuations in the middle stream during the rise. Then it decreases without any fluctuations during the fall and finally takes a flat shape after around 300K. Fig. 22(b) depicts the plot for the parametric study at inlet fuel velocity 15 m/s and $y/D = 15$ for velocity. The velocity profile starts decaying at around 12 m/s and finally reaches a value of about 1 m/s before taking a flat shape without any fluctuations. Fig. 22(c) depicts the plot for the parametric study at inlet fuel velocity 15 m/s and $y/D = 15$ for mixture fraction. The mixture fraction profile starts at around 1. and finally dies to zero without fluctuations.

4.3.2 Parametric study of inlet fuel velocity 20 m/s and $y/D = 15$ for temperature, velocity, and mixture fraction

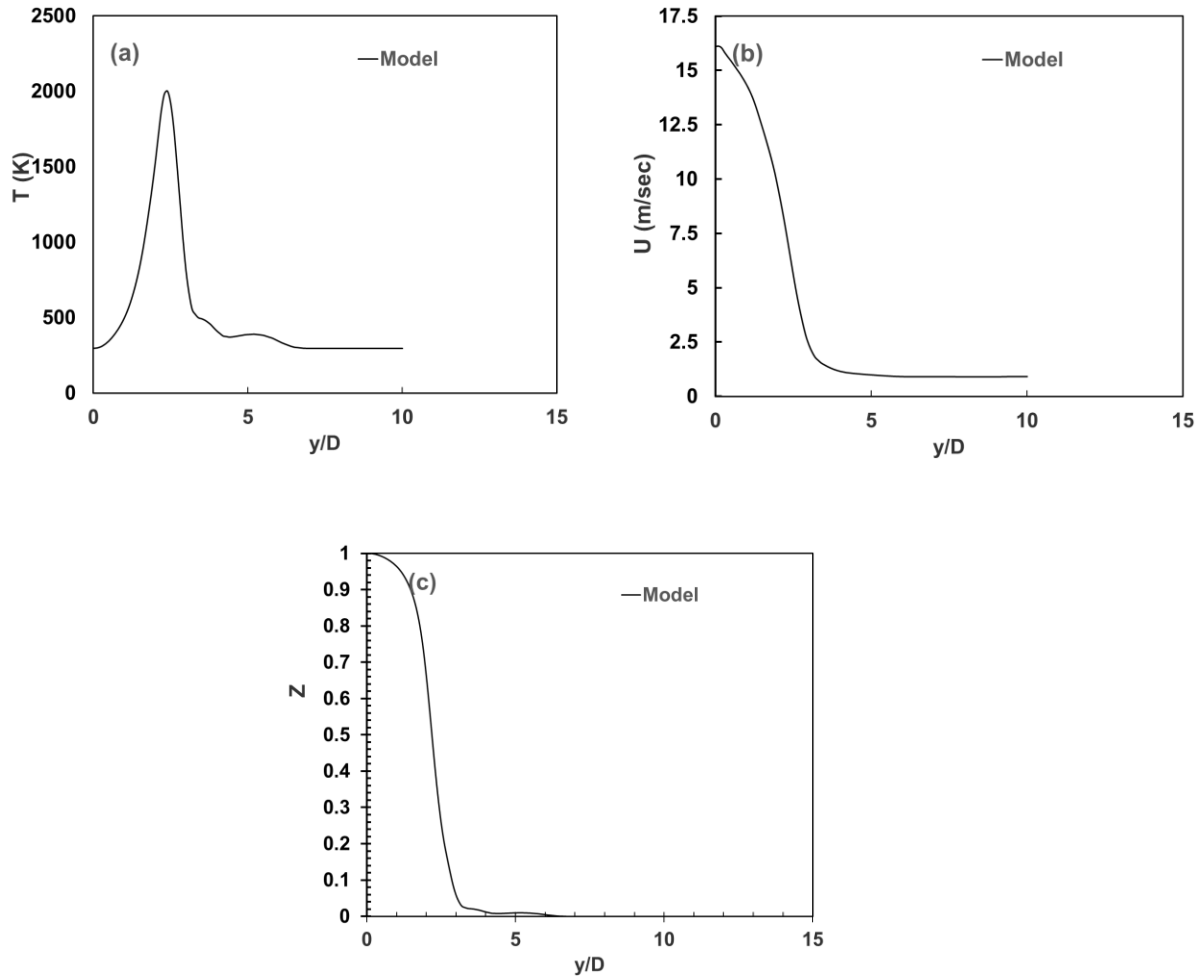
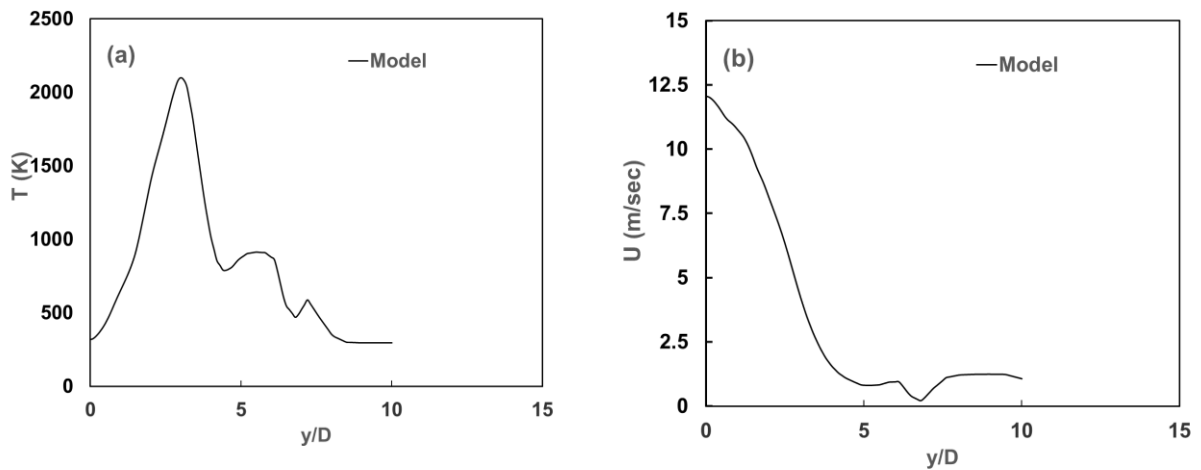


Figure 23: (a). Temperature vs $y/D = 15$ at inlet velocity = 20 m/s, (b) Velocity vs $y/D = 15$ at inlet velocity = 20 m/s, (c) Mixture fraction vs $y/D = 15$ at inlet velocity = 20 m/s

Fig. 23(a) depicts the temperature plot for the parametric study at inlet fuel velocity 20 m/s and $y/D = 15$. The temperature profile starts at around 300 K and rises to a value of around 2000 K without any fluctuations in the middle stream during the rise. Then it decreases without any fluctuations during the fall and finally takes a flat shape after around 300 K after moderate fluctuations. So, at the location $y/D = 15$, there is minimal difference despite the increase in

velocity from 15 m/s to 20 m/s besides few fluctuations downstream during decay. Fig. 23(b) depicts the velocity plot for the parametric study at inlet fuel velocity 20 m/s and $y/D = 15$. The velocity profile starts decaying at around 16 m/s and finally reaches a value of about 1 m/s before taking a flat shape without any fluctuations. Hence, the major difference is the starting point of velocity which in previous case was a little bit lower because of the low inlet velocity of course. Fig. 23(c) depicts the plot for the parametric study at inlet fuel velocity 20 m/s and $y/D = 15$ for mixture fraction. The mixture fraction profile starts at around 1 and finally dies to zero without fluctuations. Hence, there is no significant difference in the mixture fraction plot at the same location i.e., $y/D = 15$ with the increase in velocity to 20 m/s from 15 m/s.

4.3.3 Parametric study of inlet fuel velocity 15 m/s and $y/D = 30$ for temperature, velocity, and mixture fraction



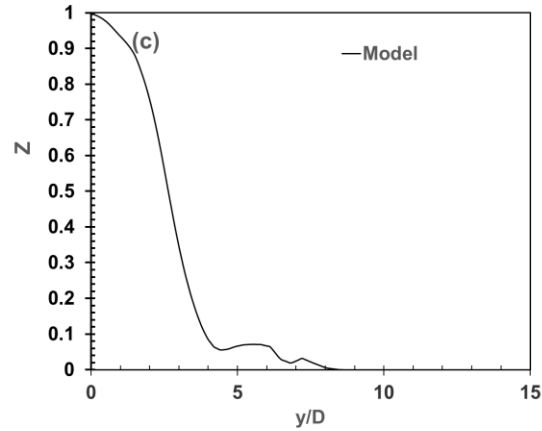


Figure 24: (a). Temperature vs $y/D = 30$ at inlet velocity = 15 m/s, (b) Velocity vs $y/D = 30$ at inlet velocity = 15 m/s, (c) Mixture fraction vs $y/D = 30$ at inlet velocity = 15 m/s

Fig. 24(a) depicts the temperature plot for the parametric study at inlet fuel velocity 15 m/s and $y/D = 30$. The temperature profile starts at around 300 K and rises to a value of around 2100 K without any fluctuations in the middle stream during the rise. Then it decreases with fluctuations during the fall at around 800 K before rising to about 900 K. Again, it decreases with fluctuations during the fall at around 400 K before rising to about 500 K and finally takes a flat shape after rising around 600 K. So, at the inlet velocity of 15 m/s, there is minimal difference despite the noticeable fluctuations downstream during decay. Fig. 24(b) depicts the velocity plot for the parametric study at inlet fuel velocity 15 m/s and $y/D = 30$. The velocity profile starts decaying at around 12 m/s and finally reaches a value of about 1 m/s before taking a flat shape with one major dip in between. Hence, the major difference is the starting point of velocity which in previous case was 11 m/s and is 12 m/s in the new location i.e., $y/D = 30$ with the same inlet velocity of 15 m/s. Fig. 24(c) depicts the plot for the parametric study at inlet fuel velocity 20 m/s and $y/D = 15$ for mixture fraction. The mixture fraction profile starts at around 1 and finally dies to zero with fluctuations. Hence, the only difference in the mixture fraction plot

at the same location i.e., $y/D = 15$ with the increase in velocity to 20 m/s from 15 m/s is the minimal fluctuations in the downstream section.

4.3.4 Parametric study of inlet fuel velocity 20 m/s and $y/D = 30$ for temperature, velocity, and mixture fraction

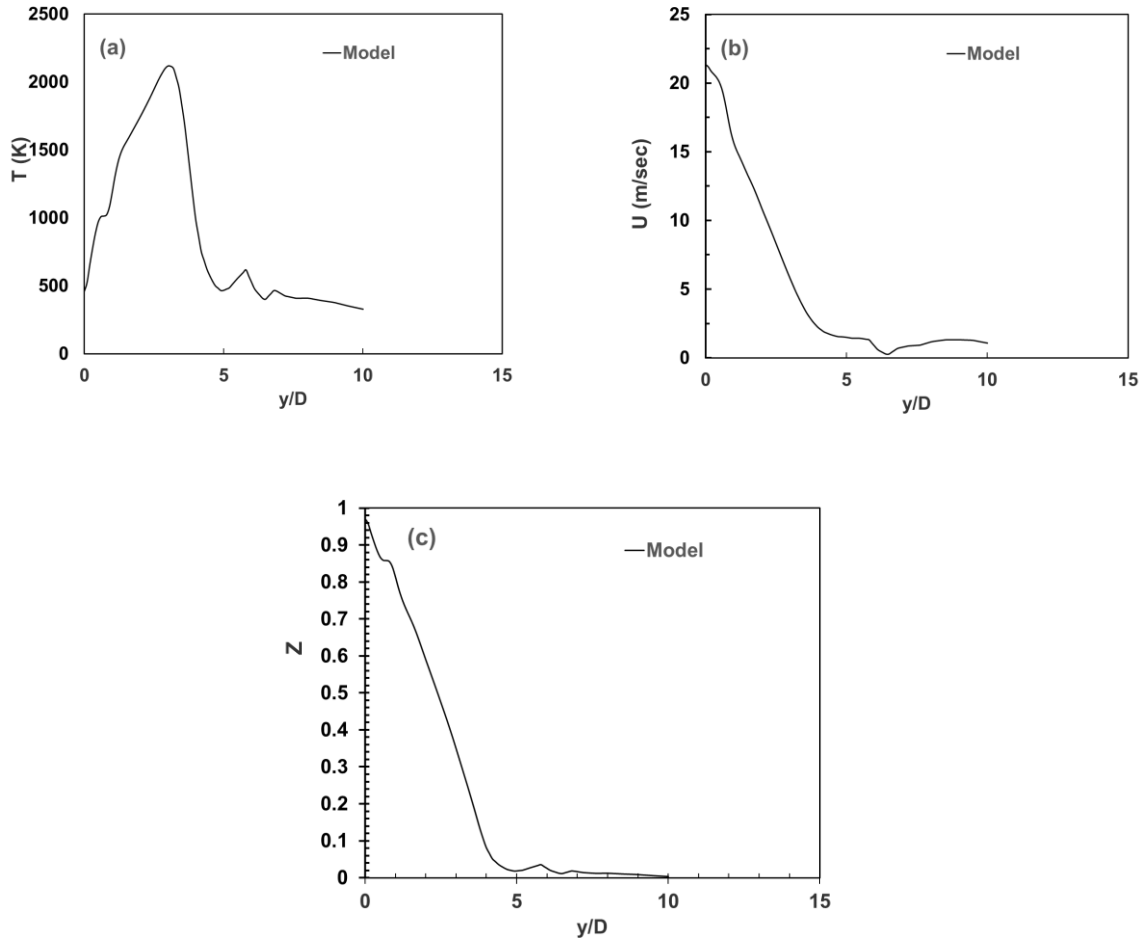


Figure 25: (a). Temperature vs $y/D = 30$ at inlet velocity = 20 m/s, (b) Velocity vs $y/D = 30$ at inlet velocity = 20 m/s, (c) Mixture fraction vs $y/D = 30$ at inlet velocity = 20 m/s

Fig. 25(a) depicts the temperature plot for the parametric study at inlet fuel velocity 20 m/s and $y/D = 30$. The temperature profile starts at around 500 K and rises to a value of around 2100 K with minimal fluctuations in the middle stream during the rise to about 2100 K. Then it decreases

without any fluctuations during the fall until about 500 K. Finally, we see some fluctuations at around 600 K and at around 400 K before finally settling down. So, at the inlet velocity of 20 m/s, there is minimal difference despite the noticeable gap during the rise and the fall. Fig. 25(b) depicts the velocity plot for the parametric study at inlet fuel velocity 20 m/s and $y/D = 30$. The velocity profile starts decaying at around 21 m/s and finally reaches a value of about 1 m/s before taking a flat shape with one major dip in between. Hence, the major differences are the starting point of velocity which in previous case was 16 m/s and is 21 m/s in the new location i.e., $y/D = 30$ with the same inlet velocity of 20 m/s and the small fluctuation with the dip in the downstream. Fig. 25(c) depicts the plot for the parametric study at inlet fuel velocity 20 m/s and $y/D = 30$ for mixture fraction. The mixture fraction profile starts at around 0.9 and finally dies to zero with minimal fluctuations. Hence, the only difference in the mixture fraction plot at the location i.e., $y/D = 15$ and $y/D = 30$ with the same velocity of 20 m/s is the minimal fluctuations in the downstream section and the starting point was 1 in the previous case compared to 0.9 in this case.

4.3.5 Parametric study of inlet fuel velocity 15 m/s and $y/D = 45$ for temperature, velocity, and mixture fraction

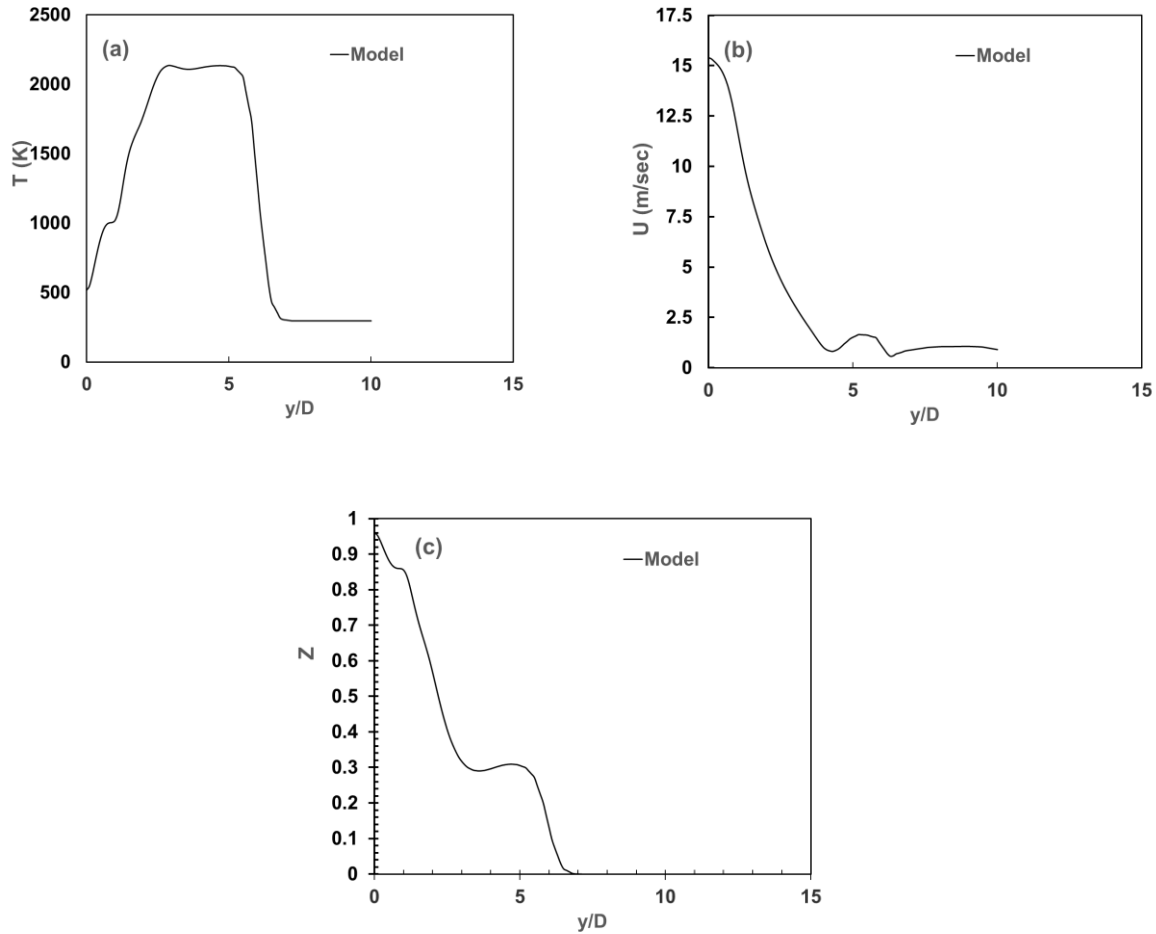


Figure 26: (a). Temperature vs $y/D = 45$ at inlet velocity = 15 m/s, (b). Velocity vs $y/D = 45$ at inlet velocity = 15 m/s, (c). Mixture fraction vs $y/D = 45$ at inlet velocity = 15 m/s

Fig. 26(a) depicts the temperature plot for the parametric study at inlet fuel velocity 15 m/s and $y/D = 45$. The temperature profile starts at around 500 K and rises to a value of around 2100 K with minimal fluctuations in the middle stream and plateauing at about 2100 K for a short time. Then it decreases without any fluctuations during the fall until flattening at about 400 K. Fig. 26(b) depicts the velocity plot for the parametric study at inlet fuel velocity 15 m/s and $y/D = 45$.

The velocity profile starts decaying at around 15 m/s and finally reaches a value of about 1 m/s before taking a flat shape with two major dips in between. Fig. 26(c) depicts the plot for the parametric study at inlet fuel velocity 15 m/s and $y/D = 45$ for mixture fraction. The mixture fraction profile starts at around 0.9 and plateaus at around 0.4 and again decreases to about zero.

4.3.6 Parametric study of inlet fuel velocity 20 m/s and $y/D = 45$ for temperature, velocity, and mixture fraction

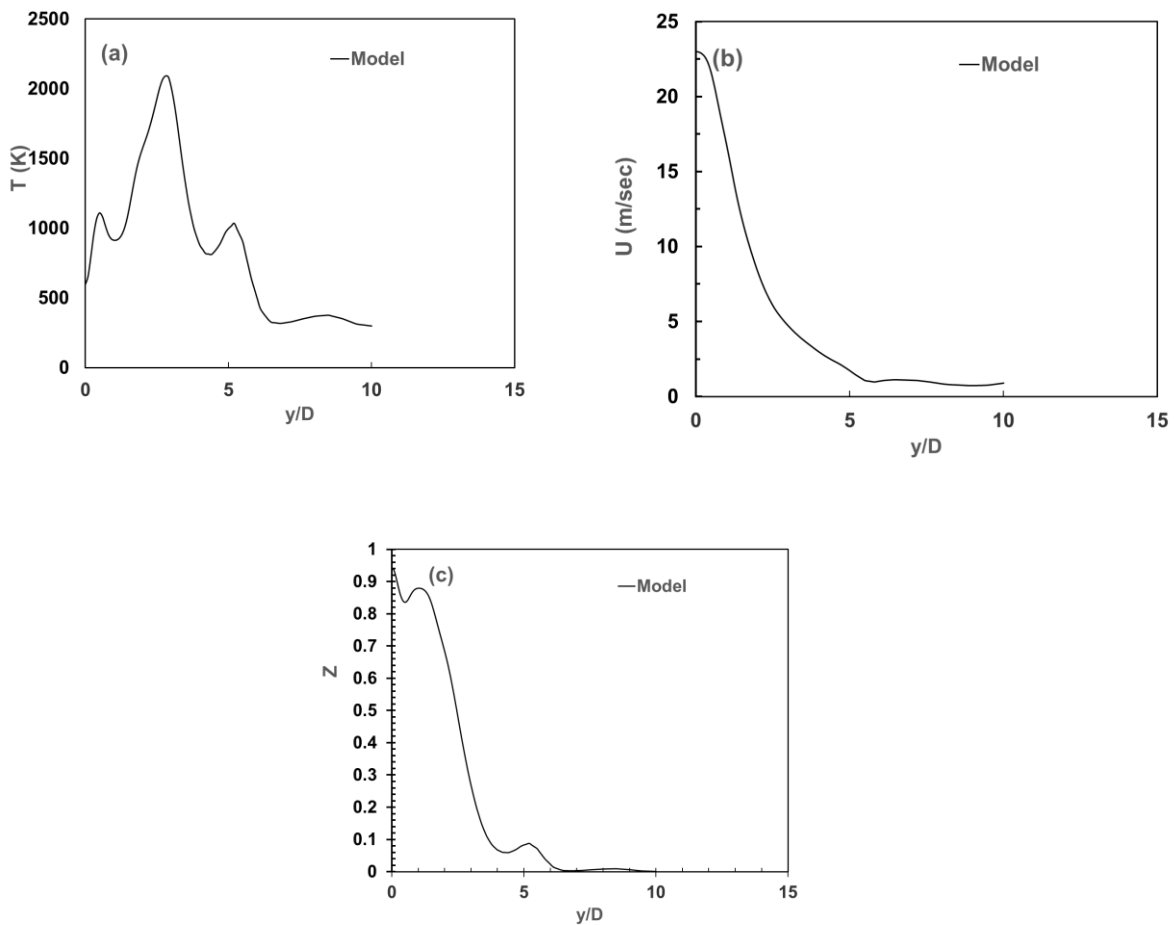


Figure 27: (a). Temperature vs $y/D = 45$ at inlet velocity = 20 m/s, (b). Velocity vs $y/D = 45$ at inlet velocity = 20 m/s, (c). Mixture fraction vs $y/D = 45$ at inlet velocity = 20 m/s

Fig. 27(a) depicts the temperature plot for the parametric study at inlet fuel velocity 20 m/s and

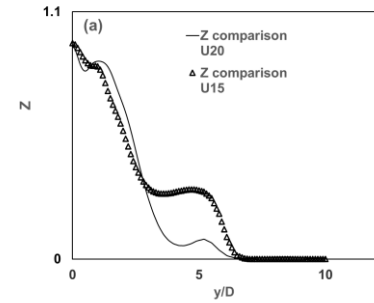
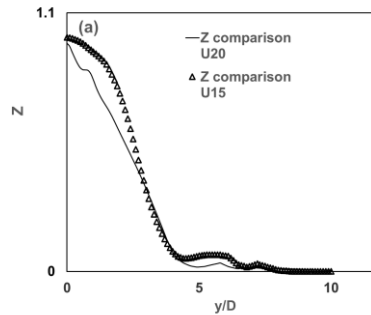
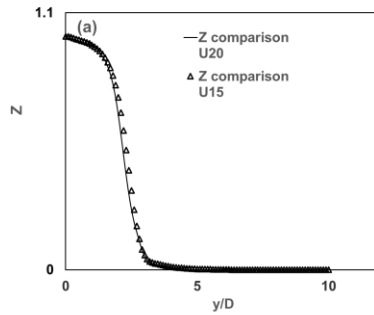
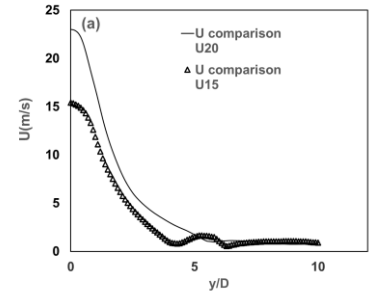
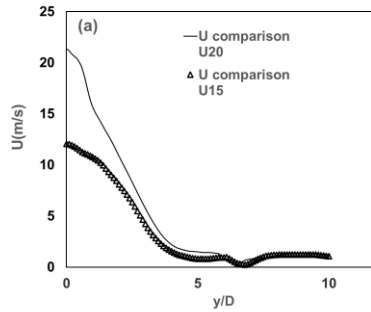
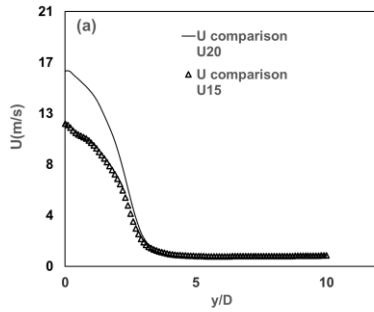
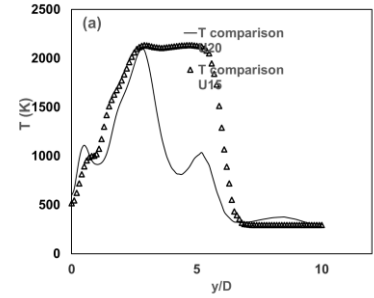
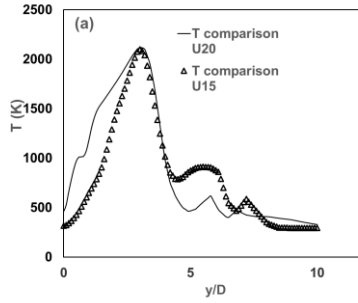
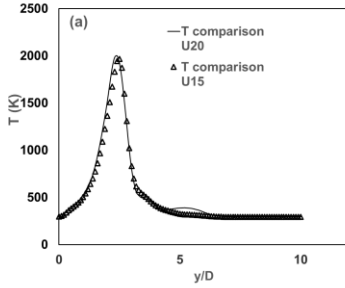
$y/D = 45$. Here, the temperature profile starts at about 600 K and rises to about 1100K. Then, it takes a dip to about 900 K and peaks at about 2100 K. After that, it starts decreasing from the peak up to about 800 K with the rise again at about 1000 K. Then finally it drops down to plateau at around 300 K. Whereas, when the velocity was 15 m/s (as in the previous case), the temperature profile starts at around 500 k and rises to a value of around 2100 K with minimal fluctuations in the middle stream and plateauing at about 2100 K for a short time. Then it decreases without any fluctuations during the fall until flattening at about 400 K. Fig. 27(b) depicts the velocity plot for the parametric study at inlet fuel velocity 20 m/s and $y/D = 45$. The velocity profile starts decaying at around 23 m/s and finally reaches a value of about 1 m/s before taking a flat shape with one major dip in between. Whereas previously, the velocity profile starts decaying at around 15 m/s and finally reaches a value of about 1 m/s before taking a flat shape with two major dips in between. Fig. 27(c) depicts the plot for the parametric study at inlet fuel velocity 20 m/s and $y/D = 45$ for mixture fraction. Here, the mixture fraction profile starts at around 0.9, takes a dip at around 0.7 and again rises and falls to about 0.1. There is one more fluctuation before eventually reaching zero. Whereas previously, the mixture fraction profile plateaus at around 0.4 and again decreases to about zero. The mixture fraction profile starts at around 0.9 and plateaus at around 0.4 and again decreases to about zero.

Summary of plot comparison for parametric study based on inlet fuel velocity

@ $y/D = 15$

@ $y/D = 30$

@ $y/D = 45$



Here, we can see the good or not so good agreement in the plots from the summary mentioned and can draw the conclusions accordingly for temperature, velocity, and mixture fraction.

4.4 Results based on heat flux wall boundary condition @ $U = 20$ m/s

4.4.1 Parametric study of heat flux at uniform gradient = 10 at $y/D = 15$ for temperature, velocity, and mixture fraction at inlet velocity 20 m/s

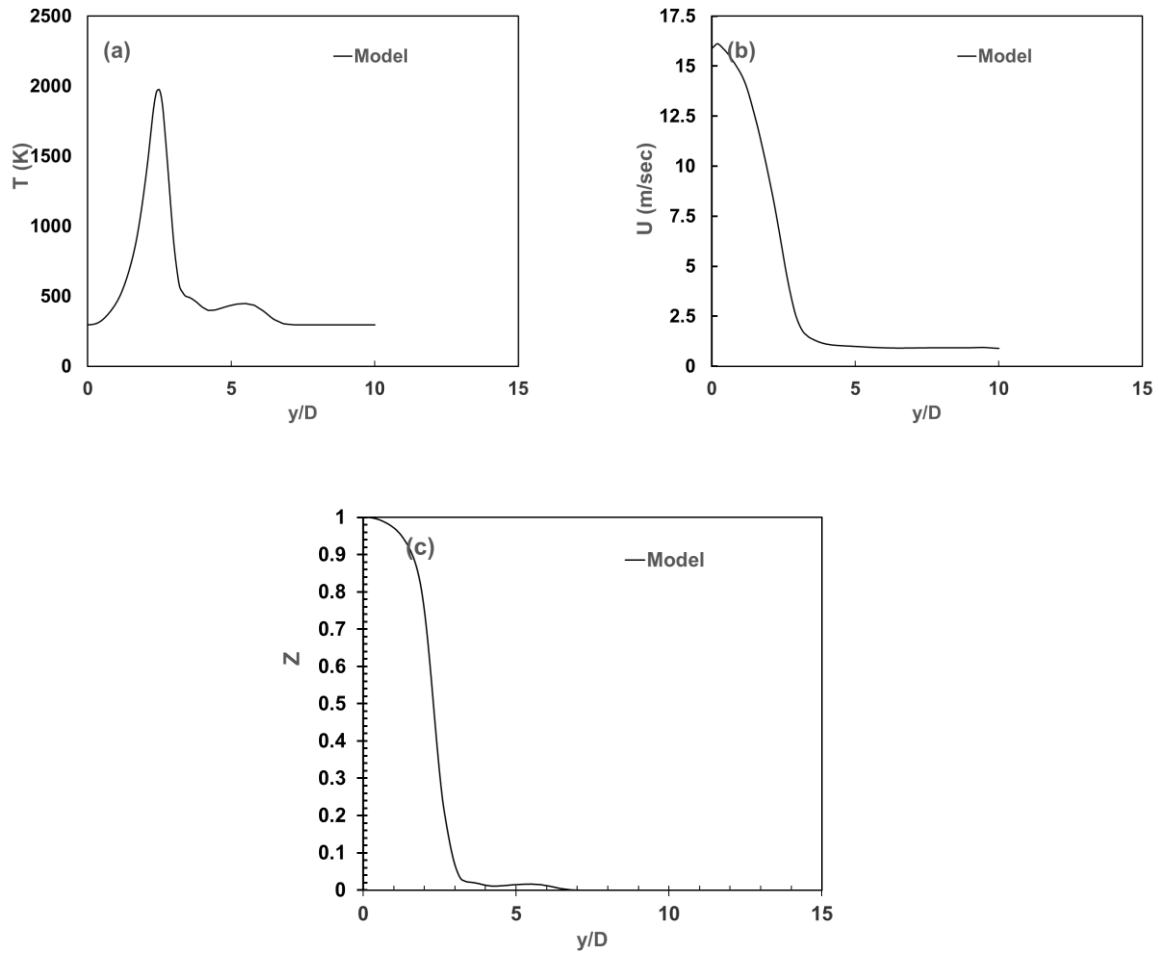


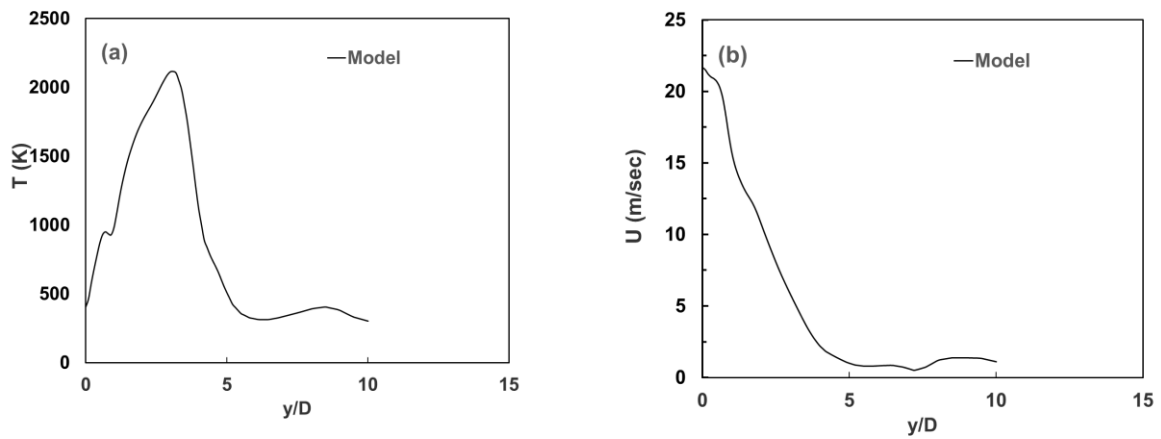
Figure 28: (a). Temperature vs $y/D = 15$ at inlet velocity = 20 m/s for heat flux = 10, (b).

Velocity vs $y/D = 15$ at inlet velocity = 20 m/s for heat flux = 10, (c). Mixture fraction vs y/D
= 15 at inlet velocity = 20 m/s for heat flux = 10

Fig. 28(a) depicts the temperature plot for the parametric study at inlet fuel velocity 20 m/s and $y/D = 15$ for heat flux of 10 per unit area. Here, the temperature profile starts at about 300 K and

risers to about 2000K. Then, it takes a straight dip to about 450 K and plateaus to about 300 K after one fluctuation. Fig. 28(b) depicts the velocity plot for the parametric study at inlet fuel velocity 20 m/s and $y/D = 15$ for heat flux of 10 per unit area. The velocity profile starts decaying at around 16 m/s and finally plateaus at a value of about 1 m/s. Fig. 28(c) depicts the mixture fraction plot for the parametric study at inlet fuel velocity 20 m/s and $y/D = 15$ for heat flux of 10 per unit area. Here, the mixture fraction profile starts at around 1 and decays.

4.4.2 Parametric study of gradient energy at heat flux = 10 at $y/D = 30$ for temperature, velocity, and mixture fraction at inlet velocity 20 m/s



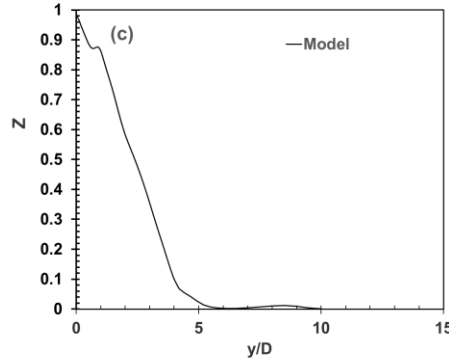


Figure 29: (a). Temperature vs $y/D = 30$ at inlet velocity = 20 m/s for heat flux = 10, (b).

Velocity vs $y/D = 30$ at inlet velocity = 20 m/s for heat flux = 10, (c) Mixture fraction vs $y/D = 30$ at inlet velocity = 20 m/s for heat flux = 10

Fig. 29(a) depicts the temperature plot for the parametric study at inlet fuel velocity 20 m/s and $y/D = 30$ for heat flux of 10 per unit area. Here, the temperature profile starts at about 500 K and rises to about 2100K. Then, it takes a straight dip to about 450 K and plateaus after one fluctuation. Fig. 29(b) depicts the velocity plot for the parametric study at inlet fuel velocity 20 m/s and $y/D = 30$ for heat flux of 10 per unit area. The velocity profile starts decaying at around 21 m/s and finally plateaus at a value of about 1 m/s after one fluctuation. Fig. 29(c) depicts the mixture fraction plot for the parametric study at inlet fuel velocity 20 m/s and $y/D = 30$ for heat flux of 10 per unit area. Here, the mixture fraction profile starts below 1 and decays.

4.4.3 Parametric study of heat flux at uniform gradient = 50 at $y/D = 15$ for temperature, velocity, and mixture fraction at inlet velocity 20 m/s

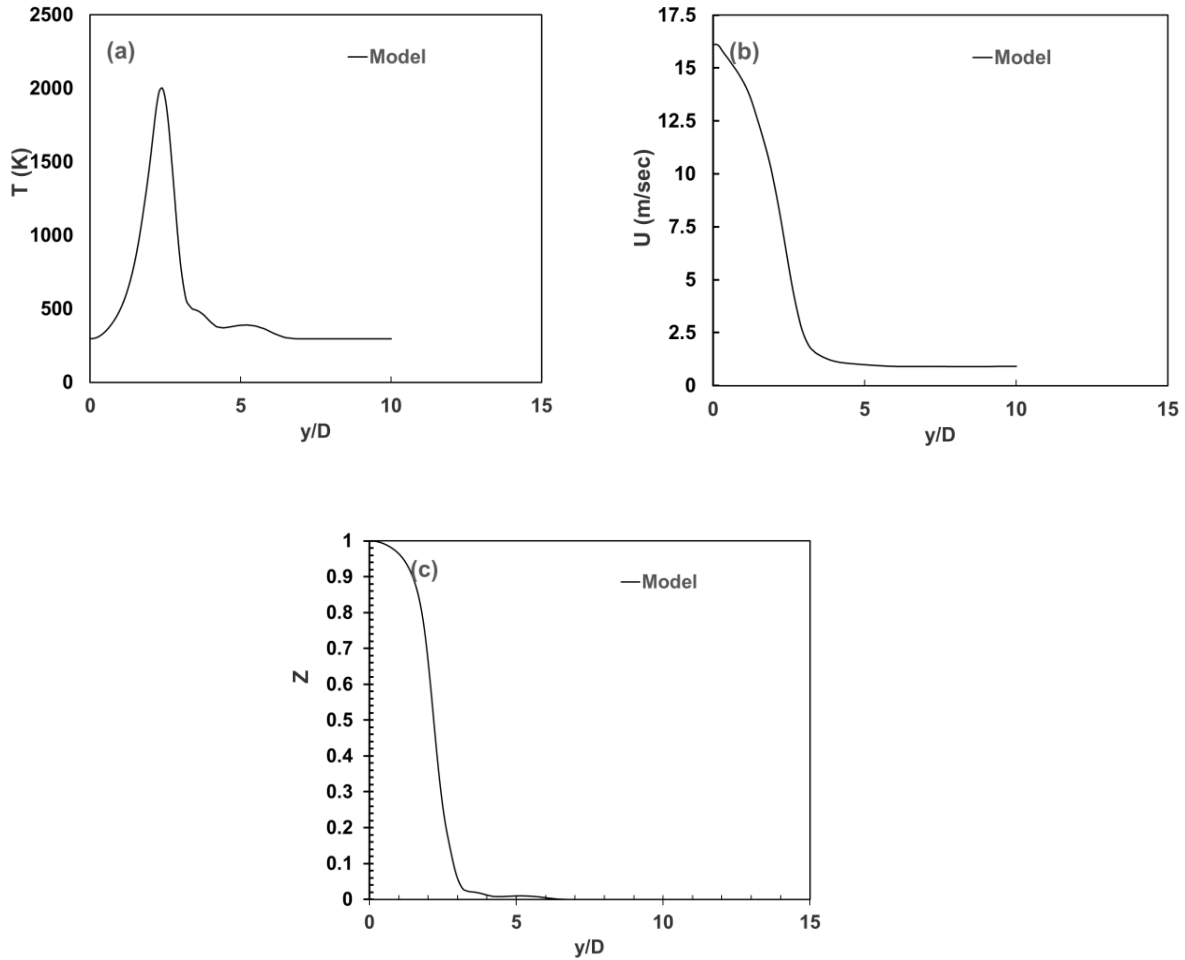


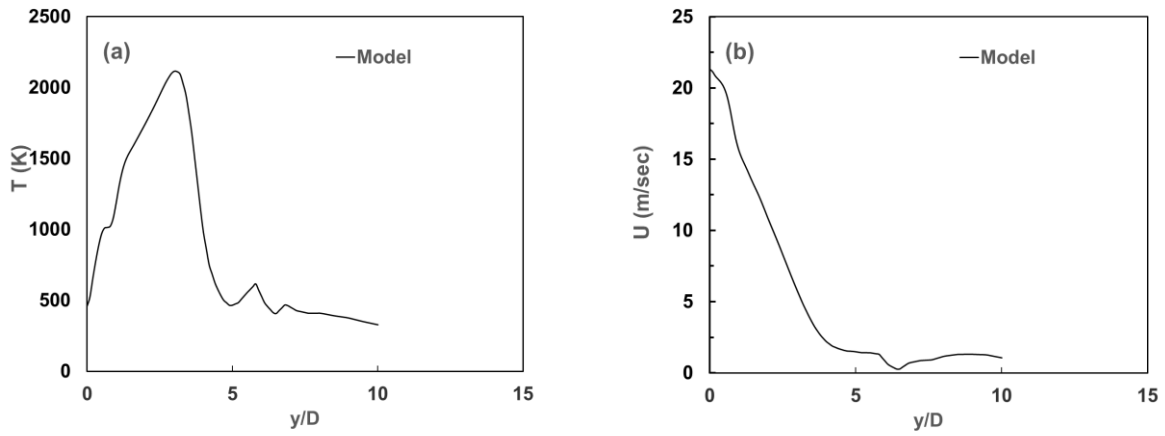
Figure 30: (a). Temperature vs $y/D = 15$ at inlet velocity = 20 m/s for heat flux = 50, (b).

Velocity vs $y/D = 15$ at inlet velocity = 20 m/s for heat flux = 50, (c). Mixture fraction vs $y/D = 15$ at inlet velocity = 20 m/s for heat flux = 50

Fig. 30(a) depicts the temperature plot for the parametric study at inlet fuel velocity 20 m/s and $y/D = 15$ for heat flux of 50 per unit area. Here, the temperature profile starts at about 300 K and rises to about 2000K. Then, it takes a straight dip to about 450 K and plateaus after one fluctuation. Fig. 30(b) depicts the velocity plot for the parametric study at inlet fuel velocity 20

m/s and $y/D = 15$ for heat flux of 50 per unit area. The velocity profile starts decaying at around 16 m/s and finally plateaus at a value of about 1 m/s without any fluctuation. Fig. 30(c) depicts the mixture fraction plot for the parametric study at inlet fuel velocity 20 m/s and $y/D = 15$ for heat flux of 50 per unit area. Here, the mixture fraction profile starts at 1 and decays.

4.4.4 Parametric study of heat flux at value = 50 at $y/D = 30$ for temperature, velocity, and mixture fraction at inlet velocity 20 m/s



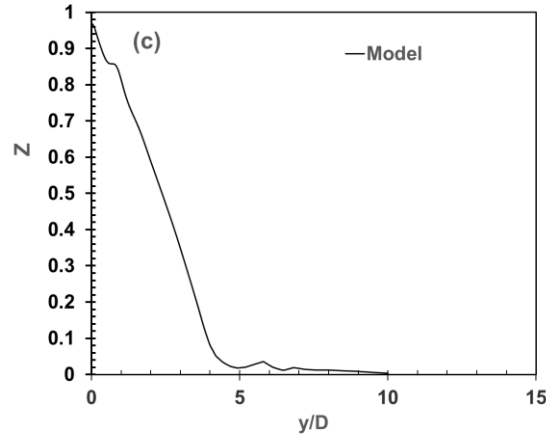


Figure 31: (a). Temperature vs $y/D = 30$ at inlet velocity = 20 m/s for heat flux = 50, Velocity vs $y/D = 30$ at inlet velocity = 20 m/s for heat flux = 50, (c). Mixture fraction vs $y/D = 30$ at inlet velocity = 20 m/s for heat flux = 50

Fig. 31(a) depicts the temperature plot for the parametric study at inlet fuel velocity 20 m/s and $y/D = 30$ for heat flux of 50 per unit area. Here, the temperature profile starts at about 500 K and rises to about 2100K. Then, it takes a straight dip to about 500 K and plateaus after two fluctuations. Fig. 31(b) depicts the velocity plot for the parametric study at inlet fuel velocity 20 m/s and $y/D = 20$ for heat flux of 50 per unit area. The velocity profile starts decaying at around 20 m/s and finally plateaus at a value of about 1 m/s with one major dip. Fig. 31(c) depicts the mixture fraction plot for the parametric study at inlet fuel velocity 20 m/s and $y/D = 30$ for heat flux of 50 per unit area. Here, the mixture fraction profile starts at below 1 and decays with few fluctuations.

4.4.5 Parametric study of heat flux at value = 500 at $y/D = 15$ for temperature, velocity, and mixture fraction at inlet velocity 20 m/s

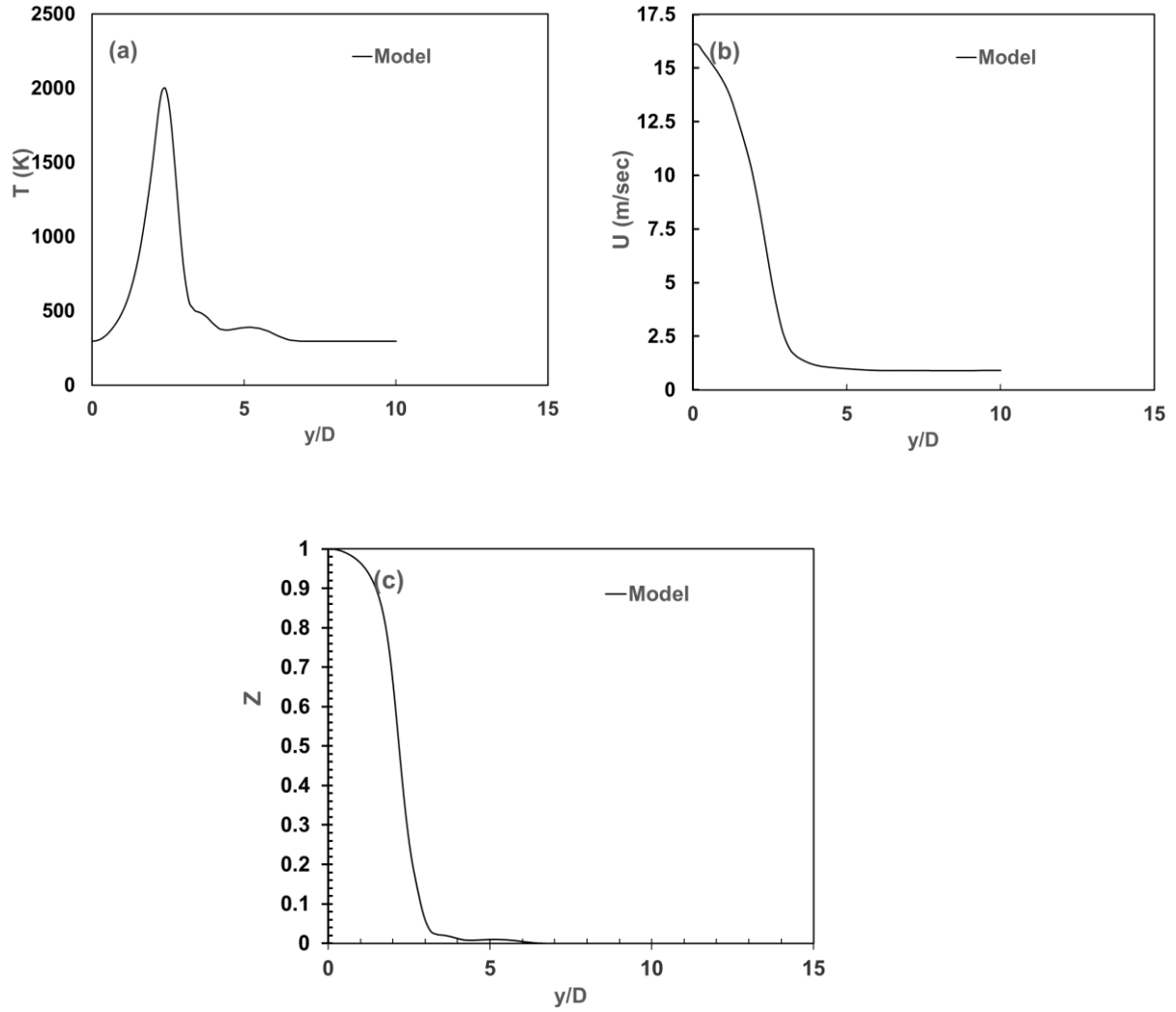


Figure 32: (a). Temperature vs $y/D = 15$ at inlet velocity = 20 m/s for heat flux = 500, (b).

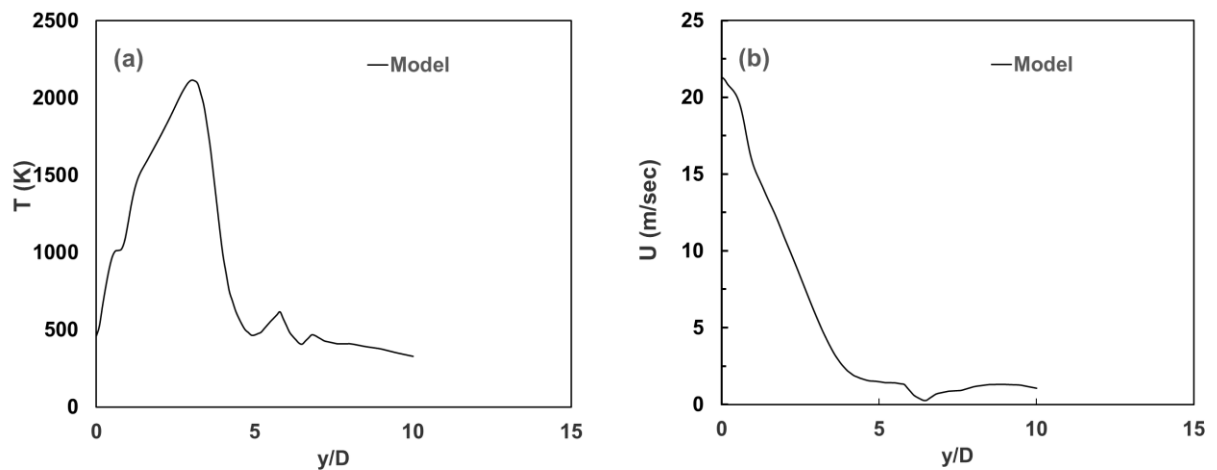
Velocity vs $y/D = 15$ at inlet velocity = 20 m/s for heat flux = 500, (c). Mixture fraction vs y/D

= 15 at inlet velocity = 20 m/s for heat flux = 500

Fig. 32(a) depicts the temperature plot for the parametric study at inlet fuel velocity 20 m/s and $y/D = 15$ for heat flux of 500 per unit area. Here, the temperature profile starts at about 300 K and rises to about 2000K. Then, it takes a straight dip to about 350 K and plateaus after two

fluctuations. Fig. 32(b) depicts the velocity plot for the parametric study at inlet fuel velocity 20 m/s and $y/D = 15$ for heat flux of 500 per unit area. The velocity profile starts decaying at around 16 m/s and finally plateaus at a value of about 1 m/s without any fluctuations. Fig. 32(c) depicts the mixture fraction plot for the parametric study at inlet fuel velocity 20 m/s and $y/D = 15$ for heat flux of 500 per unit area. Here, the mixture fraction profile starts at 1 and decays without fluctuations.

4.4.6 Parametric study of heat flux at value = 500 at $y/D = 30$ for temperature, velocity, and mixture fraction at inlet velocity 20 m/s



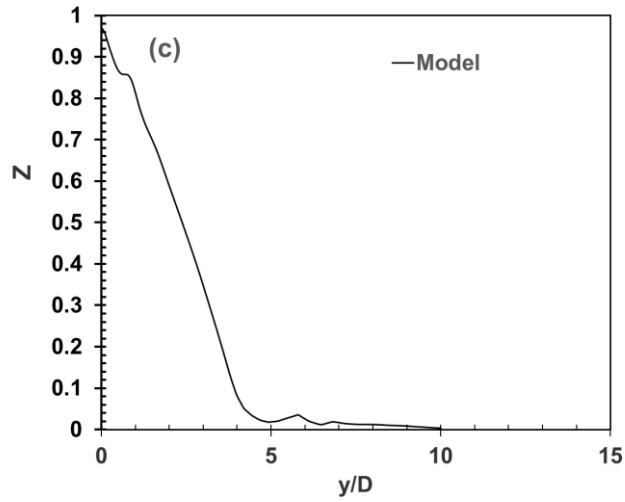


Figure 33: (a). Temperature vs $y/D = 30$ at inlet velocity = 20 m/s for heat flux = 500, (b).

Velocity vs $y/D = 30$ at inlet velocity = 20 m/s for heat flux = 500, (c). Mixture fraction vs $y/D = 30$ at inlet velocity = 20 m/s for heat flux = 500

Fig. 33(a) depicts the temperature plot for the parametric study at inlet fuel velocity 20 m/s and $y/D = 30$ for heat flux of 500 per unit area. Here, the temperature profile starts at about 500 K and rises to about 2150K. Then, it takes a straight dip to about 450 K and plateaus after two fluctuations. Fig. 33(b) depicts the velocity plot for the parametric study at inlet fuel velocity 20 m/s and $y/D = 30$ for heat flux of 500 per unit area. The velocity profile starts decaying at around 21 m/s and finally plateaus at a value of about 1 m/s with one major dip. Fig. 33(c) depicts the mixture fraction plot for the parametric study at inlet fuel velocity 20 m/s and $y/D = 30$ for heat flux of 500 per unit area. Here, the mixture fraction profile starts at below 1 and decays with minimal fluctuations.

4.4.7 Parametric study of heat flux at value = 1000 at $y/D = 15$ for temperature, velocity, and mixture fraction at inlet velocity 20 m/s

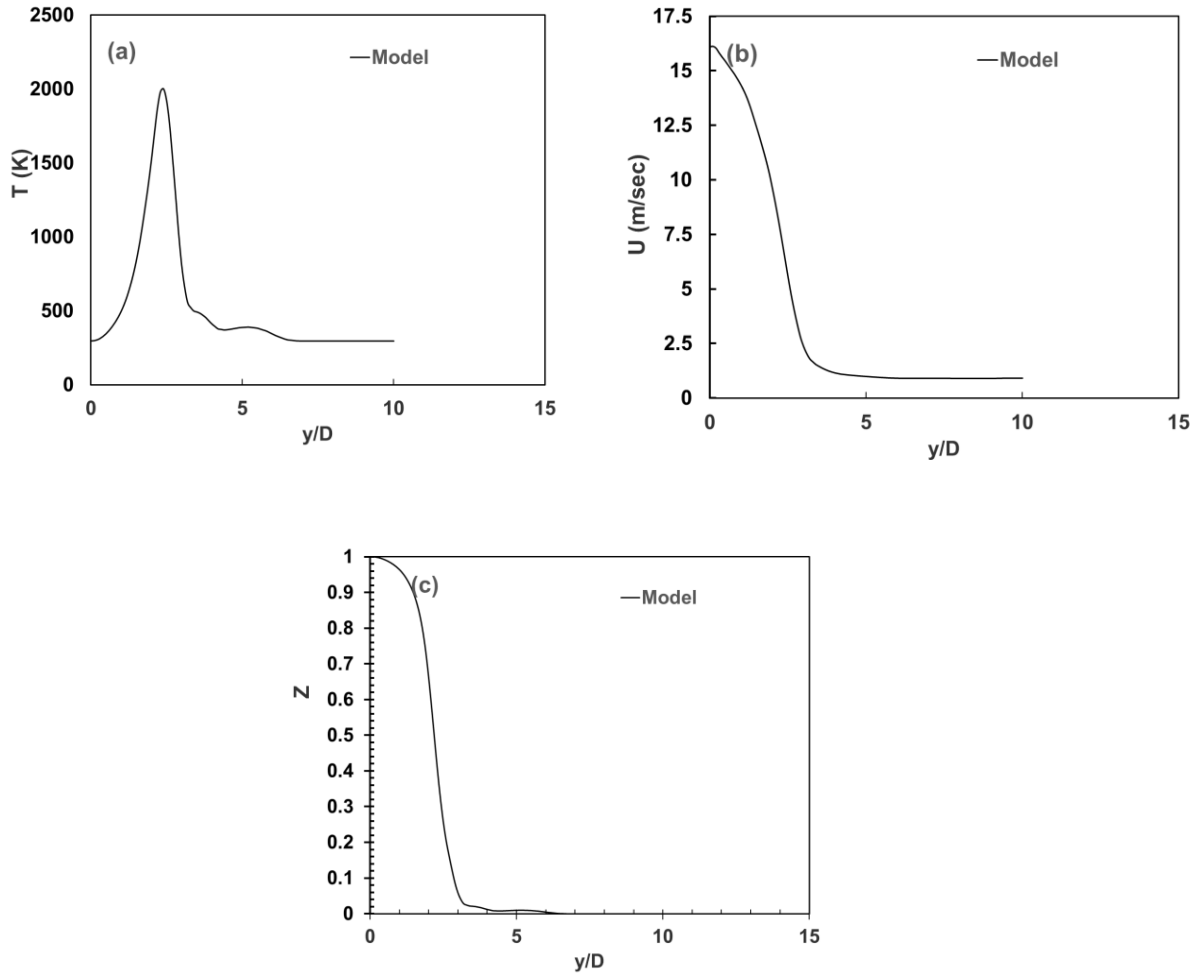


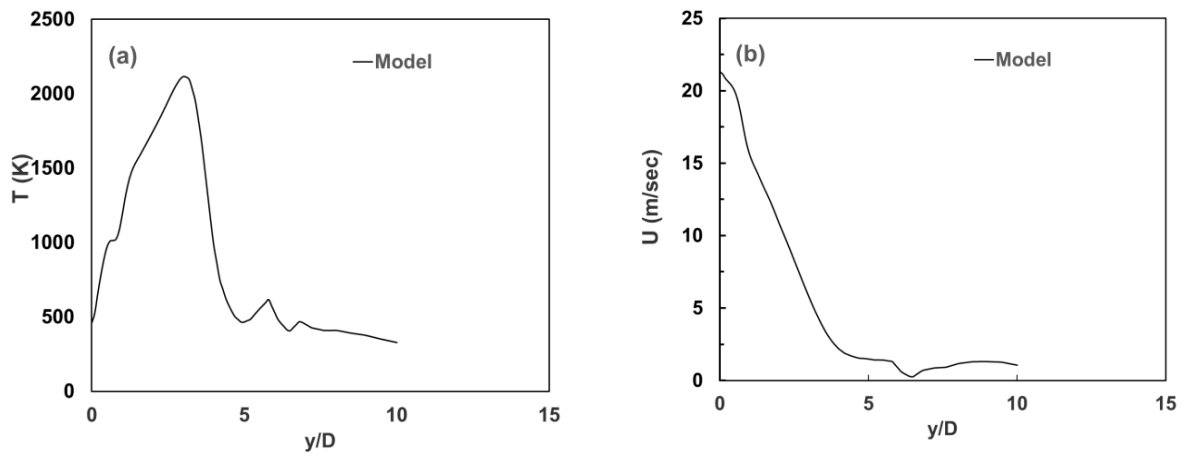
Figure 34: (a). Temperature vs $y/D = 15$ at inlet velocity = 20 m/s for heat flux = 1000, (b).

Velocity vs $y/D = 15$ at inlet velocity = 20 m/s for heat flux = 1000, (c). Mixture fraction vs $y/D = 15$ at inlet velocity = 20 m/s for heat flux = 1000

Fig. 34(a) depicts the temperature plot for the parametric study at inlet fuel velocity 20 m/s and $y/D = 15$ for heat flux of 1000 per unit area. Here, the temperature profile starts at about 300 K and rises to about 2000K. Then, it takes a straight dip to about 300 K and plateaus after two fluctuations. Fig. 34(b) depicts the velocity plot for the parametric study at inlet fuel velocity 20

m/s and $y/D = 15$ for heat flux of 1000 per unit area. The velocity profile starts decaying at around 16 m/s and finally plateaus at a value of about 1 m/s without any fluctuations. Fig. 34(c) depicts the mixture fraction plot for the parametric study at inlet fuel velocity 20 m/s and $y/D = 15$ for heat flux of 1000 per unit area. Here, the mixture fraction profile starts at 1 and decays without fluctuations.

4.4.8 Parametric study of heat flux at value = 1000 at $y/D = 30$ for temperature, velocity, and mixture fraction at inlet velocity 20 m/s



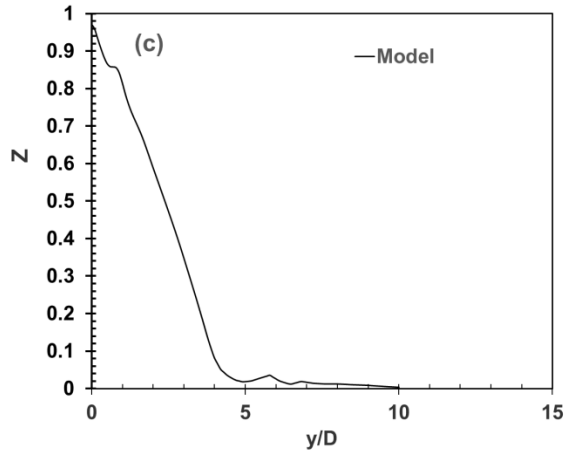


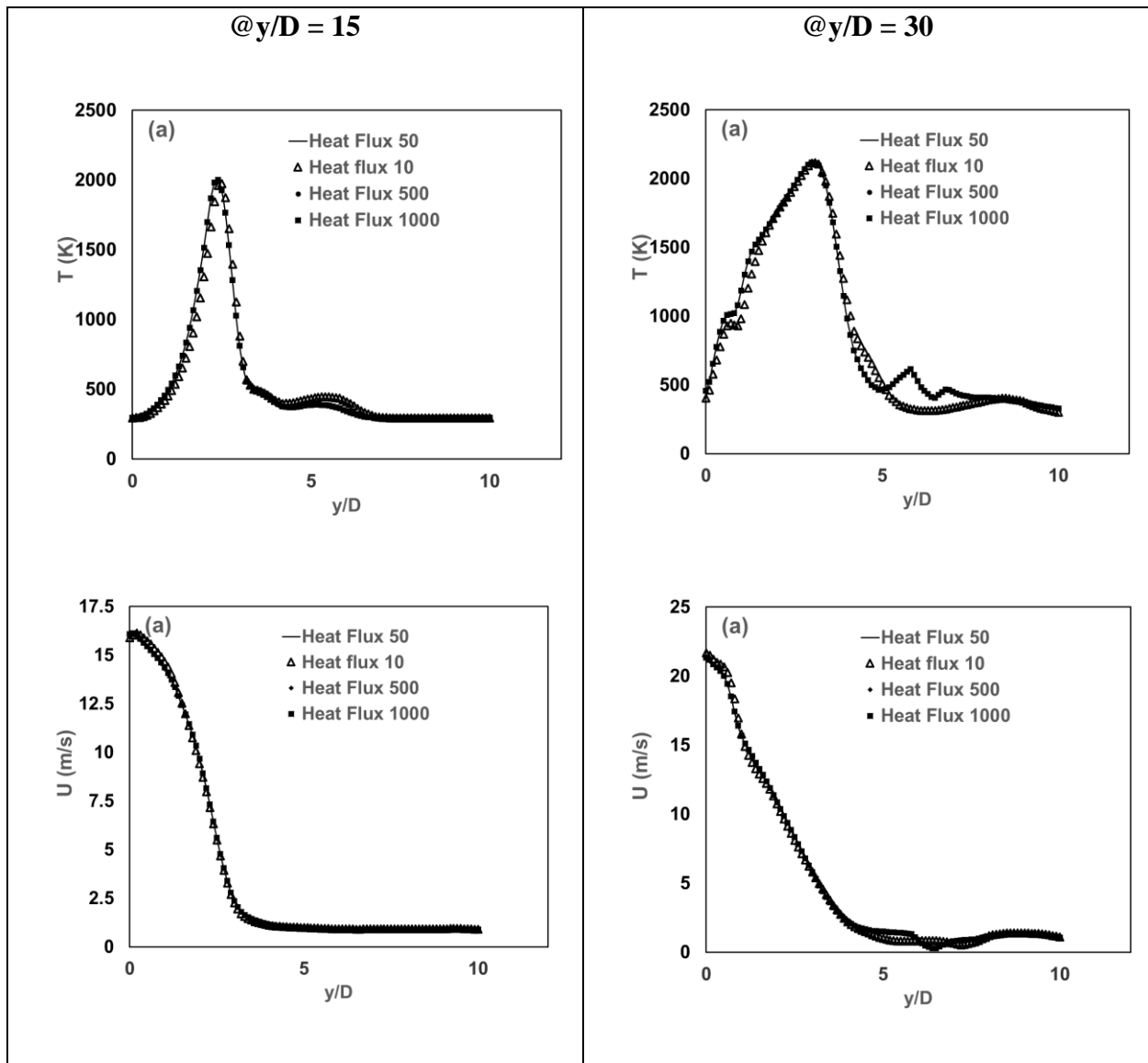
Figure 35: (a). Temperature vs $y/D = 30$ at inlet velocity = 20 m/s for heat flux = 1000, (b). Velocity vs $y/D = 30$ at inlet velocity = 20 m/s for heat flux = 1000, (c). Mixture fraction vs $y/D = 30$ at inlet velocity = 20 m/s for heat flux = 1000

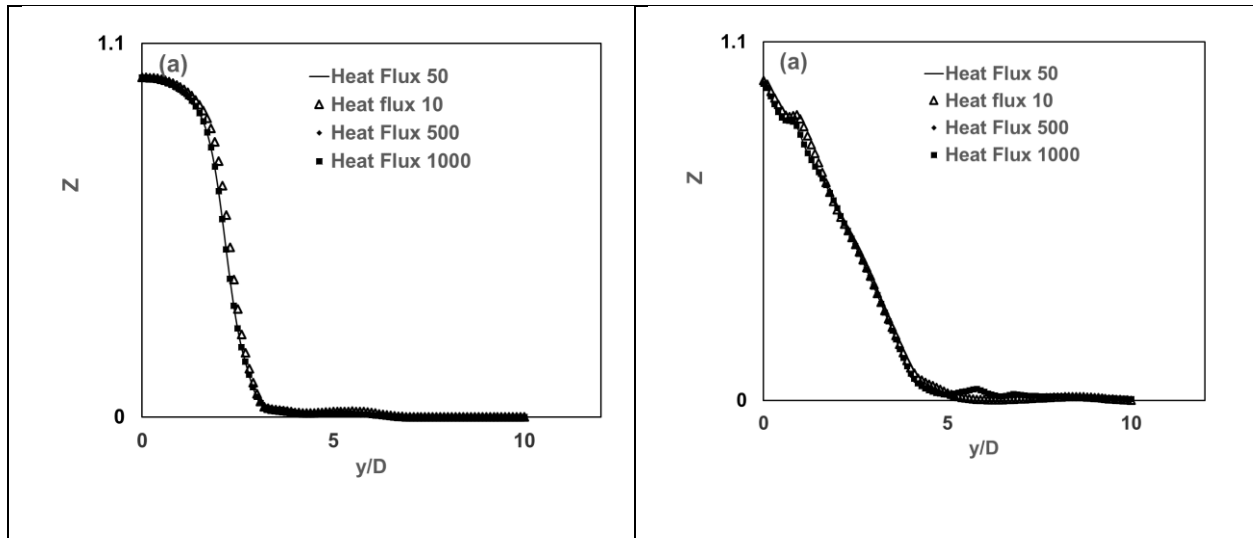
Fig. 35(a) depicts the temperature plot for the parametric study at inlet fuel velocity 20 m/s and $y/D = 30$ for heat flux of 1000 per unit area. Here, the temperature profile starts at about 500 K and rises to about 2100K. Then, it takes a straight dip to about 500 K and plateaus after two fluctuations to a value of about 300 K. Fig. 35(b) depicts the velocity plot for the parametric study at inlet fuel velocity 20 m/s and $y/D = 30$ for heat flux of 1000 per unit area. The velocity profile starts decaying at around 21 m/s and finally plateaus at a value of about 1 m/s with one major dip in between. Fig. 35(c) depicts the mixture fraction plot for the parametric study at inlet fuel velocity 20 m/s and $y/D = 30$ for heat flux of 1000 per unit area. Here, the mixture fraction profile starts at below 1 and decays with minimal fluctuations.

Conclusion for the heat flux effect

Hence, there are no major differences with the change in the heat fluxes. The only noticeable difference is the starting point and the presence and the absence of the fluctuations for temperature, velocity, and the mixture fraction plots.

Summary of the comparison of plots based on heat flux (10 W/m², 50W/m², 500W/m², 1000W/m²)





4.5 Demonstration of temperature profile at 0.26 seconds during validation after all the blocks were added

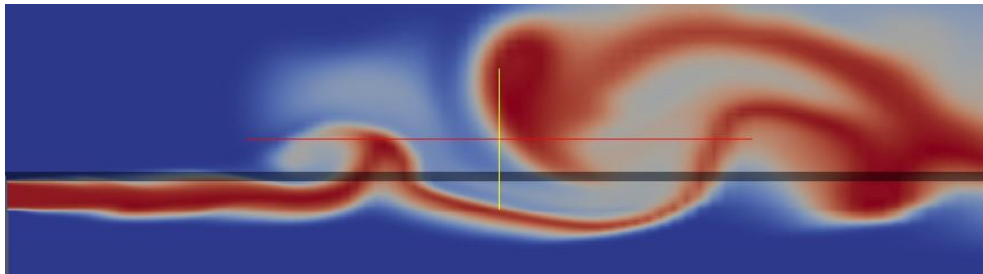


Figure 36: Temperature profile after validation for 0.26 seconds

Fig. 36 demonstrates the temperature profile after validation for 0.26 seconds.

4.6 Demonstration of velocity profile at 0.26 seconds during validation after all the blocks were added

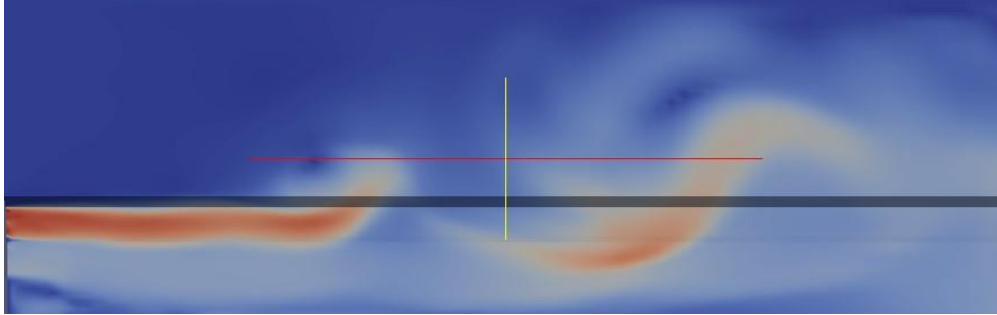


Figure 37: Velocity profile after validation for 0.26 seconds

Fig. 37 demonstrates the velocity profile after validation for 0.26 seconds.

4.7 Demonstration of mixture fraction profile at 0.26 seconds during validation after all the blocks were added

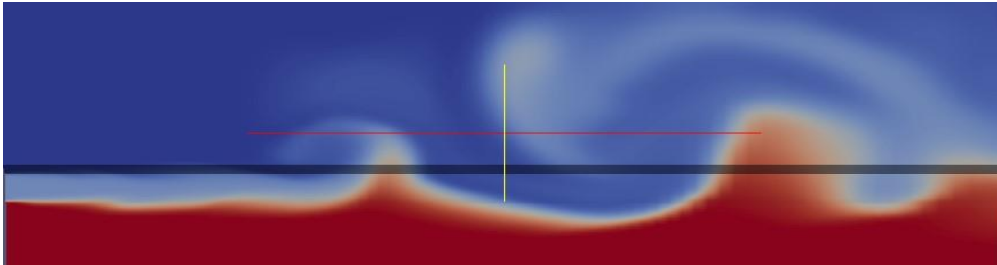


Figure 38: Mixture fraction profile after validation for 0.26 seconds

Fig. 38 demonstrates the mixture fraction profile after validation for 0.26 seconds

4.8 Demonstration of temperature profile at 0.26 seconds during validation after all the blocks were added for longer geometry (four times)

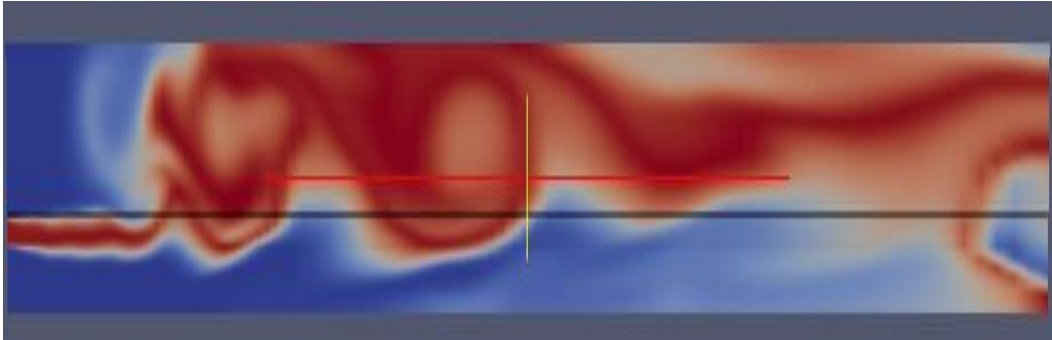


Figure 39: Temperature profile after validation for 0.26 seconds for longer geometry (four times)

4.9 Demonstration of velocity profile at 0.26 seconds during validation after all the blocks were added for longer geometry (four times)

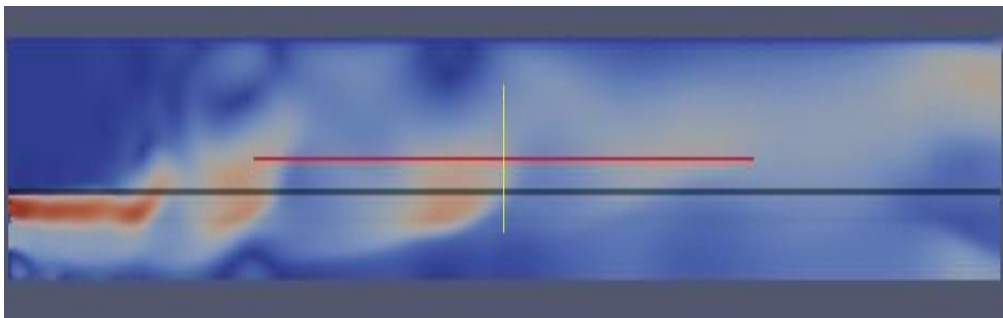


Figure 40: Velocity profile after validation for 0.26 seconds for longer geometry (four times)

4.10 Demonstration of mixture fraction profile at 0.26 seconds during validation after all the blocks were added for longer geometry (four times)

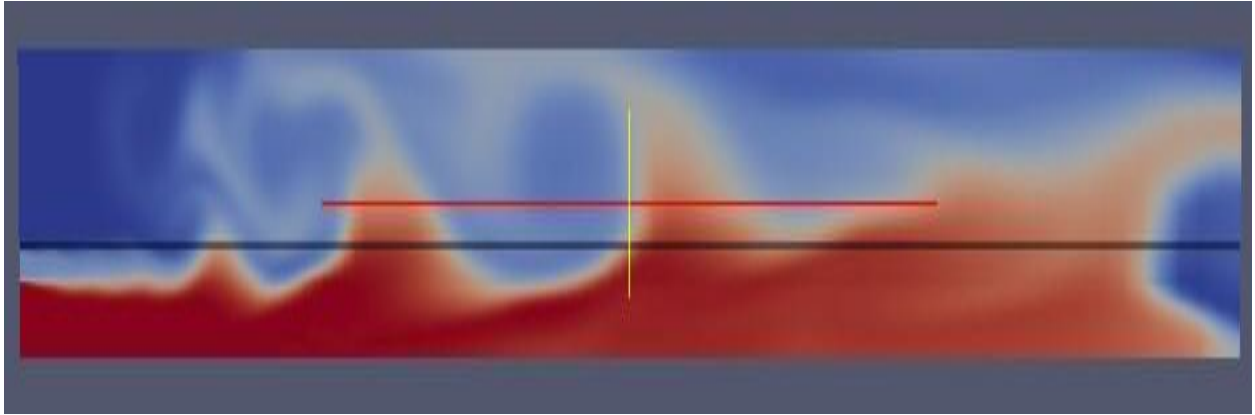


Figure 41: Mixture fraction profile after validation for 0.26 seconds for longer geometry (four times)

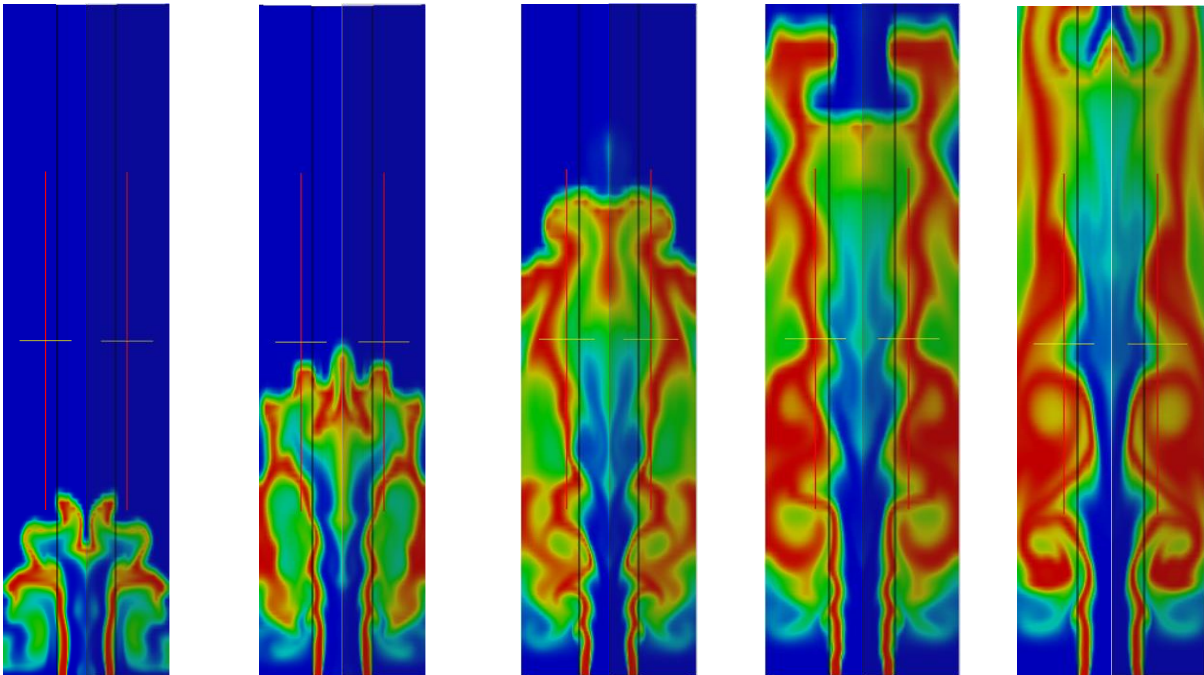


Figure 42: Temperature contour

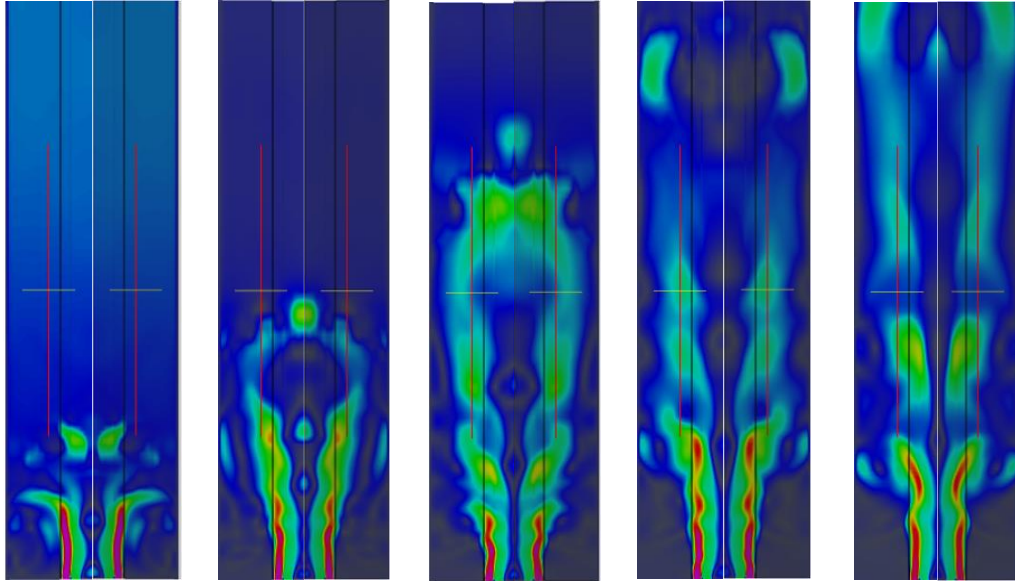


Figure 43: Velocity contour

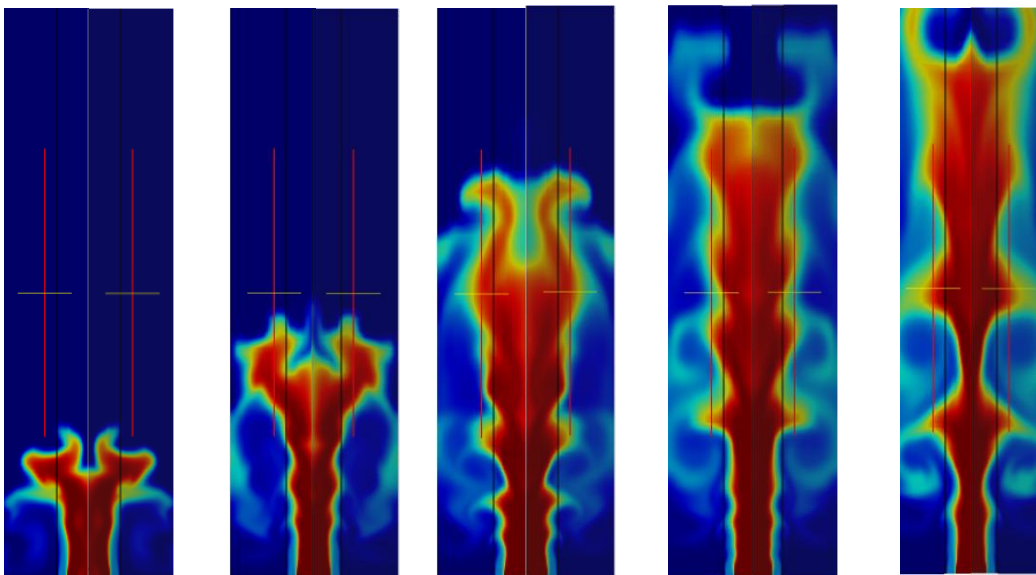


Figure 44: Mixture fraction contour

Converting ANSYS mesh to open foam mesh: command

fluent3DMeshToFoam

The three solid cylinders were modeled in solidworks and then imported to Ansys to mesh them. Then, the meshed model from ANSYS was imported into open foam and the above command was used to create the polymesh mesh file. In order to do so, we had to delete the previously contained blockMesh file in order to create the new polymesh file and then change the pressure and velocity accordingly. we have to change the boundaries that we set in ANSYS file for the pressure and velocity [18]. We have to change the inlet type from patch to inlet and outlet respectively [18]. To set our case in order to display the mesh in paraview, we need to copy the boundaries in the files in the zero folder [18]. When opening those ones, we find different boundaries and we change the setup as seen in the newly generated polymesh folder.

Problems faced:

- The entire case could not run and the error messages are attached above. The other reason may be the limitation of the fluent mesh [19]. But finally, it was solved. When we went through the blogs, it was mentioned in the thread to increase the space and it was resolved. It just took 20 minutes to run the entire case as follows.
- Different versions of ubuntu and open Foam were tried and tested in order to see which one works well with each other because some commands depend on the version of ubuntu and open Foam.

CHAPTER 5. CONCLUSIONS AND RECOMMENDATIONS FOR FUTURE RESEARCH

5.1 Concluding remarks

In this graduation thesis, we experimentally investigated the effect of burner geometry (flat, converging, and diverging) on the stability of a turbulent non-premixed burner flame.

Experiments were performed at standard temperature, pressure, variable inlet fuel velocities and the inlet fuel composition was kept constant (75% CH₄ and 25% CO₂). In this study, burner geometry, inlet velocities, heat fluxes, mesh and temperature were varied. There was an attempt to also simulate the results for the 3D model by trying to find out the balance between the finer and coarser mesh by always keeping track of the Courant number. Also, there was an attempt to validate the plots from the large eddy simulation of the Cambridge/Sandia stratified flame with flamelet-generated manifolds with the diameters of 23.6 mm for fuel and 34.8 mm for pilot air with the results noticing at 0.26 s. The most important findings of this study can be summarized as follows.

- Mathematically and numerically modeled effect of wall thermal boundary conditions in non-premixed flame dynamics
- Presented detailed parametric studies based on nozzle shape, fuel inlet velocities, and gradientEnergy boundary condition at different locations using Open FOAM.
- Visually seen differences in temperature, velocity, and mixture fraction at different locations for different boundary conditions.
- After the model was simulated, the impacts of stretching were investigated.
- The velocity fields, species mass fraction, equivalence ratio, and temperature simulation and

experimental data were determined to be in satisfactorily good agreement.

- Pursuit of simulation and results based on externalWallHeatFlux boundary condition for the conjugate case is still in progress.
- It was demonstrated that there were few excellent agreements between the mixture fraction, temperature, and velocity profiles and the experimental data and there were few disagreements.

Thus, the stage of finding the effects of boundary conditions in flame stability and propagation is still in progress and remains a challenge. Hence, further research is needed to better understand fuel combustion and consequently develop strategies to improve flame stability.

5.2 Recommendations for future research

The outcomes are anticipated to be further enhanced by a more comprehensive model that takes into account all heat loss (including radiation), preferred diffusion, stretch effects, and other factors. Future research will need to be done on this.

REFERENCES

- [1] *Flames*. (2011, February 14). A-to-Z Guide to Thermodynamics, Heat & Mass Transfer, and Fluids Engineering Online. <https://thermopedia.com/content/766/>
- [2] Pachpute, D. S. (2021, June 26). *CFD modeling of turbulent combustion · CFD Flow Engineering*. CFD Flow Engineering. Retrieved October 8, 2022, from <https://cfdflowengineering.com/cfd-modeling-of-turbulent-combustion/>
- [3] Lucchini, T., D'Errico, G., Onorati, A., Frassoldati, A., Stagni, A., & Hardy, G. (2017, March 28). *Modeling non-premixed combustion using tabulated kinetics and different fame structure assumptions*. SAE International Journal of Engines. Retrieved October 8, 2022, from <https://www.sae.org/publications/technical-papers/content/2017-01-0556/>
- [4] *Fluent tutorial guide - FEM.IR*. (2022). Retrieved October 9, 2022, from http://www.ansys.fem.ir/ansys_fluent_tutorial.pdf
- [5] Pachpute, D. S. (2021, June 26). *CFD modeling of turbulent combustion · CFD Flow Engineering*. CFD Flow Engineering. Retrieved October 8, 2022, from <https://cfdflowengineering.com/cfd-modeling-of-turbulent-combustion/>
- [6] *Fluent tutorial guide 182 [QN8RR0XMWKL1]*. [qn8rr0xmwkl1]. (2022). Retrieved October 8, 2022, from <https://idoc.pub/documents/fluent-tutorial-guide-182-qn8rr0xmwkl1>
- [7] Kassem, H. I., Saqr, K. M., Aly, H. S., Sies, M. M., & Wahid, M. A. (2010, December 16). *Implementation of the Eddy dissipation model of turbulent non-premixed combustion in openfoam*. International Communications in Heat and Mass Transfer. Retrieved October 8, 2022, from <https://www.sciencedirect.com/science/article/pii/S0735193310002964>
- [8] Ap. (2022, October 7). *AP News Summary at 12:14 a.m. EDT*. Watertown Daily Times. Retrieved October 8, 2022, from https://www.wdtimes.com/news/national/ap-news-summary-at-12-14-a-m-edt/article_a319157a-ff2f-5cfd-9012-ff5de43490c3.html
- [9] *Valerio Parisi - Google scholar*. (n.d.). Retrieved October 9, 2022, from <https://scholar.google.com/citations?user=FaagiogAAAAJ>
- [10] Author Cadence CFD. (2021, December 16). *The Reynolds-averaged navier-stokes (RANS) equations and models*. Cadence. Retrieved October 8, 2022, from <https://resources.system-analysis.cadence.com/blog/msa2021-the-reynolds-averaged-navier-stokes-rans-equations-and-models>
- [11] *2.2.1.3 depth averaged shallow water equations - tuhh*. (2022). Retrieved October 9, 2022, from http://daad.wb.tu-harburg.de/fileadmin/BackUsersResources/Flood_Probability/2D/Steffi-2D/pdf/Depth-averaged_shallow_water_equation.pdf
- [12] OpenFOAM. (2022). Retrieved October 8, 2022, from <https://www.openfoam.com/>
- [13] Asmedigitalcollection.asme.org. (n.d.). Retrieved October 8, 2022, from <https://asmedigitalcollection.asme.org/ICEF/proceedings-abstract/ICEF2020/84034/V001T06A018/1092296>

- [14] *Effect of wall boundary conditions on flame propagation in micro-chambers*. (2022). Retrieved October 9, 2022, from https://www.researchgate.net/publication/301445657_Effect_of_Wall_Boundary_Conditions_on_Flame_Propagation_in_Micro-Chambers
- [15] Ugarte-Almeyda, Orlando J., "Effect of Boundary Conditions on Propagation and Morphology of Premixed Flames in Narrow Conduits" (2015). Graduate Theses, Dissertations, and Problem Reports. 6846.
- [16] Reddy Shetty, Swathi, "Effect of Thermal Boundary Conditions on Propagation of Non-Equidiffusive Flames in Pipes" (2017). Graduate Theses, Dissertations, and Problem Reports. 6488.
- [17] kscottrichey. (2013, March 27). *Density of a gas mixture*. YouTube. Retrieved October 8, 2022, from <https://www.youtube.com/watch?v=hwkr7XP6fdc>
- [18] YouTube. (2020, June 3). *How to convert fluent .MSH mesh to openfoam polymesh using fluent3dmeshstof foam #asmaahadane*. YouTube. Retrieved October 8, 2022, from <https://www.youtube.com/watch?v=CfTE5U7AAAdA>
- [19] *Fluentmeshtof foam*. OpenFOAMWiki. (2022). Retrieved October 8, 2022, from <https://openfoamwiki.net/index.php/FluentMeshToFoam>
- [20] Barlow, R. S., and Frank, J. H., Proc. Comb. Inst. 27:1087 (1998).
- [21] TNF Workshop, <http://www.ca.sandia.gov/TNF>, R. Barlow, Eds., Sandia National Laboratories.
- [22] Borujeni, M. M., & Norouzi, H. R. (2022). *Sandia D Flame Reactingfoam*. Scribd. Retrieved September 22, 2022, from <https://www.scribd.com/document/513034825/Sandia-D-Flame-ReactingFoam>
- [23] Masudi, H, Samudrala, S, and Hudson, C. Effect of burner settings on flame stability during the combustion of coal-water slurry fuel. United States: N. p., 1997. Web.
- [24] S. R. Koirttyohann and E. E. Pickett, "The Role of Flame Shape and Burner Configuration in Emission Analysis," Appl. Spectrosc. 23, 597-600 (1969)
- [25] Lee CW, Kim IS, Hong JG. Experimental Investigation on the Effects of the Geometry of the Pilot Burner on Main Flame. *Energies*. 2021; 14(4):1115. <https://doi.org/10.3390/en14041115>
- [26] Aggarwal, S.K. Extinction of Laminar Partially Premixed Flames. Prog. Energy Combust. Sci. 2009, 35, 528–570.
- [27] Syred, N. A Review of Oscillation Mechanisms and the Role of the Precessing Vortex Core (PVC) in Swirl Combustion Systems. Prog. Energy Combust. Sci. 2006, 32, 93–161.
- [28] Lee, S.Y.; Seo, S.; Broda, J.C.; Pal, S.; Santoro, R.J. An Experimental Estimation of Mean Reaction Rate and Flame Structure During Combustion Instability in a Lean Premixed Gas Turbine Combustor. Proc. Combust. Inst. 2000, 28, 775–782.
- [29] Al-abdeli, Y.M.; Masri, A.R. Review of Laboratory Swirl Burners and Experiments for Model Validation. Exp. Therm. Fluid Sci. 2015, 69, 178–196.
- [30] Galley, D.; Ducruix, S.; Lacas, F.; Veynante, D. Mixing and Stabilization Study of a Partially Premixed Swirling Flame Using Laser Induced Fluorescence. Combust. Flame 2011, 158, 155–171.

- [31] Lee, T.W.; Fenton, M.; Shankland, R. Effects of Variable Partial Premixing on Turbulent Jet Flame Structure. *Combust. Flame* 1997, 109, 117545.
- [32] Huang, Y.; Yang, V. Dynamics and Stability of Lean-Premixed Swirl-Stabilized Combustion. *Prog. Energy Combust. Sci.* 2009, 35, 293–364.
- [33] Akbarzadeh, M.; Birouk, M. Liftoff of a Co-Flowing Non-Premixed Turbulent Methane Flame: Effect of the Fuel Nozzle Orifice Geometry. *Flow Turbul. Combust.* 2014, 92, 903–929.
- [34] Akbarzadeh, M.; Birouk, M. Liftoff of a Co-Flowing Non-Premixed Turbulent Methane Flame: Effect of the Fuel Nozzle Orifice Geometry. *Flow Turbul. Combust.* 2014, 92, 903–929.
- [35] Wang, X.; Cheng, X.; Lu, H.; Pan, F.; Qin, L.; Wang, Z. Effect of Burner Diameter on Structure and Instability of Turbulent Premixed Flames. *Fuel* 2020, 271, 536–548.
- [36] Yu, S.; Bai, X.S.; Zhou, B.; Wang, Z.; Li, Z.S.; Aldén, M. Numerical Studies of the Pilot Flame Effect on a Piloted Jet Flame. *Combust. Sci. Technol.* 2019.
- [37] Xi, Zhongya & Fu, Zhongguang & Hu, Xiaotian & Sabir, Syed Waqas & Jiang, Yibo. (2018). An Investigation on Flame Shape and Size for a High-Pressure Turbulent Non-Premixed Swirl Combustion. *Energies*. 11. 930. 10.3390/en11040930.
- [38] Al-Abbasi, AM. (2019). Burner Geometry Effect on the Stability of a Swirling Premixed Biogas Flame [master's thesis, University of Manitoba]
- [39] *J. Chem. Phys.* 11, 75 (1943); <https://doi.org/10.1063/1.1723808>
- [40] X. Liu, Z. Yan, and Z.-B. Yue, “Biogas,” *Compr. Biotechnol.*, pp. 99–114, 2011.
- [41] Q. Zhang, D. R. Noble, A. Meyers, K. Xu, and T. Lieuwen, “Characterization of Fuel Composition Effects in H₂/CO/CH₄ Mixtures Upon Lean Blowout,” *Aerosp. Eng.*, vol. 129, no. July, pp. 1–13, 2005.
- [42] N. Syred- K. R. Dahmen- A. C. Styles- S. A. Najim, “A review of combustion problems associated with low calorific value gases.” *J. Inst. Fuel*, p. 13, 1977.
- [43] J. Chomiak, J. P. Longwell, and A. F. Sarofim, “Combustion of low calorific value gases, Problems and Prospects,” *Prog. Energy Comb. Sci.*, vol. 15, pp. 109–129, 1989.
- [44] H. S. Zhen, Z. L. Wei, C. W. Leung, C. S. Cheung, and Z. H. Huang, “Emission of impinging biogas/air premixed flame with hydrogen enrichment,” *Int. J. Hydrogen Energy*, vol. 41, no. 3, pp. 2087–2095, 2016.
- [45] C. Karagiannaki, G. Paterakis, K. Souflas, E. Dogkas, and P. Koutmos, “Performance Evaluation of a Model Swirl Burner under Premixed or Stratified Inlet Mixture Conditions,” *J. Energy Eng.*, vol. 141, no. 2, pp. 1–9, 2015.
- [46] P. Taylor, “Combustion Science and Technology A Review of NO_x Formation Under Gas-Turbine Combustion Conditions,” no. October 2012, pp. 37–41, 1992.
- [47] C. Kulsheimer and H. Büchner, “Combustion dynamics of turbulent swirling flames,” *Combust. Flame*, vol. 131, no. 1–2, pp. 70–84, 2002.
- [48] G. E. Ballachey and M. R. Johnson, “Prediction of blowoff in a fully controllable lowswirl burner burning alternative fuels: Effects of burner geometry, swirl, and fuel composition,” *Proc. Combust. Inst.*, vol. 34, no. 2, pp. 3193–3201, 2013.

- [49] M. Saediamiri, M. Birouk, and J. A. Kozinski, "On the stability of a turbulent nonpremixed biogas flame: Effect of low swirl strength," *Combust. Flame*, vol. 186, no. 10–11, pp. 1460–1477, 2014.
- [50] M. Birouk, M. Saediamiri, and J. A. Kozinski, "Non-Premixed Turbulent Biogas Flame: Effect of The Co-Airflow Swirl Strength on the Stability Limits," *Combust. Sci. Technol.*, vol. 186, no. 10–11, pp. 1460–1477, 2014.
- [51] F. El-Mmahallawy, A. Abdelhafez, M. Mansour*, and M. Mansour, "Mixing and Nozzle Geometry Effects on Flame Structure and Stability," *Combust. Sci. Technol.*, vol. 179, no. 1–2, pp. 249–263, 2007.
- [52] B. Yan et al., "Structures and stabilization of low calorific value gas turbulent partially premixed flames in a conical burner," *Exp. Therm. Fluid Sci.*, vol. 34, no. 3, pp. 412–419, 2010.
- [53] E. A. R. V. A. Arkhipov, O. V. Matvienko, "Influence of Geometric and Regime Parameters on Flame Stabilization of a Swirl Burner," *Combust. Explos. Shock Waves*, vol. 35, no. 5, 1999.
- [54] T. Lieuwen, V. McDonell, E. Petersen, and D. Santavicca, "Fuel Flexibility Influences on Premixed Combustor Blowout, Flashback, Autoignition, and Stability," *J. Eng. Gas Turbines Power*, vol. 130, no. 1, p. 011506, 2008.
- [55] W. Jerzak and M. Kuźnia, "Experimental study of impact of swirl number as well as oxygen and carbon dioxide content in natural gas combustion air on flame flashback and blow-off," *J. Nat. Gas Sci. Eng.*, vol. 29, pp. 46–54, 2016.
- [56] Driscoll, James & Temme, Jacob. (2011). Role of Swirl in Flame Stabilization. 10.2514/6.2011108.
- [57] Lecture 5. laminar premixed flames structures and propagation. (n.d.). Retrieved October 9, 2022, from https://www.lth.se/fileadmin/fm/Education/Courses/Combustion/Lect5_pf_2.pdf
- [58] Lecture 11 premixed turbulent combustion: The regime diagram. (n.d.). Retrieved October 9, 2022, from <https://cefr.princeton.edu/sites/g/files/toruqf1071/files/Files/2010%20Lecture%20Notes/Norbert%20Peters/Lecture11.pdf>
- [59] Cloney, C. (2019, July 18). Differences between premixed and non-premixed flames. Dust Safety Science. Retrieved October 8, 2022, from <https://dustsafetyscience.com/premixed-vs-non-premixed-flames/>
- [60] Gestione. (2022, April 2). Turbulence models in CFD - rans, DES, Les and DNS. IdealSimulations. Retrieved October 8, 2022, from <https://www.idealsimulations.com/resources/turbulence-models-in-cfd/>
- [61] Malalasekera, W, Ibrahim, SS, Masri, AR et al. (2 more authors) (2010) Large eddy simulation of premixed and non-premixed combustion. In: Proceedings of the 37th National & 4th International Conference on Fluid Mechanics and Fluid Power. 37th National & 4th International Conference on Fluid Mechanics and Fluid Power, Chennai, India. , Chennai .
- [62] Parisi, Valerio. Large Eddy Simulation of a Stagnation Point Reverse Flow Combustor. Diss. Georgia Institute of Technology, 2006.

- [63] Zhang, Jian, LiPo Wang, and YuQing Guo. "Non-premixed turbulent combustion modeling based on the filtered turbulent flamelet equation." *SCIENCE CHINA Physics, Mechanics & Astronomy* 63.4 (2020): 1-6.
- [64] Ihme, M., & Pitsch, H. (2005, January). LES of a non-premixed flame using an extended flamelet/progress variable model. In the 43rd AIAA Aerospace Sciences Meeting and Exhibit (p. 558).
- [65] Zhang, W., Karaca, S., Wang, J., Huang, Z., & Oijen, J. van. (2021). Large eddy simulation of the cambridge/sandia stratified flame with flamelet-generated manifolds: Effects of non-unity lewis numbers and stretch. *Combustion and Flame*, 227, 106–119. <https://doi.org/10.1016/j.combustflame.2021.01.004>